# Magma chamber dynamics at Soufrière Hills volcano, Montserrat

Crystal P. Mann

Department of Earth and Planetary Sciences

McGill University

Montreal, Quebec, Canada

April 2010

## Abstract

Implicit in active, steady-state magmatic systems is their persistent activity and unchanging behavior in terms of composition and eruptive styles. The ongoing eruption (July 1995 – April 2010) of the Soufrière Hills volcano (SHV), Montserrat, provides an ideal setting for understanding this steady-state behavior. Mafic enclaves are ubiquitous in andesitic magma erupted from SHV. The mafic enclaves are basalt to basaltic andesite (49 – 56 wt. % $SiO_2$) in composition. Based on their chemistry, mineralogy and petrology, they are divided into three types. Prior to intrusion, basaltic magma underwent significant differentiation of amphibole at deep crustal levels. Type 1 (T1) and Type 2 (T2) enclaves represent hybrid magmas which are a mixture of differentiated basaltic magma and the host andesite, while Type 3 (T3) enclaves represent basaltic magma which ponded prior to intrusion and underwent significant additional fractionation of plagioclase. The T1 enclaves sample a vesiculated upper portion of the mixing horizon, while the T2 enclaves sample a less vesiculated, deeper, and slightly more rigid portion of this horizon. The T3 enclaves were near the temperatures of the andesite reservoir at the time of their intrusion; they demonstrate mixing on a physical mixing only, i.e., crystal transfer. The T1 enclaves formed when they reached buoyancy due to vesiculation and detached from the mixing horizon to rise upward in the andesite, whereas T2 enclaves formed during subsequent intrusions, during mafic overturn. The SHV demonstrates periodic and regular explosive activity, for which we can quantify changes in volatile content over time. Volatile analyses from phenocryst-hosted melt inclusions sampled from andesitic pumice cluster at 2.8 – 5.4 wt. % $H_2O$, with ~ 3000 ppm Cl and negligible $CO_2$. We interpret these volatile contents to mirror conditions in the lower conduit and upper magma reservoir beneath the volcano. Our model of the SHV magmatic system suggests that 1) the mafic magma is providing heat, mass and volatiles to the

magmatic system, 2) the magmatic system is unable to evolve to more felsic compositions due to buffering by this mafic magma, 3) $CO_2$ is degassed and lost from the mafic magma as it rises from the deep crust, 4) S exsolves during mixing of the mafic magma and andesitic host and 5) explosive eruptions are sampling magma which is stored in the upper portions of the magma chamber.

**Résumé**

Une caractéristique des systèmes magmatiques à l'équilibre est leur activité persistante et leur comportement constant en termes de compositions et styles d'éruption. L'éruption en cours (Juillet 1995 – Avril 2010) du volcan de Soufrière Hills (SHV), Montserrat, représente une configuration idéale pour comprendre cet état d'équilibre éruptif. Les enclaves mafiques sont omniprésentes dans les magmas andésitiques émis à SHV. La composition de ces enclaves varie de basaltes à andésites basaltiques (49 – 56 % $SiO_2$). Elles se répartissent en trois types selon leur chimie, minéralogie et pétrologie. Avant intrusion dans le magma andésitique, les magmas basaltiques ont fractionné une quantité importante d'amphibole dans la croûte profonde. Les enclaves de type 1 (T1) et type 2 (T2) représentent des magmas hybrides, soit un mélange de basalte différencié et d'andésite hôte, tandis que les enclaves de type 3 (T3) représentent un magma basaltique qui a stagné avant intrusion et a subi un fractionnement additionnel de plagioclase. Les enclaves T1 proviennent de portions vésiculaires de la partie supérieure du front de mélange, tandis que les T2 proviennent d'un niveau moins vésiculaire, plus profond et légèrement plus rigide ce cet horizon. Les enclaves T3 étaient proches de la température du réservoir andésitique au moment de leur intrusion et ne montrent du mélange que d'une manière physique, soit des transferts de cristaux. Les enclaves se sont formées lorsqu'elles sont devenues moins denses à cause de la vésiculation et se sont détachées de l'horizon de mélange pour monter dans le magma andésitique, tandis que les T2 se sont formées durant des intrusions successives, causant de la convection mafique. Le SHV connaît une activité explosive et régulière, pour laquelle il est possible de quantifier des changements en volatiles au cours du temps. Des analyses des volatiles dans les inclusions vitreuses des phénocristaux issus de ponces andésitiques indiquent des concentrations de 2.7 – 5.4% $H_2O$, ~ 3000 ppm Cl et négligeables en

$CO_2$. Nous interprétons ces concentrations de volatiles comme reflétant les conditions dans le conduit inférieur et le haut du réservoir magmatique. Notre modèle du système magmatique du SHV suggère que 1) les magmas mafiques apportent de la chaleur, de la masse et des volatiles au système magmatique, 2) le système magmatique n'est pas capable d'évoluer vers des compositions plus felsiques car tamponné par les apports de magmas mafiques, 3) le $CO_2$ dégaze et quitte le magma mafique à mesure que celui-ci monte depuis la croûte profonde, 4) S subit une exsolution lors du mélange du magma mafique et de l'hôte andésitique, et 5) les éruptions explosives capturent du magma accumulé dans les portions supérieures de la chambre magmatique.

**Contributions of authors**

This thesis is a manuscript based thesis with three main chapters (Chapters 1, 2 and 3) and to be submitted to journals. I am the main author on each chapter. I have one co-author on Chapters 1 and 3 and two co-authors on Chapter 2. I developed the ideas and proposed the models for each paper, I performed all the fieldwork, sample preparation, sample analysis, data interpretation, writing, table and figure design. John Stix, my research supervisor, provided advice on data interpretation and guidance in idea development, as well as editing of each chapter.

## Acknowledgements

This thesis would not have been possible without the support of many people. First I would like to thank my supervisor, John Stix, for his constant support, encouragement and excitement for this project. I would like to thank the Kristy Thornton and Anne Kosowski for their help with McGill red tape and always looking out for my best interests. I would like to thank Shi Lang and Brigitte Dionne for their technical support with machines that have a mind of their own. I would like to thanks my research committee members Willy Williams-Jones and Don Francis for their advice and suggestions during committee meetings. I thank Guillaume Girard for translating the abstract on such short notice during the Stanley Cup playoffs and I thank the members of the volcanology group and my friends from the EPS department for their constant support over the years.

I want to acknowledge the first floor of FDA. I thank the hydro group, Bernardo Brixel, Laura Maharaj and Micheal Barear for their constant support, the late night pizza and willingness to help me with anything right down to the last minute. I thank Jack Wilcock, Michelle Campbell, Christoph Helo and Marc-Antoine Longpré for their friendship. Without these four I many not have met my goal. I thank Jack for breakfast, lunch and dinner and helping me with last minute corrections, Michelle for her help in proofreading when I couldn't see it anymore, Christoph and Marc-Antoine for their words of wisdom.

Lastly I would like to thank my family and friends from Seattle for their constant encouragement and support of my studies.

**Table of Contents**

# List of Tables

**Chapter 1**

**Chapter 2**

No tables

**Chapter 3**

No tables

# List of Figures

## Chapter 1

## Chapter 2

## Chapter 3

# List of Appendicies

# General Introduction

# Introduction

*Arc volcanism*

Arc volcanism is among the most impressive displays of nature's power on Earth. Arc volcanoes contribute gas and ash to the atmosphere, have a hand in destruction of lives and livelihoods and provide us with a glimpse of dynamics below the Earth's surface. Some examples include, Mt. Pinatubo, Phillipines; Vesuvius, Italy: Mount St. Helens, U.S.A; and Soufrière Hills volcano, Montserrat.  The importance of studying active volcanism is the opportunity to correlate visual changes observed at the surface with processes occurring at depth. Visual changes can be witnessed and documented, but the information on subsurface processes comes in the form of magma erupted at the surface and volatiles observed in the gas plume. Once this link is made to better understand the mechanisms which control eruptions, we can improve mitigation strategies. However, the reasons why arc volcanoes re-activate after years of dormancy, the mechanisms contributing to their longevity and the significance of the petrologic processes operating at depth are still poorly understood.

*Magma replenishment as an eruption trigger*

Volcanic eruptions may have a common mechanism, i.e., the replenishment of shallow reservoirs during intrusion of new magma. The intrusive magma can be either more mafic or more felsic than the resident magma composition (Andrews et al., 2008; Browne et al., 2006; Eichelberger et al., 2000; Murphy et al., 2000; Turner et al., 2008). Upon intrusion, the replenishing magma contributes mass, heat and volatiles to the shallow reservoir, increasing pressure and causing disequilibrium within the magmatic system (Bachmann and Bergantz, 2003; Eichelberger, 1980; Huppert et al., 1982; Huppert and Woods, 2002; Sparks and Marshall,

1986). Recognition of a replenishment event is often inferred from magmatic enclaves which have a different composition compared to the resident magma.

*Significance of mafic enclaves*

The presence of mafic enclaves in igneous rocks has long been documented in andesitic to rhyolitic lava domes (Bacon, 1986b; Eichelberger, 1975), as well as in the plutonic record (Wiebe, 1974). Their presence has been attributed to the incorporation of solid country rock xenoliths (Chappell *et al.*, 1987), cumulate fragments derived from the crystalline rinds of upper crustal magma reservoirs (Arculus and Wills, 1980), hot mafic magma intruded and chilled as blobs in a cooler, more silicic host (Bacon, 1986a), or the more mafic components of a stratified chamber incorporated into the more silicic host due to convective mixing (Mattson *et al.*, 1986).

The textural characteristics of magmatic enclaves in volcanic rocks can distinguish a liquid state at the time of their incorporation into the host. These characteristics include 1) acicular, tabular, swallowtail and skeletal habits of groundmass microphenocrysts, 2) an ellipsoidal shape, 3) chilled or crenulate margins, 4) abundant interstitial residual glass and 5) vesicular textures (Bacon, 1986a; Eichelberger, 1980). The best examples of these phenomena occur when the difference in temperature between the two magmas is large, hence the degree of undercooling is at a maximum (Coombs et al., 2003; Martin et al., 2006).

*The Soufrière Hills volcano*

After ~ 400 years of quiescence, on 18 July 1995 phreatomagmatic explosions announced the re-awakening of the Soufrière Hills volcano (SHV) (Aspinall et al., 1998). Volcanic unrest began in 1992, when an intense earthquake swarm occurred beneath Montserrat, followed by another intense swarm in late 1994 (Aspinall et al., 1998). Similar swarms had occurred

frequently during the last two centuries, with seismic crises recorded in 1987, 1933 and 1966 at approximately 30 year intervals (Robertson et al., 2000). These swarms are thought to represent magma rising beneath the volcano and ponding before reaching the surface (Perret, 1939; Shepherd et al. 1971). The seismic activity in 1992-1994 just prior to the onset of extrusion comprised 15 episodic swarms of volcano-tectonic earthquakes located at ~ 15 km beneath SHV, which were interpreted as movement of mafic magma (Aspinall et al., 1998).

The ongoing eruption is characterized by 1) multiple episodes of growth and collapse of andesitic lava domes (Cole et al., 1998; Herd et al., 2005; Simmons et al., 2005), 2) generation of andesitic block and ash flows by explosive and gravitational collapse of these domes (Cole et al., 1998; Loughlin, 2002), and 3) generation of pyroclastic flows of vesicular andesite by fountain collapse of Vulcanian eruption columns (Clarke, 2000; Cole, 2002; Druitt et al., 2002). It is typical to see dome growth and collapse cycles followed by vulcanian explosions, with a hiatus in dome growth for intervals of years (Herd et al., 2005). The dome growth – dome collapse cycles are thought to be initiated by intrusions of more mafic magma at depth contributing volume, heat and volatiles which together push the magmatic system towards a state of disequilibrium (Murphy et al., 2000).

*Lavas and volatiles observed at SHV*

The extrusion of non-juvenile material began in the summit region in September of 1995, with sustained extrusion of andesite lava starting in November 1995 (Young et al., 1998b). The extruded lavas are porphyritic hornblende-hypersthene andesites comprising 45 – 55 vol% phenocrysts (30 – 35 % plagioclase, 6-10 % amphibole, 2-4 % titanomagnetite, < 0.5 % quartz, < 0.5 % clinopyroxene), set in a partly crystalline groundmass (Murphy et al., 2000; Murphy et al., 1998). The interstitial glass is rhyolitic and represents 5 – 35 % of the rock by volume. It has

been suggested that the abundant disequilibrium features of the phenocrysts are products of a chemically homogeneous, convecting andesitic magma heated from below and cooled from above (Couch et al., 2001). The erupted lavas are host to basaltic to basaltic andesite enclaves (Murphy et al., 2000; Murphy et al., 1998; Rea, 1974; Wadge and Isaacs, 1988; Zellmer et al., 2003). Previous studies have demonstrated that the mafic enclaves are not related to the more mafic South Soufrière Hills (SSH) volcano to the south nor are parental to the andesitic host (Murphy et al., 2000; Zellmer et al., 2003). Since the injection of mafic magma into a more silicic host is often a triggering mechanism for volcanic eruptions (Bacon, 1986a; Eichelberger, 1980; Sparks et al., 1977) and mafic magma observed as enclaves is an obvious hint of intrusion of mafic material, the enclaves are therefore an important source of information to better comprehend the volcano's behavior.

At SHV, gas monitoring includes $SO_2$, HCl and $CO_2$ (Christopher et al., 2010; Edmonds et al., 2003; Edmonds et al., 2002; Galle et al., 2003; Hammouya et al., 1998). Increases in $SO_2$ emission rate accompany increasing magma extrusion rates during certain periods of the eruption and correlate with seismic activity over short timescales during cycles of inflation and deflation associated with upper conduit pressure fluctuations (Watson *et al.*, 2000). It is also common to see $SO_2$ spikes immediately after dome collapse (Herd et al., 2005; Young et al., 1998a). The mafic magma is thought to be the source of S and $CO_2$ for the magmatic system (Christopher et al., 2010; Edmonds et al., 2003).

*Magma reservoir models*

The andesitic magma is interpreted as a long-lived body thermally sustained by intrusions from depth (Murphy et al., 2000). The reservoir volume is estimated to be on the order of several cubic kilometers (Voight et al., 2010). The volume of resident andesite magma relative to that of

intrusive mafic magma is unclear, but the volume of erupted andesite extruded at the surface is maybe caused by an equivalent volume of mafic magma displacing the andesite at depth (Voight *et al.*, 2010). Magma storage comprises either 1) two magma chambers at ~ 5 km and ~ 12 km connected by a conduit which transfers magma, or 2) a vertically extensive reservoir centered at ~ 10 km (Barclay et al., 1998; Devine et al., 2003; Murphy et al., 2000; Voight et al., 2010).

## Thesis rationale

The presence of a mafic component clearly influences volcanism at SHV, and its importance in triggering volcanic eruption has been established. The obvious presence of more mafic magma, coupled with a plethora of literature on SHV over the last 15 years as well as real time monitoring at the volcano, provide an ideal site for study. In this thesis I focus on mafic enclaves observed at the Soufrière Hills volcano (SHV). I assess their physical and chemical contribution to the ongoing eruption at the SHV, first by conducting a detailed petrologic study of the mafic enclaves observed in the recent (1996 – 2006) deposits, followed by a volatile study on phenocryst-hosted melt inclusions observed in the vulcanian pumice.

## Thesis organization

This thesis is divided into a general introduction, three main chapters, and a concluding chapter. Each of the three main chapters is a manuscript to be submitted to relevant journals. The last concluding chapter summarizes the main findings and contributions to knowledge, and also presents some directions for future research.

The main objectives of this thesis are:

1) To determine the petrogenesis of the mafic magma from the upper mantle to enclave formation.

2) To establish the contribution of mafic magma to the andesite magma body in terms of bulk composition, heat and volatiles.

3) To identify the role and influence of the mafic magma in the longevity of the current eruption.

Chapter 1 is a characterization of the mafic enclaves. I use bulk rock major element, trace element and rare earth element chemistry, as well as glass chemistry, to determine the enclave compositions and their compositional variability. I then model the differentiation of the mafic magma to reproduce the enclave compositions observed. Mineral compositions are used to determine intensive variables such as temperatures and pressures of enclave formation, while textural data are used to establish when the mafic enclaves formed and how they evolved after formation.

Chapter 2 is an analysis of the phenocryst-hosted melt inclusions in vulcanian pumice. I collect major element and volatile compositions in phenocryst hosted melt inclusions from the vulcanian pumice to determine volatile concentrations in the magma chamber prior to eruption. I use these data to establish which volatile species were present, their concentrations and their evolution in the SHV reservoir.

Chapter 3 is a synthetic paper which proposes a model of the SHV magmatic system that accounts for the intrusion of mafic enclaves and the observed volatile concentrations. I establish the role of the mafic magma in terms of the longevity of the magmatic system and the role it plays in the evolution of the magma chamber.

## References

Andrews, B.J., Gardner, J.E., and Housh, T.B., 2008, Repeated recharge, assimilation, and hybridization in magmas erupted from El Chichón as recorded by plagioclase and amphibole phenocrysts: Journal of Volcanology and Geothermal Research, v. 175, p. 415-426.

Arculus, R.J., and Wills, K.J.A., 1980, The Petrology of Plutonic Blocks and Inclusions from the Lesser Antilles Island Arc: J. Petrology, v. 21, p. 743-799.

Aspinall, W.P., Miller, A.D., Lynch, L., Stewart, R.C., White, R.A., and Power, J.A., 1998, Soufrière Hills eruption, Montserrat 1995-1997: volcanic earthquake locations and fault plane solutions: Geophysical Research Letters, v. 25, p. 3397-3400.

Bachmann, O., and Bergantz, G.W., 2003, Rejuvenation of the Fish Canyon magma body: A window into the evolution of large-volume silicic magma systems: Geology, v. 31, p. 789-792.

Bacon, C., 1986a, Magmatic inclusions in silicic and intermediate volcanic rocks: Journal of Geophysical Research, v. 91, p. 6091-6112.

Bacon, C.R., 1986b, Magmatic Inclusions in Silicic and Intermediate Volcanic Rocks: J. Geophys. Res., v. 91.

Barclay, J., Rutherford, M.J., Carroll, M.R., Murphy, M.D., Devine, J.D., Gardner, J.E., and Sparks, R.S.J., 1998, Experimental phase equilibria constraints on pre-eruptive storage

conditions of the Soufrière Hills magma: Geophysical Research Letters, v. 25, p. 3437-3440.

Browne, B.L., Eichelberger, J.C., Patino, L.C., Vogel, T.A., Dehn, J., Uto, K., and Hoshizumi, H., 2006, Generation of Porphyritic and Equigranular Mafic Enclaves During Magma Recharge Events at Unzen Volcano, Japan: J. Petrology, v. 47, p. 301-328.

Chappell, B.W., White, A.J.R., and Wyborn, D., 1987, The Importance of Residual Source Material (Restite) in Granite Petrogenesis: J. Petrology, v. 28, p. 1111-1138.

Christopher, T., Edmonds, M., Humphreys, M.C.S., and Herd, R.A., 2010, Volcanic gas emissions from Soufrière Hills Volcano, Montserrat 1995-2009, with implications for mafic magma supply and degassing: Geophys. Res. Lett., v. 37, p. L00E04.

Clarke, A.B., 2000, Modeling of transient vulcanian eruptions at the Soufrière Hills Volcano, Montserrat: IAVCEI general assembly 2000; Exploring volcanoes; utilization of their resources and mitigation of their hazards.

Cole, P., 2002, Deposits from dome-collapse and fountain-collapse pyroclastic flows at Soufrière Hills Volcano, Montserrat: Memoirs of the Geological Society of London, p. 231-262.

Cole, P.D., Calder, E.S., Druitt, T.H., Hoblitt, R., Robertson, R., Sparks, R.S.J., and Young, S.R., 1998, Pyroclastic flows generated by gravitational instability of the 1996-1997 Lava Dome of Soufrière Hills Volcano, Montserrat: Geophys. Res. Lett., v. 25, p. 3425-3428.

Coombs, M.L., Eichelberger, J.C., and Rutherford, M.J., 2003, Experimental and textural

    constraints on mafic enclave formation in volcanic rocks: Journal of Volcanology and

    Geothermal Research, v. 119, p. 125-144.

Couch, S., Sparks, R.S.J., and Carroll, M.R., 2001, Mineral disequilibrium in lavas explained by

    convective self-mixing in open magma chambers: Nature, v. 411, p. 1037(3).

Devine, J.D., Rutherford, M.J., Norton, G.E., and Young, S.R., 2003, Magma Storage Region

    Processes Inferred from Geochemistry of Fe-Ti Oxides in Andesitic Magma, Soufrière

    Hills Volcano, Montserrat, W.I: J. Petrology, v. 44, p. 1375-1400.

Druitt, T.H., Young, S.R., Baptie, B., Bonadonna, C., Calder, E.S., Clarke, A.B., Cole, P.D.,

    Harford, C.L., Herd, R.A., Luckett, R., Ryan, G., and Voight, V., 2002, Episodes of

    cyclic vulcanian explosive activity with fountain collapse at Soufrière Hills Volcano,

    Montserrat, *in* Druitt, T.H., and Kokelaar, B.P., eds., The eruption of Soufrière Hills

    Volcano, Montserrat, from 1995 to 1999, Volume 21: Geological Society, London,

    Memoirs: London, The Geological Society of London, p. 281-306.

Edmonds, M., Oppenheimer, C., Pyle, D.M., Herd, R.A., and Thompson, G., 2003, SO2

    emissions from Soufrière Hills volcano and their relationship to conduit permeability,

    hydrothermal interaction and degassing regime: Journal of Volcanology and Geothermal

    Research, v. 124, p. 23-43.

Edmonds, M., Pyle, D., and Oppenheimer, C., 2002, HCl emissions at Soufrière Hills Volcano, Montserrat, West Indies, during a second phase of dome building: November 1999 to October 2000: Bulletin of Volcanology, v. 64, p. 21-30.

Eichelberger, J.C., 1975, Origin of andesite and dacite: Evidence of mixing at Glass Mountain in California and at other circum-Pacific volcanoes: Geological Society of America Bulletin, v. 86, p. 1381-1391.

—, 1980, Vesiculation of mafic magma during replenishment of silicic magma reservoirs: Nature, v. 288, p. 446-450.

Eichelberger, J.C., Chertkoff, D.G., Dreher, S.T., and Nye, C.J., 2000, Magmas in collision: Rethinking chemical zonation in silicic magmas: Geology, v. 28, p. 603-606.

Galle, B., Oppenheimer, C., Geyer, A., McGonigle, A.J.S., Edmonds, M., and Horrocks, L., 2003, A miniaturised ultraviolet spectrometer for remote sensing of SO2 fluxes: a new tool for volcano surveillance: Journal of Volcanology and Geothermal Research, v. 119, p. 241-254.

Hammouya, G., Allard, P., Jean-Baptiste, P., Parello, F., Semet, M.P., and Young, S.R., 1998, Pre and syn-eruptive geochemistry of volcanic gases from Soufrière Hills volcano, Montserrat W.I.: Geophysical Research Letters, v. 25, p. 3685-3688.

Herd, R.A., Edmonds, M., and Bass, V.A., 2005, Catastrophic lava dome failure at Soufrière Hills Volcano, Montserrat, 12-13 July 2003: Journal of Volcanology and Geothermal Research, v. 148, p. 234-252.

Huppert, H.E., Sparks, R.S.J., and Turner, J.S., 1982, Effects of volatiles on mixing in calc-alkaline magma systems: Nature, v. 297, p. 554-557.

Huppert, H.E., and Woods, A.W., 2002, The role of volatiles in magma chamber dynamics: Nature, v. 420, p. 493-495.

Loughlin, S.C., 2002, Pyroclastic flows and surges generated by the 25 June 1997 dome collapse, Soufrière Hills Volcano, Montserrat: Memoirs of the Geological Society of London, p. 191-209.

Martin, V.M., Holness, M.B., and Pyle, D.M., 2006, Textural analysis of magmatic enclaves from the Kameni Islands, Santorini, Greece: Journal of Volcanology and Geothermal Research, v. 154, p. 89-102.

Mattson, S.R., Vogel, T.A., and Wilband, J.T., 1986, Petrochemistry of the silicic-mafic complexes at Vesturhorn and Austurhorn, Iceland: evidence for zoned/stratified magma: Journal of Volcanology and Geothermal Research, v. 28, p. 197-223.

Murphy, M.D., Sparks, R.S.J., Barclay, J., Carroll, M.R., and Brewer, T.S., 2000, Remobilization of Andesite Magma by Intrusion of Mafic Magma at the Soufrière Hills Volcano, Montserrat, West Indies: J. Petrology, v. 41, p. 21-42.

Murphy, M.D., Sparks, R.S.J., Barclay, J., Carroll, M.R., Lejeune, A.M., Brewer, T.S., Macdonald, R., Black, S., and Young, S.R., 1998, The role of magma mixing in triggering the current eruption at the Soufrière Hills volcano, Montserrat, West Indies: Geophysical Research Letters, v. 25, p. 3433-3436.

Rea, W.J., 1974, The volcanic geology and petrology of Montserrat, West Indies: Journal of the

    Geological Society, v. 130, p. 341-366.

Robertson, R.E.A., Aspinall, W.P., Herd, R.A., Norton, G.E., Sparks, R.S.J., and Young, S.R.,

    2000, The 1995-1998 Eruption of the Soufrière Hills Volcano, Montserrat, WI:

    Philosophical Transactions: Mathematical, Physical and Engineering Sciences, v. 358, p.

    1619-1637.

Simmons, J., Elsworth, D., and Voight, B., 2005, Classification and idealized limit-equilibrium

    analyses of dome collapses at Soufrière Hills volcano, Montserrat, during growth of the

    first lava dome: November 1995-March 1998: Journal of Volcanology and Geothermal

    Research, v. 139, p. 241-258.

Sparks, R.S.J., and Marshall, L.A., 1986, Thermal and mechanical constraints on mixing

    between mafic and silicic magmas: Journal of Volcanology and Geothermal Research, v.

    29, p. 99-124.

Sparks, S.R.J., Sigurdsson, H., and Wilson, L., 1977, Magma mixing: a mechanism for triggering

    acid explosive eruptions: Nature, v. 267, p. 315-318.

Turner, M.B., Cronin, S.J., Smith, I.E., Stewart, R.B., and Neall, V.E., 2008, Eruption episodes

    and magma recharge events in andesitic systems: Mt Taranaki, New Zealand: Journal of

    Volcanology and Geothermal Research, v. 177, p. 1063-1076.

Voight, B., Widiwijayanti, C., Mattioli, G., Elsworth, D., Hidayat, D., and Strutt, M., 2010,

    Magma-sponge hypothesis and stratovolcanoes: Case for a compressible reservoir and

quasi-steady deep influx at Soufrière Hills Volcano, Montserrat: Geophys. Res. Lett., v. 37, p. L00E05.

Wadge, G., and Isaacs, M.C., 1988, Mapping the volcanic hazards from Soufrière Hills Volcano, Montserrat, West Indies using an image processor: Journal of the Geological Society, v. 145, p. 541-551.

Watson, I.M., Oppenheimer, C., Voight, B., Francis, P.W., Clarke, A., Stix, J., Miller, A., Pyle, D.M., Burton, M.R., Young, S.R., Norton, G., Loughlin, S., and Darroux, B., 2000, The relationship between degassing and ground deformation at Soufrière Hills Volcano, Montserrat: Journal of Volcanology and Geothermal Research, v. 98, p. 117-126.

Wiebe, R.A., 1974, Coexisting Intermediate and Basic Magmas, Ingonish, Cape Breton Island: The Journal of Geology, v. 82, p. 74-87.

Young, S.R., Francis, P.W., Barclay, J., Casadevall, T.J., Gardner, C.A., Darroux, B., Davies, M.A., Delmelle, P., Norton, G.E., Maciejewski, A.J.H., Oppenheimer, C.M.M., Stix, J., and Watson, I.M., 1998a, Monitoring SO2 emission at the Soufrière Hills Volcano: Implications for changes in eruptive conditions: Geophys. Res. Lett., v. 25, p. 3681-3684.

Young, S.R., Sparks, R., Aspinall, W.P., Lynch, L., Miller, A.D., Robertson, R., and Shepherd, J.B., 1998b, Overview of the eruption of the Soufrière Hills volcano, 18 July 1995 to December 997: Geophysical Research Letters, v. 25, p. 3389-3392.

Zellmer, G.F., Hawkesworth, C.J., Sparks, R.S.J., Thomas, L.E., Harford, C.L., Brewer, T.S.,

and Loughlin, S.C., 2003, Geochemical Evolution of the Soufrière Hills Volcano,

Montserrat, Lesser Antilles Volcanic Arc: J. Petrology, v. 44, p. 1349-1374.

## Link to Chapter 1

In the general introduction, I have emphasized the importance of replenishment by mafic magmas in the evolution of magmatic systems. Mafic recharge is widely invoked as a catalyst in volcanic eruptions, but the role of the mafic magma is poorly understood. Using the Soufrière Hills volcano, Montserrat, as a case study, we analyze mafic enclaves observed in the field to 1) determine the evolution of the mafic magma from the deep crust/upper mantle, 2) examine the interaction of the mafic magma with the andesitic host once it intrudes into the magma chamber, and 3) model the formation of the mafic enclaves after intrusion.

**Chapter 1**

# Magmatic enclaves record magma mixing at the Soufrière Hills volcano, Montserrat, Lesser Antilles

**Crystal P. Mann[1*], John Stix[1] and Thomas Christopher[2]**

**[1]Department of Earth and Planetary Sciences, McGill University, QC H3A 2A7, Canada**

**[2] Montserrat Volcano Observatory, Flemmings, Montserrat, W.I.**

**\* Corresponding author. E-Mail: crystal.mann@mail.mcgill.ca**

## Abstract

Mafic to intermediate composition enclaves are distributed pervasively throughout the andesitic block and ash flows erupted from the Soufrière Hills volcano from 1996 to 2006. The mafic enclaves are similar in composition and texture over time. This study documents the textural, chemical and petrological characteristics of these enclaves. The enclaves can be divided into three types based on their textures, mineralogy, and geochemistry. The Type 1 and Type 2 enclaves represent hybrid magmas as a result of mixing between a basaltic magma and the andesitic host. The Type 3 magma is not as well mixed and represents further differentiation of a basaltic liquid at shallower levels. The basaltic magma underwent significant fractionation of amphibole at deep crustal levels and during ascent through the crust. At crustal discontinuities some basaltic batches stall, undergoing further differentiation of plagioclase, while other batches intersect the active andesitic magma. This basaltic liquid directly intrudes the andesitic reservoir and mixes with the resident magma at a mixing horizon. A boundary layer develops a rigid framework of crystals and a bubble-rich layer at the top. The T1 enclaves are samples from this upper layer of the mixing horizon and form due to buoyancy as the basaltic magma vesiculates. The T2 enclaves are representative of slightly deeper portions of the boundary horizon, which is disrupted during subsequent intrusions of mafic magma.

**Introduction**

The presence of mafic enclaves in igneous rocks has long been documented in andesitic to rhyolitic lava domes (Bacon, 1986; Eichelberger, 1975), as well as in the plutonic record (Wiebe, 1974; Blundy and Sparks, 1992). Their presence has been attributed to the incorporation of solid country rock xenoliths (Chappell *et al.*, 1987), cumulate fragments derived from the crystalline rinds of upper crustal magma reservoirs (Arculus & Wills, 1980), hot mafic magma intruded and chilled as blobs in a cooler, more silicic host (Bacon, 1986; Costa and Singer, 2002), or the more mafic components of a stratified chamber incorporated into the more silicic host due to convective mixing (Mattson *et al.*, 1986). The textural characteristics of magmatic enclaves in volcanic rocks can distinguish a liquid state at the time of incorporation into the host reservoir (Bacon, 1986a; Eichelberger, 1980).

Injection of a more mafic magma into a silicic magma reservoir contributes mass, heat, volume and volatiles to the shallow reservoir, increasing pressure and causing disequilibrium within the magmatic system (Bachmann and Bergantz, 2003; Eichelberger, 1980; Huppert et al., 1982; Pallister et al., 1996; Huppert and Woods, 2002; Sparks and Marshall, 1986) and is commonly invoked as a triggering mechanism for volcanic eruptions (e.g. Sparks *et al.*, 1977; Eichelberger, 1980; Bacon, 1986; Clynne, 1999; Halama et al. 2006; Zellmer and Turner 2007). However, the extent to which the mafic magma and the more silicic magma mix is dependant upon their density, temperature, and viscosity contrasts (Sparks and Marshall, 1986) and thus the extent of mixing will be highly variable. Efficient mixing can form an andesitic magma (Kent et al., 2010; Schiano et al., 2010), while less efficient mixing can preserve evidence of the magmatic endmembers, such as crystals and mingling textures, thus providing clues as to the mixing relationships during and after intrusion.

Careful study of magmatic enclaves are used to infer both physical and chemical magma reservoir processes. The size and spatial distribution of mafic enclaves are used to suggest pre-eruptive stratification of the magma reservoir (Feeley et al., 2008; Turnbull et al., 2010). Morphological and textural changes of mafic enclaves can be used to distinguish between different enclave types and suggest the extent of mixing between the basalt and silicic endmembers (Browne et al., 2006). Thus determination of enclave compositions may provide important information into the evolution of the magma reservoir and the reservoir dynamics.

The Soufrière Hills volcano, Montserrat, is an ideal place to study mafic enclaves, as the eruptive products are rich in these enclaves. The contemporaneous existence of basaltic to basaltic andesite enclaves at the Soufrière Hills volcano testify to the importance of mafic magma in the andesitic system. Outstanding issues at Soufrière Hills volcano are the causes of the renewed activity and the longevity of the eruption, as well as the general underlying petrologic processes operating at depth (Barclay et al., (2010); Christopher et al., (2010); Devine et al (1998, 2003); Edmonds et al. (2001, 2010); Genareau and Clarke (2010)). However, the interpretation of mafic enclaves is not straightforward; for example, are mafic enclaves representative of a magma parental to the magmatic system, or are they unrelated? Do the enclaves represent more than one mafic recharge event? In this study, we use field observation, geochemistry and mineralogy of basaltic to basaltic-andesite enclaves to infer magma chamber processes during and after intrusion of mafic magma. We first divide the enclaves into 3 distinct types (T1, T2 and T3). Secondly, we demonstrate that the enclaves are hybrid magmas between a more mafic magma and silicic endmember and quantify the extent of mixing. We suggest that formation of the T1 and T2 enclaves occurred within the magma reservoir at the contact between the mafic and more silicic endmembers. The T3 enclave is distinguished from the T1 and T2

enclave by geochemistry, which indicates additional fractionation of plagioclase from basalt at shallow levels. We end with a model of petrogenesis of the mafic magma from intrusion into the andesitic reservoir to enclave formation and link our model of enclave formation into the current models of the plumbing system at the Soufrière Hills volcano. We contribute the first complete description of the mafic enclaves observed at the Soufrière Hills volcano. The petrogenesis of the of the different enclaves provides criteria which can be used to trace the evolution of the mafic enclaves, thus providing powerful insights into the evolution of the magmatic system over time.

**Background**

The Lesser Antilles intra-oceanic island arc is a 750 km long chain of volcanic islands formed as a result of the westward subduction of the Atlantic oceanic lithosphere beneath the Caribbean plate (Fig. 1). The islands which comprise the arc display large variations in physical and chemical characteristics, including magma compositions which range from low-K tholeiites through calc-alkaline basalts to alkali basalts and andesite (Brown *et al.,* 1977). The island of Montserrat, located in the northward section of the chain, comprises three volcanic massifs, the youngest of which is the South Soufrière Hills- Soufrière Hills complex, located in the southernmost part of the island (Fig. 1).

The Soufrière Hills volcano (~170 ka) is a composite of at least five andesitic lava domes, (Harford *et al.*, 2002). The Soufrière Hills volcano began erupting in July 1995 after approximately 350 years of quiescence. Lava extrusion started in November 1995, and the eruption continues at the time of writing (April 2010). The recent (>1995) eruptive history is divided into multiple phases of dome growth with a range of 1.5 to ~4 years in duration. The dome growth is commonly followed by a large dome collapse and a subsequent pause in dome growth up to ~ two years. New growth of the dome defines the beginning of the subsequent phase. The active vent is located in a horseshoe shaped crater which is open to the east (Fig. 1).

**Methodology**
*Field sampling*
Selected samples are from a variety of collections, including the University of Bristol, the

Montserrat Volcano Observatory (MVO) and samples collected by us during two summer field

campaigns in 2005 and 2006. Due to the ongoing eruption, it was impossible to sample the dome

directly. Therefore, the dome rock and associated enclaves were collected from well documented

block and ash flows and other primary dome collapse material. For this study, we chose a subset

of mafic enclaves sampled from the 17 September 1996, 25 June 1997, 21-29 September 2002, 8

December 2002, and 30 June 2006 block and ash flows. The field description is based on an

evaluation of 25 boulders, ranging in volume from 1 $m^3$ to 25 $m^3$, and the general appearance,

shape, grain size and contact relationships of ~ 240 enclaves within the andesite from the 8

December 2002 block and ash flow deposited in White's Ghaut (Fig. 1).


*X-ray fluorescence analyses (XRF)*
Major and trace element analyses were performed using X-ray fluorescence (XRF) spectrometry.

Samples were crushed in a steel jaw crusher to produce rock fragments <1 cm and powdered in

an alumina shatterbox. X-ray fluorescence of whole rock powders was carried out with a Philips

PW2440 4 kW automated XRF spectrometer system at the Geochemical Laboratories, McGill

University, Canada. Major elements (Si, Ti, Al, Fe, Mn, Mg, Ca, Na, K, P) and trace elements

(Ba, Cr, Ni and V) were analyzed as 32-mm diameter fused beads while trace elements (Ga, Nb,

Pb, Rb, Sr, Zr) were analyzed as 40-mm diameter pressed powder pellets. Analysis of

international standard reference materials (SRM) (Govindaraju, 1994) indicates that the overall

precision (i.e., sample preparation and instrument analysis) is within 0.5% relative, and the

instrumental precision is within 0.3% relative. Accuracy for $SiO_2$ is better than 0.5% and for all

other major elements better than 1%. For trace elements, accuracy is better than 5%. We

analyzed standards UTR-2 and SR7 as internal checks as well as MVO107, previously analyzed by the University of Bristol, to double check precision and accuracy across different labs. All results exhibit good reproducibility (Supplemental Data Table1)

*Inductively coupled plasma mass spectrometry (ICP- MS)*
Analyses of the rare earth elements (REE), Th, U and Y were performed on solutions using a PerkinElmer/SciEx Elan 6100 DRCplus ICP-MS. Samples (0.4 g, corrected for loss-on-ignition) were fused using a lithium metaborate mixture, then dissolved into nitric acid and diluted. Standards and calibration solutions were prepared from fusion blanks, and rhenium was used as an internal standard. Oxide corrections on the middle and heavy REE were made off-line using oxide production rates determined daily from single REE standard solutions. Rock-sample detection limits (based on three times the background standard deviation) are 10 ppb for Y and La through Pr, and 5 ppb for Nd through Lu. A set of three internal laboratory reference materials were fused and run with each batch of samples to evaluate long-term precision. Precision was also evaluated through repeat measurements of samples, including repeat fusions and dilution; it is better than 3% RSD in all cases. Accuracy was evaluated using a series of six standard reference materials that span the sample concentration range, prepared using the same procedure as the samples. Our determinations agree with the accepted values for these SRM with discrepancies of less than 5%.

*Electron microprobe analysis*
Major element compositions of mineral phases and matrix glasses from the enclaves were analyzed at McGill University using a JEOL JXA-8900 electron microprobe equipped with five wavelength dispersive spectrometers and one energy dispersive spectrometer. For all mineral phases, we used an accelerating voltage of 15 keV, a beam current of 20 nA and a beam diameter

of 2-5 μm and calibrated our analyses with a set of natural and synthetic mineral standards. For

the matrix glass analyses we used an accelerating voltage of 15 kV, a beam current of 15 nA and

a beam diameter of 10 μm. For glass, Si, Al, Fe, Na and K were calibrated with an anhydrous

peralkaline rhyolitic glass standard (UTR-2) while Mg, Ca, P, and Ti were calibrated with a

basaltic glass (BMAK). Mn was calibrated with spessartine, Ba with Ba-Orth, Cl with KN9

(3100 ppm Cl) and S with a pyrrhotite standard (#507: 38.25 wt. % S). Analytical techniques

were optimized to minimize loss of sodium while ensuring good precision.  Elements were

analyzed in the same order and for the same length of time for both standards and unknowns, and

the ZAF correction model was applied. For analysis of chlorine and sulfur, we increased the

count times to improve statistical precision. The counting times for S and Cl (100 seconds)

reduced detection limits to ~140 ppm for S and ~70 ppm for Cl. The matrix glass was analyzed

over multiple sessions; therefore we report the standard data as a pooled average and a pooled

standard deviation (Supplemental data Table 2). For major elements, precision for Si and Mg is

better than 0.6 %, Al, Ca and K better than 1 %, and Fe and Na better than 3 %.  For trace

elements, precision for Ti is better than 1.6 %, P and Cl better than 3.1 %, Mn better than 8.5 %,

and S better than 7.9 %. Ba is better than 2 % based on repeat measurements of Ba in Ba-Orth

(Supplemental data Table 2).


**Results**
The mafic enclaves are separated into three enclave types based on field observation,

geochemistry and mineralogy. We first, describe differences in enclave textures between the T1

and T2 enclave from field observations. Secondly, we report similar whole-rock geochemistry

between the T1 and T2 enclaves and more evolved geochemistry of the T3 enclave. Lastly, we

report the differences in mineralogy between the T1, T2 and T3 enclaves. A summary of the field

textures and geochemistry is presented in Table 1, the whole-rock geochemistry is presented in

Table 2 and a summary of mineral compositions and mineral textures are presented in Table 3.

*Field Observations*

In general, the enclaves are ellipsoidal with glassy margins to blocky with crenulate margins and

comprise ~5 vol. % of the boulder (Fig. 2a; Table 1). It is common to see all three types of

enclaves in the same boulder, and many of the small inclusions are proximal to the larger ones

(Fig. 2b).

The Type 1 (T1) enclaves are ellipsoidal in shape, range from 1 – 15 cm in diameter and

are rimmed by a glassy rind in contact with the andesite (Fig. 2c). The void space decreases from

the core of the enclave to its rim (Fig. 2d). Some T1 enclaves are observed with partially slightly

angular margins.

The Type 2 enclaves (T2) are blocky in shape, range from 1 – 28 cm (measuring the

longest side) and are defined by a crenulate or scalloped margins in contact with the andesite

(Fig. 3a). At the contact between the T2 enclaves and the andesite, we commonly observe a

higher concentration of amphibole on the enclave side of the contact and a higher plagioclase

phenocryst-rich layer on the andesite side of the contact (Fig. 3b). Mafic fingers at the edge of

the enclaves intrude into the andesite (Fig. 3c). It is common to observe T2 enclaves pulled apart

or fractured although still intact (Fig. 3a). Some partially fractured T2 enclaves are filled with an

exceptionally plagioclase-rich andesite (Fig. 2b), and we observe higher concentration zones of

plagioclase crystals, typically on the outermost edges of the larger T2 enclaves, which

correspond to a color change from black to dark gray (Fig. 2b).

The Type 3 enclaves (T3) are blocky in shape with crenulate margins in contact with the

andesite. They range in size from ~1- 15 cm and are closer in color to the andesite than the T1 or

T2 enclave. They are easily mistaken for the T2 enclaves in the field.

Other studies describe similar enclaves to what we observe. Murphy et al. (2000)

described mafic enclaves erupted between December 1995 and January 1998 as ellipsoidal with

glassy margins to angular with crenulate margins. Murphy et al. (2000) suggest that the

ellipsoidal shape with glassy margins are dominant and the enclaves represent ~ 1 % of the rock.

Based on observations from the 9 December 2002 block and ash flow, we observe the same

enclave shapes and enclave margins as Murphy et al (2000), but observe a dominance of blocky

enclaves with crenulate margins  and a general increase of enclaves to ~ 5 % hosted by the

andesite. Barclay et al. (2010) have similar field observations to us and Murphy et al (2000) from

block and ash flows in 2007 and suggest that the percentage of enclaves observed in the andesite

have increased to ~7 %. Comparing this study to Murphy et al. (2000) and Barclay et al., (2010)

which span the eruption from 1995 to 2007, the Soufrière Hills volcano continues to erupt

enclave types 1 and 2 as described in this study with the erupted percentage increasing over time.

*Whole-rock major and trace elements*

Major and trace element data were compiled from our new analyses and the literature (Harford *et al.*, 2002; Murphy *et al.*, 2000; Zellmer *et al.*, 2003; Barclay *et al.*, 2010) to represent a suite of

rocks from 1996 to 2007. Representative data from this study are given in Table 2. The mafic

enclaves are high alumina basalt to basaltic-andesites (Fig. 4a-b), ranging from 49.8 – 56 wt. %

$SiO_2$ (Le Bas *et al.*, 1986). In general, whole-rock Ti, Al, Fe, Mg, Ca, and V concentrations of the

enclaves decrease with increasing silica content, whereas Na, K, Ba, Zr and Rb increase (Fig. 4a-

d, Fig. 5a). Zr is lower for the T3 enclaves relative to T1 and T2 (Fig. 5a). Ni demonstrates an

overall decrease with increasing silica content, although the T1 enclaves record the highest Ni

contents, while T3 has the lowest Ni concentrations (Fig. 5b). T1 and T2 appear to be constant in

Y at ~ 20 ppm with increasing silica, but T3 clusters at significantly higher levels between 27

and 40 ppm (Fig. 5c). Finally, Sr appears to be constant in all three types of enclaves, with

slightly higher concentrations in the T3 enclave, for increasing silica contents (Fig. 5d).

If we first consider just our sample set, we observe no systematic changes (i.e. increasing

silica contents with time) in bulk composition of the mafic enclaves or andesite since 1996. The

T1 and T2 enclaves from 1996 to 2002 overlap in composition and texture (Fig. 4a-d; Fig. 5a-d).

Our sample set shows good comparison and overlap with compositions reported by Murphy et al.

(2000). Whole-rock analyses reported by Barclay et al, (2010) are higher in major element

compositions such as MgO, $Al_2O_3$ and $K_2O$ at the same $SiO_2$. For example, at ~ 51 wt. % $SiO_2$

we report ~ 5 wt. % MgO and Barclay et al. (2010) report ~ 5.5 MgO (100% anhydrous).

*Rare earth elements*

Rare earth elements (REE) are shown in Table 2 and plotted in Fig. 6a-c. Chondrite-normalized

REE patterns demonstrate a clear enrichment of light rare earth elements (LREE; La to Nd)

relative to the middle rare earth elements (MREE; Sm to Ho) and heavy rare earth elements

(HREE; Er to Lu), with slight enrichment of HREE relative to MREE forming a trough-shaped

profile. All three types of enclaves, as well as the andesite, display this similar trough-shaped

profile, but the T3 enclaves are enriched in REE with more pronounced negative Eu anomalies

(average $[Eu/Eu^*]_{CN} = 0.85$) relative to the T1 and T2 enclaves, which have average $[Eu/Eu^*]_{CN}$

values of 0.98 and average 0.96 respectively.

*Mineralogy*

We now describe the mineral compositions, mineral textures and groundmass characteristics

such as glass composition and void space in the T1, T2 and T3 enclaves (Table 3). The rationale

for the size divisions among phenocrysts at > 450 μm (longest dimension), microphenocrysts at

450 – 100 μm and microlites at <100 μm is based on mineral textures observed in thin section. The division between phenocrysts and microphenocrysts is based on the smallest plagioclase crystal which demonstrates the same sieve patterns as we observe in the T2 plagioclase. The division between microphenocrysts and microlites is based on the smallest crystal we could distinguish with the microscope.

T1 enclaves are porphyritic with 0 – 15 vol. % phenocrysts, 45 – 65 vol. % microphenocrysts, up to 10 vol. % microlites, < 5 vol. % glass and 10 – 15 vol. % void space, The phenocrysts include plagioclase, amphibole, pyroxene and quartz, all typically mantled by overgrowth textures. The crystal framework is dominated by subhedral to euhedral, tabular microphenocrysts of plagioclase with lesser amounts of needlelike pyroxene. Microlites comprise a much smaller population made of plagioclase and pyroxene. The groundmass texture is diktytaxitic with void space (40 μm to ~ 900 μm in length) ranging in shape from irregular spheres to odd angular spaces, with microphenocrysts protruding into the void space. The glass is both transparent and brown in color, filling void space and clinging to crystal edges. The brown glass sometimes has radiating needles of feldspar.

T2 enclaves are porphyritic in texture consisting of 0 – 15 vol. % phenocrysts, 50 – 70 vol. % microphenocrysts, up to 10 vol. % microlites, < 5 vol. % glass and 5 - 10 vol. % void space. The porphyritic texture is characterized by a low percentage of plagioclase and acicular amphibole phenocrysts in a finer-grained groundmass. Occasionally we observe minor pyroxene phenocrysts with reaction rims but do not observe quartz. The fine-grained groundmass comprises subhedral to euhedral, tabular to blocky plagioclase microphenocrysts and needle-shaped to prismatic amphibole microphenocrysts. Microlites include plagioclase and amphibole with occasional pyroxene. The groundmass texture is diktytaxitic with void space ~40 μm to ~

400 μm in length ranging in shape from irregular spheres to more angular spaces. In some cases the microphenocrysts protrude into the void space. Glass is observed as clear to brown in color, sometimes with radiating needles and observed as patches and clinging to crystals.

T3 enclaves are porphyritic consisting of 5 – 15 % phenocrysts, 60 – 70 % microphenocrysts, < 10 % microlites, < 5 % glass and < 10 % void space. The margins are crenulate. The porphyritic texture is characterized by plagioclase and amphibole phenocrysts in a finer-grained groundmass. The microphenocrysts are plagioclase and amphibole; in most thin sections amphibole crystals are almost completely replaced by pyroxene and Fe-Ti oxides. The groundmass has a diktytaxitic texture with void space (~40 um to ~450 um in length) ranging in shape from irregular spheres to angular spaces. In some cases the microphenocrysts protrude into the void spaces. The glass is brown and sometimes with radiating needles of feldspar.

*Plagioclase* - Plagioclase is the most abundant mineral phase in all mafic enclaves, ranging in size from ~ 3 mm to < 100 um. Plagioclase occurs as single phenocrysts, in clusters with multiple plagioclase crystals, as microphenocrysts, microlites, and inclusions within amphibole phenocrysts and as intergrowths with pyroxene and magnetite, formed by the breakdown of amphibole. We identify four distinct plagioclase groups on the basis of mineral texture and composition (Table 4).

The first group of plagioclase crystals are observed in T1 enclaves. They are large (~0.7 – 3.0 mm), subhedral to anhedral, reversely zoned crystals with relatively sodic cores ($An_{47-67}$) and more calcic rims ($An_{71-84}$) (Fig. 7a, Fig. 8). Many cores have small-scale oscillatory zoning or patches up to $An_{68}$. The cores and rims are separated by a sieve-textured zone. Boundaries between the sodic cores and sieve-textured regions are rounded to irregular in shape; in many cases they truncate the small-scale oscillatory zones of the sodic cores. The rims range up to

~100 um thick, and many remain calcic to the crystal edge; occasionally we observe a more sodic rim ($An_{62-72}$).

The second group of plagioclase crystals observed in the T2 enclaves are large (~ 0.65 – 1 mm), subhedral to anhedral and normally zoned (Fig. 9a). Crystals have highly calcic ($An_{75-87}$) and extensively sieved cores with slightly less calcic rims ($An_{61-81}$) up to ~100 μm thick (Fig. 8; Fig. 9a). The sieve texture is a network of highly calcic plagioclase with small pockets (< 20 μm) of glass.

The third group of plagioclase crystals comprise medium to small crystals (< 650 μm) and are observed as part of the framework mineral assemblage in both the T1 and T2 enclaves. These microphenocrysts (650 to 100 μm) are tabular (Fig. 7a) with overlapping core ($An_{69-79}$) and rim compositions ($An_{70-83}$). Microlites (<100 μm) appear blocky to needlelike in shape with compositions of $An_{76-82}$. Individual microlites generally have a narrow compositional range of ± 7 An. The group 3 plagioclases overlap in An content with the rim compositions of plagioclase from groups 1 and 2 (Fig. 8).

The fourth group of plagioclase crystals is observed in the T3 enclaves and comprises microphenocrysts and phenocrysts up to ~1.5 mm (Fig. 9c). These crystals are subhedral to euhedral in shape and normally zoned with a range of core compositions from sodic to more calcic ($An_{49-90}$) with more sodic rims ($An_{49-62}$) (Fig. 8). There is no sieved zone present between the calcic core and more sodic rim. This plagioclase group is unique in its similarity to plagioclase phenocrysts observed in the andesite; rim compositions are similar to the andesite phenocryst core compositions while compositional zoning resembles plagioclase inclusion compositions hosted by amphibole in the andesite (Murphy et al., 2000; Electronic Appendix 3).

In summary, the three types of enclaves host different plagioclase types. The first group, which is reversely zoned with the core separated from the rim by a sieve texture, is found in the T1 enclaves. The second group, normally zoned with a highly calcic core which is pervasively sieved and a slightly less calcic rim, is found in the T2 enclaves. We occasionally observe both types of phenocrysts in the same thin section. The third group of calcic microphenocrysts and microlites is similar in composition to the rim compositions of the group 1 and 2 phenocrysts, and both are found in the T1 and T2 enclaves. The fourth group, observed in the T3 enclaves, comprises phenocrysts to microphenocrysts which are made up of a range of core compositions from calcic to sodic and rimmed by a much more sodic composition.

*Amphibole* - Amphibole is divided into three groups based on composition and texture. Amphibole is the second most abundant crystal phase in the mafic enclaves, ranging in size from ~ 6 mm to < 100 μm in length. Amphibole is present as single crystals, microphenocrysts, microlites and is host to inclusions of pyroxene, plagioclase and Fe-Ti oxides. The amphibole is commonly hosted by plagioclase. All amphiboles are calcic in the fields of magnesiohornblende and tschermakite (Leake *et al.*, 1997) (Fig. 10; Table 5). In the T1 enclaves, phenocrysts are magnesiohornblende which are prismatic in shape, typically with an extensive overgrowth of pyroxene, plagioclase and Fe-Ti oxides (Fig. 7b). In the T2 enclaves, the amphibole is defined by tschermakite observed as phenocrysts, microphenocryts, microlites and inclusions. The phenocrysts and microphenocrysts are acicular in shape, while the microlites are more needlelike (Fig. 9b). In the T3 enclaves, the phenocrysts and microphenocrysts are magnesiohornblende, anhedral in shape with overgrowths of pyroxene needles (Fig. 9c). Tschermakite observed in the T2 enclaves is slightly lower in Mg# relative to tschermakite in the T1 enclaves (Fig. 10).

*Pyroxene* - Pyroxene occurs as phenocrysts up to ~1.4 mm, microphenocrysts, microlites and as a component in reaction rims observed on amphibole and quartz. Pyroxene compositional data are reported in Table 6 and plotted in Fig. 11. Phenocrysts are subhedral to anhedral in shape; when present, the crystals comprise 1-3 grains per thin section. The microphenocrysts are equant to tabular and subhedral to anhedral in shape. In the T1 enclaves the phenocryst cores are enstatite ($En_{57}$ $Wo_3$), while the rims are more calcic with compositions of augite to diopside ($En_{87-85}$ $Wo_{45-43}$) (Fig. 7c). The microlites and microphenocrysts are enstatite ($En_{77-63}$ $Wo_{4-3}$) and range from augite to diopside ($En_{75}$ $Wo_{26}$ to $En_{87}$ $Wo_{48}$). Both phenocryst cores and rims in the T2 enclaves are enstatite ($En_{62-57}$ $Wo_{3-1}$), but the microphenocrysts are largely enstatite ($En_{67-57}$ $Wo_{5-2}$) to pigeonite ($En_{67-60}$ $Wo_{16-5}$) with a minor amount of augite ($En_{75-62}$ $Wo_{52-39}$). Phenocryst cores from the T3 enclaves are enstatite ($En_{63-61}$ $Wo_{3-2}$) with augite rims ($En_{82-78}$ $Wo_{41-30}$). The microphenocrysts are enstatite ($En_{69-61}$ $Wo_{3-2}$) and augite ($En_{82-81}$ $Wo_{40-41}$).

In summary, phenocrystic pyroxene in the T1 enclaves is orthopyroxene rimmed by clinopyroxene with microphenocrysts and microlites of both. The cores and rims of the T2 phenocrystic pyroxene are enstatite with slightly more Fe rich rims, while the microphenocrysts and microlites range from enstatite to augite and dominated by pigeonite. All crystals in the T2 enclaves are Fe rich relative to those observed in the T1 and T3 enclaves. The T3 enclaves comprise phenocrysts of orthopyroxene with clinopyroxene rims and orthopyroxene microphenocrysts. Orthopyroxene compositions in the T1 and the T2 enclaves are similar.

*Fe-Ti oxides* - Fe-Ti compositional data are reported in Table 7 and Fig. 12. Titanomagnetite is the dominant Fe-Ti oxide, appearing as phenocrysts, microphenocrysts, microlites, inclusions in plagioclase and as a component in amphibole breakdown products in all

enclave types. The phenocrysts, microphenocrysts and microlites appear blocky, subhedral to euhedral in shape occurring as individual grains and as clusters. The microphenocrysts and microlites are observed as both individual grains and as inclusions in plagioclase phenocrysts. We do not observe magnetite grains with ilmenite exsolution, but a few ilmenite microphenocrysts are observed in the T2 and T3 enclaves.

*Quartz* - We observe quartz in the T1 enclaves only. When present, quartz occurs as embayed individual crystals ~ 1 mm in size, typically with only one or two grains per thin section. All crystals have reaction rims of clinopyroxene, and many are host to rhyolitic melt inclusions and Fe-Ti oxides (Fig. 7d).

*Matrix glass* - The enclave matrix glasses are rhyolitic with 72.8 - 77.5 wt. % $SiO_2$ (normalized to 100 wt. % anhydrous; Table 8). Overall, Ti, Al, Fe, Ca, Na and Mg decrease with increasing silica content while K increases. While these trends are expected for an evolved liquid, we make two important observations. 1) Andesite matrix glass overlaps with enclave glass compositions (Fig. 13a, b). 2) Glass compositions on each side of the contact between the andesite and T1 enclaves are different in composition (Fig. 14a, b).

The glass comprises two groups: a Na + Ca-rich glass and a K + Fe-rich glass. In the Na + Ca rich we also observe radiating needles of quartz and feldspar. Due to the absence of a potassic phase in the observed crystallizing assemblage, we consider the high K + Fe glass to be a true glass and the high Ca + Na glass to be devitrified. To ensure that we are only considering true glass in our interpretation, we eliminated glass which we observe to be devitrified and with K + Fe < 2 wt. % (Electronic Appendix 4).

**Intensive parameters**
*Pressure and temperature estimates*

We estimate pressure and temperature of enclave formation based on mineral compositions of the microphenocrysts, which we assume to form in the hybrid magma. For the T1 enclaves, clinopyroxene/liquid geothermobarometry indicate a pressure range from 380 – 440 MPa and temperatures of 1086 – 1109°C (Putirka et al., 2003). Plagioclase - liquid thermometry of plagioclase rims in equilibrium with the liquid range from 980 – 1100°C (400 MPa). For the T2 enclave, we use the pressure estimates for the T1 enclaves and pigeonite thermometry to estimate temperatures of formation at 1098 ± 20°C (400 MPa). Plagioclase-liquid thermometry for the T2 enclaves show temperatures of 979-1026°C (400 MPa) (Putirka, 2008). For the T3 enclave we use one magnetite/ilmenite microphenocryst pair with mineral recalculation done according to Carmichael (1967) and temperatures calculated using ILMAT (Lepage, 2003) for an estimate of 897 ± 16°C. Hence T1 and T2 enclaves have similar temperatures, while the T3 enclaves are the coolest and similar in temperature to the estimates for the andesite magma reservoir (Barclay *et al.*, 1998; Rutherford & Devine, 2003)

The range of enclave temperatures calculated for this study demonstrates consistency with enclave temperatures calculated by previous authors. Murphy et al. (2000) used QUILF to determine crystallization of orthopyroxene phenocryst cores at ~1020 – 1060°C (Andersen *et al.*, 1993) . Humphries et al. (2008) used a two-pyroxene geothermometer on microphenocrysts to determine temperatures of 1,110°C and the hornblende-plagioclase geothermometer of to determine a temperature of ~ 878 ± 40 °C (Holland & Blundy, 1994).

**Discussion**

*Origin of crystals*
In the T1 enclaves, plagioclase is reversely zoned, orthopyroxene and quartz have overgrowth rims of clinopyroxene and amphibole is commonly observed with reaction rims (Fig. 7a-d). The

quartz and the orthopyroxene are unlikely to be phenocrysts in the mafic magma, as their

survival is ascribed to the presence of the clinopyroxene rims. The reversely zoned plagioclase

crystals suggest their last residence in a more mafic composition. Clearly the quartz,

orthopyroxene and plagioclase are xenocrysts in the T1 enclaves. The amphibole is more

difficult to interpret, as the observed disequilibrium rims are similar to the dehydration rims

observed on amphibole in the andesite (Buckley *et al.*, 2006; Devine *et al.*, 1998; Rutherford &

Hill, 1993). Compositionally, the amphibole observed in the T1 enclaves is similar to that

observed in the andesite (Fig. 10). In the T2 enclaves the plagioclase phenocrysts are normally

zoned, and the amphibole phenocrysts are tschermakite in composition, similar to the

microphenocrysts and microlites (Fig. 9a; Fig. 10). We observe orthopyroxene sometimes with

overgrowths of clinopyroxene. We suggest that the plagioclase and amphibole are phenocrysts

and some orthopyroxene may be xenocrystic.

*Magma evolution*
In largely molten crustal reservoirs, magmas typically differentiate by at least two well

established processes: 1) crystal fractionation and 2) magma mixing. In this section we establish

that the T1 and T2 enclaves are hybrid compositions between a more mafic endmember and the

andesite. We suggest that crystal fractionation of mafic magma may take place during intrusion

but is secondary to magma mixing.

    *Magma Mixing* - The linear trends on Harker variation diagrams suggest that mixing

could play a role in SHV magma petrogenesis (Fig. 4a-d; Fig. 5a). Using the least-squares mass

balance calculation method of Bryan et al (1969) and the mixing equations from Langmuir et al.

(1977), we calculate the major element best fit compositions of datapoints intermediate between

the basaltic magma and andesitic magma endmembers.

For the purpose of the magma mixing modeling, we use the most mafic sample CM65 as representative of the mafic magma endmember and CM25 as the most evolved endmember and mix them to reproduce the T1 and T2 enclave series (Table 9). To evaluate a good solution, we report both the residual sum of squares ($\Sigma r^2$) and the major element analytical error.

We successfully model the major elements of the T1 enclaves with various degrees of mixing (Table 9). We show a good fit of the chemical composition for the most evolved T1 enclave (CM28 with 54.77 wt. % $SiO_2$) by mixing ~46 % basalt and ~53 % andesite for an observed fit of 54.73 wt. % $SiO_2$ and a good fit for a less evolved enclave (CM1448 with 52.83 wt. % $SiO_2$) using ~70 % basalt and ~30% andesite for a calculated fit of 52.63 wt. % $SiO_2$.

The T2 enclaves have $\Sigma r^2$ values ranging from 0.09 – 0.52. The best solution suggests mixing of 58 % basalt and 42 % andesite to reproduce a hybrid with ~ 53.67 wt. % $SiO_2$, which fits well with an observed $SiO_2$ value of 53.73 wt. %. Solutions with a higher $\Sigma r^2$ value (i.e. $\Sigma r^2$ 0.52) predicts lower FeO and $K_2O$ and higher MgO and $Na_2O$ than observed. We suggest that the discrepancy between the predicted and the actual hybrid compositions could be do to some crystal fractionation at the time of intrusion. For example, as hot mafic magma interacts and mixes with cooler andesitic magma, it is chilled hence crystallizes. Crystallization of Tschermakite would lower the MgO contents and the crystallization of plagioclase could lower the $Na_2O$ contents. As a further test of magma mixing we apply the mixing equations to the trace element and REE data. We use La and Ba, as they are highly incompatible in this system and both the T1 and T2 mixing trends demonstrate very good reproducibility and consistency with the major element mixing percentages (Fig. 15 a, b)

*Crystal Fractionation* - Magma mixing explains the trends we observe in the major element and trace elment models, but we model crystal fractionation to explore if the hybrid

magma can fractionate to the andesite. Major element variations are modeled using the Igpet petrologic mixing program (Carr, 1990). The fractional crystallization equation is based on the least-squares mass balance which subtracts the compositions of the liquidus mineral phases from the least evolved sample to derive a residual liquid that is consistent with the composition of the most evolved sample (Bryan et al., 1969). The Σr2 should be <0.2 for an acceptable solution.

To test the possibility of the hybrid magma fractionating to andesite, we model magma evolution in two steps: basalt to basaltic andesite, and basaltic andesite to andesite. The bulk distribution coefficients from the estimated mineral assemblages and partition coefficients from the literature based on similar compositions are reported in Table 10. In the T1 and T2 enclaves, phenocrysts comprise < 15 % of the thin section as they are dominated by microphenocrysts. When present, orthopyroxene comprises one or two phenocrysts per thin section; based on this observation, we model the first step with a combination of plagioclase, amphibole, magnetite ± orthopyroxene. All combinations including orthopyroxene indicate unrealistic phenocryst phase proportions, hence we exclude orthopyroxene from further discussion. An $\Sigma r^2$ with a range of 0.56 – 0.86 indicates crystal fractionation is not a good explanation for differentiation of the basalt to basaltic-andesite (Table 11). Conversely, an $\Sigma r^2$ with a range of 0.17 – 0.21 may indicate that the more evolved enclaves could fractionate from basaltic andesite to andesite. The hybrid would need to fractionate ~ 50% plagioclase, ~ 39 % amphibole, and ~11 % magnetite for a total crystallinity of ~ 21%. Murphy et al. (2000) report 30-35% plagioclase, 6-10% amphibole, 1-5% orthopyroxene, 2-4% magnetite and < 0.5 % quartz in the andesite for a total crystallinity of ~ 50 %.

In an effort to further quantify our results, we use the Rayleigh fractionation equation (Rollinson, 1993) to solve for concentrations of trace elements and REE in the remaining liquid

of the fractionating assemblage. We model both types of enclaves using the same whole rock

compositions. In the first step, the most mafic sample (CM65) is $C_O$ and a more evolved enclave

(MVO107 and CM28) is $C_L$. We are unable to find a reasonable crystallizing assemblage which

works for trace elements; furthermore, we are unable to model crystal fractionation from basaltic

andesite to andesite using the phenocryst proportions from the best fit of major elements.

Based on this modeling, we conclude that the compositional variations that we observe in

the T1 and T2 enclaves are principally the result of magma mixing with the andesite. Evidence

of magma mixing can be seen from field observations, geochemistry and mineralogy of the

samples. In the field, basaltic to basaltic-andesite enclaves are observed in the andesite. The large

crystals in the T1 enclaves are xenocrystic to the enclave magma as indicated by the reverse

zoning of plagioclase, clinopyroxene rims on orthopyroxene, the low Mg amphiboles and the

existence of quartz with clinopyroxene rims. In the T1 enclaves xenocrysts dominate, whereas in

the T2 enclaves phenocrysts dominate and xenocrysts are rare. Nevertheless, we acknowledge

that the evolution of the enclaves is complex, and magma mixing may be coupled to crystal

fractionation in some cases (i.e. variable $\Sigma r^2$ values). Hence coupled magma mixing – crystal

fractionation may be a viable scenario to explain some of the compositional range for T1 and T2

enclaves.

The variation of La/Yb and Dy/Yb versus $SiO_2$ wt. % (Fig. 16) and the pronounced

trough-shaped REE profile (Fig. 6a-c) argue strongly for amphibole as an important phase in the

differentiation of mafic magma prior to mixing (Davidson et al., 2007). In general the T1 and T2

enclaves have small to negligible Eu anomalies, which indicate minor fractionation of

plagioclase. The strong amphibole signature coupled with the absence of olivine and

clinopyroxene may suggest that an appreciable amount of amphibole crystallization has already

occurred at mid to deep crustal levels by the time the enclave magma reaches shallow crustal levels (Barclay & Carmichael, 2004; Davidson *et al.*, 2007)

The T3 enclaves are distinct from the T1 and T2 enclaves. They are more enriched in REE than the T1 and T2 enclaves and more enriched then the andesite (Fig. 6c). Hence they cannot be mixtures of basalt and andesite. They have generally parallel MREE and HREE trough shaped patterns, and a pronounced negative Eu anomaly. The variably enriched REE patterns and negative Eu anomalies argue for significant amounts of plagioclase involvement most likely at shallow crustal levels, while the trough-shaped REE patterns suggest prior crystallization of amphibole at deeper levels. The shallow crystallization of the T3 enclave is supported by our relatively low estimated temperatures of $897 \pm 16°C$. The normally zoned plagioclase with highly calcic cores suggests that not much mixing took place after intrusion and the similar temperatures would suggest that the T3 magma intruded more as a dike, with a relatively high viscosity, preserving a more angular shape.

**Mixing and crystallization predate enclave formation**

The T1 and T2 enclave magmas are a hybrid between an intruding mafic magma and the andesite. We suggest that mixing of the mafic magma and andesite takes place after intrusion and before enclave formation, at a mixing layer between the two endmembers. Mixing between two magmas with different compositions will depend on density, temperature, and viscosity contrasts between them (Sparks & Marshall, 1986). Here the intruding mafic endmember is a plagioclase bearing, water-rich high aluminium basalt at ~ 1100°C, while the andesitic magma is at a temperature of ~ 850°C (Murphy *et al.*, 2000). To mix these two magmas efficiently requires similar densities and viscosities which can be achieved by fractional crystallization or closed system crystallization of the more mafic magma, thereby lowering its temperature and driving

volatile exsolution, while at the same time locally heating the andesite (Huppert *et al.*, 1982;Sparks & Marshall, 1986). The groundmass plagioclase textures and crystal morphologies observed in the enclaves (Figs. 7a, 9b) are a function of the degree of undercooling between the replenishing magma and the resident magma (Bacon, 1986;Coombs *et al.*, 2003;Eichelberger, 1980;Huppert *et al.*, 1982), the acicular textures representing higher degrees of undercooling and the tabular textures lower degrees of undercooling. As undercooling decreases, plagioclase crystals begin to impinge on each other to form a touching framework, increasing the rigidity of the enclave (Fig. 7b) (Martin *et al.*, 2006). Simultaneously, vesiculation driven by crystallization forms bubbles which rise through the crystal framework, towards the top of the mafic-andesitic interface, forming a foam horizon (Eichelberger, 1980).

**Boundary layer breakup and enclave formation**

Disruption of the boundary layer takes place when the bulk density of the boundary layer falls below that of the resident magma. The increase in bubbles at the top of the boundary horizon causes the uppermost portions to become sufficiently unstable to separate and rise into the reservoir as a series of foam blobs (Eichelberger, 1980). The similar crystal size from the center of the enclaves to the rims for both T1 and T2 enclaves suggests that they were mostly crystalline before separating from the boundary horizon, otherwise larger crystals would occur towards the center (Coombs *et al.*, 2003). The glassy rims of the T1 enclaves (Fig. 2c) can be explained by gas filter pressing (Sisson & Bacon, 1999). Residual liquid oversaturated in volatiles will exsolve from an increase in vapor pressure. Due to lack of space the liquid is pushed into previously formed void spaces towards the enclave margins (Bacon, 1986), decreasing the void space from the enclave's core to its rim (Fig. 2d). Glass compositions of certain enclaves are higher in $K_2O$, with slightly lower to similar $TiO_2$ contents compared to the

glass of the andesite (Fig. 14a), while other enclaves are lower in $K_2O$ with similar $TiO_2$ glass compositions relative to the andesite glass (Fig. 14b). Buckley et al. (2006) attribute the higher $K_2O$ in the andesite to the breakdown of amphibole, while Humphreys et al. (2010) attribute higher $K_2O$ in the andesite glass to diffusive exchange between the mafic liquid with the andesite liquid. The enclaves were rigid at the time of enclave formation, as can be seen by the similar crystal size from the core to rim and by broken crystals on the margins (Fig. 3f) (Coombs *et al.*, 2003; Martin *et al.*, 2006). The enclaves essentially evolved as closed systems after enclave formation with respect to the physical transfer of crystals and liquid. The higher $K_2O$ contents in the mafic enclaves may be explained by 1) a higher K content in the mafic source, 2) the degree of magma interaction at the mixing horizon, 3) the breakdown of amphibole in the mafic enclave (Fig. 7b), 4) diffusive processes, 5) extensive crystallization of the mafic enclave, or a combination of the above processes. We suggest that the variable $K_2O$ contents may be higher in the enclaves which have formed more recently, in which $K^+$ has had less time to diffuse and equilibrate with the surrounding andesite. Rounding of the enclaves is most likely to occur by loss of weakly bound crystals from the enclave margins through mechanical processes during ascent, which could account for the broken crystals we observe and the calcium rich microlites observed in the andesite (Humphreys *et al.*, 2008). The more angular margins of the T2 enclaves represent a slightly more rigid enclave. We observe these enclaves as partially to completely fractured, but coherent in the field (Fig. 3a) This fracturing may occur when mostly rigid, brittle material is disrupted during mafic overturn or when the rigid mixing horizon is broken up during subsequent recharge events.

**Model for evolution of the mafic magma and formation of the enclaves**

We propose that replenishment events at SHV are characterized by the intrusion of a hydrous, high-alumina, plagioclase bearing basaltic magma into the base of a an andesitic magma chamber (Fig. 17) (Snyder & Tait, 1995; Wiebe, 1994). Upon ascent from the mantle wedge the basalt undergoes differentiation, fractionating amphibole at mid to deep crustal levels (Barclay & Carmichael, 2004; Davidson *et al.*, 2007). Upon intrusion into the andesitic reservoir, the basalt cools against portions of the andesite and begins to crystallize as the andesite heats. When the densities and viscosities of the two magmas become similar, they mix creating a hybrid magma (Sparks & Marshall, 1986). This hybrid continues to crystallize and exsolve bubbles. The bubbles rise to the top of the mixing horizon creating a buoyant upper layer (Eichelberger, 1980;Huppert *et al.*, 1982). Eventually this layer separates from the mixing horizon forming the T1 enclaves. In the last stages of crystallization, the liquid is pushed to open pore space as the last volatiles are exsolved (Bacon, 1986;Sisson & Bacon, 1999), creating the glassy rims. The T2 enclaves are formed when the mixing horizon undergoes overturn. They either are segregated from the mixing zone by reaching buoyancy where they can rise into the overlying magma or are mobilized due to another mafic intrusion. The T3 enclaves intrude the andesitic reservoir from a shallow chamber. They are similar in temperature and density, therefore chemical mixing is limited, but we do observe transfer of crystals.

**Conclusions**

1) The mafic enclaves are similar in composition and texture over time from 1996 to 2006.

2) The mafic enclaves are essentially hybrid compositions of a high Al, water saturated basaltic endmember and an andesite which have mixed prior to enclave formation.

3) The mafic enclaves can be divided into three distinct types (T1, T2 and T3) based on their enclave texture, mineralogy, mineral textures, and geochemistry.

4) All enclaves have undergone significant amphibole fractionation at mid to deep crustal levels.

5) Replenishment events at the SHV are characterized by the intrusion of high-alumina, plagioclase-bearing basaltic magma which mixes with andesite at the base of the shallow reservoir. The hybrid magma undergoes crystallization and exsolution of volatiles. The T1 enclaves represent the upper portions of the mixed layer which are buoyant due to bubbles, while the T2 enclaves represent the more degassed lower portions of the mixing horizon which are mobilized due to mafic overturn and subsequent intrusions. The T3 enclaves represent differentiated basalt which has undergone plagioclase fractionation.

6) Our model suggests that mafic magma continues to heat the magmatic reservoir, mixing andesite with more mafic compositions. This process prevents the andesitic reservoir from fractionating towards more evolved compositions (e.g., dacite).

7) Our observations are consistent with observations from other volcanoes (Bacon, 1986;Browne *et al.*, 2006) and highlight the importance of open system replenishment by deeper magmas in triggering volcanic eruptions.

## References

Aignertorres, M., Blundy, J., Ulmer, P. and Pettke, T. (2007). Laser Ablation ICPMS study of trace element partitioning between plagioclase and basaltic melts: an experimental approach. *Contributions to Mineralogy and Petrology* **153**, 647-667.

Andersen, D. J., Lindsley, D. H. & Davidson, P. M. (1993). QUILF: A pascal program to assess equilibria among Fe---Mg---Mn---Ti oxides, pyroxenes, olivine, and quartz. *Computers & Geosciences* **19**, 1333-1350.

Arculus, R. J. & Wills, K. J. A. (1980). The Petrology of Plutonic Blocks and Inclusions from the Lesser Antilles Island Arc. *Journal of Petrology* **21**, 743-799.

Bacon, C. (1986). Magmatic inclusions in silicic and intermediate volcanic rocks. *Journal of Geophysical Research* **91**, 6091-6112.

Barclay, J., Herd, R.A., Edwards, B.R., Christopher, T, Kiddle, E. J., Plail, M., Donovan, A. (2010) Caught in the act: Inplications for the increasing abundance of mafic enclaves during the recent eruptive episodes of the Soufrière Hills Volcano, Montserrat. Geophysical Research Letters 37: L00E09.

Barclay, J. & Carmichael, I. S. E. (2004). A Hornblende Basalt from Western Mexico: Water-saturated Phase Relations Constrain a PressureTemperature Window of Eruptibility. *Journal of Petrology* **45**, 485-506.

Barclay, J., Rutherford, M. J., Carroll, M. R., Murphy, M. D., Devine, J. D., Gardner, J. E. & Sparks, R. S. J. (1998). Experimental phase equilibria constraints on pre-eruptive storage conditions of the Soufrière Hills magma. *Geophysical Research Letters* **25**, 3437-3440.

Bindeman, I.N., Davis, A.M. and Drake, M.J. (1998). Ion microprobe study of plagioclase-basalt partition experiments at natural concentration levels of trace elements. *Geochimica et Cosmochimica Acta* **62**(7): 1,175-1,193.

Blundy, J. & Cashman, K. (2001). Ascent-driven crystallisation of dacite magmas at Mount St Helens, 1980-1986. *Contributions to Mineralogy and Petrology* **140**, 631-650.

Blundy, J & Sparks R.S.J. (1992). Petrogenesis of Mafic Inclusions in Granitoids of the Adamello Massif, Italy. Journal of Petrology 33:1039-1104

Browne,  (1977). Geochim cosmochim acta 41: 785-801.

Browne, B. L., Eichelberger, J. C., Patino, L. C., Vogel, T. A., Dehn, J., Uto, K. & Hoshizumi, H. (2006). Generation of Porphyritic and Equigranular Mafic Enclaves During Magma Recharge Events at Unzen Volcano, Japan. *Journal of Petrology* **47**, 301-328.

Bryan, W. B., Finger, L. W. & Chayes, F. (1969). Estimating Proportions in Petrographic Mixing Equations by Least-Squares Approximation. *Science* **163**, 926-927.

Buckley, V. J. E., Sparks, R. S. & Wood, B. J. (2006). Hornblende dehydration reactions during magma ascent at Soufrière Hills Volcano, Montserrat. *Contributions to Mineralogy and Petrology* **151**, 121-140.

Carmichael, Ian S.E. (1967). The iron-titanium oxides of salic volcanic rocks and their associated ferromagnesian silicates. *Contributions to Mineralogy and Petrology* **14**, 36-64.

Carr, M. (1990). IGPET for Windows. Rutgers University.

Cashman, K. V. (1992). Groundmass crystallization of Mount St. Helens dacite, 1980–1986: a tool for interpreting shallow magmatic processes. *Contributions to Mineralogy and Petrology* **109**, 431-449.

Chappell, B. W., White, A. J. R. & Wyborn, D. (1987). The Importance of Residual Source Material (Restite) in Granite Petrogenesis. *Journal of Petrology* **28**, 1111-1138.

Coombs, M. L., Eichelberger, J. C. & Rutherford, M. J. (2003). Experimental and textural constraints on mafic enclave formation in volcanic rocks. *Journal of Volcanology and Geothermal Research* **119**, 125-144.

Costa, F. and Singer, B. (2002) Evolution of Holocene Dacite and Compositionally Zoned Magma, Volcan San Pedro, Southern Volcanic Zone, Chile. Journal of Petrology 43:1571-1593.

Davidson, J., Turner, S., Handley, H., Macpherson, C. & Dosseto, A. (2007). Amphibole "sponge" in arc crust? *Geology* **35**, 787-790.

Devine, J. D., Rutherford, M. J. & Gardner, J. E. (1998). Petrologic determination of ascent rates for the 1995-1997 Soufrière Hills volcano andesitic magma. *Geophysical Research Letters* **25**, 3673-3676.

Devine, J.D., Rutherford, M.J., Norton, G.E., Young, S.E. (2003) Magma storage region processes inferred from geochemistry of the Fe-Ti oxides in andesitic magma, Soufrière Hills Volcano, Montserrat, W.I. *Journal of Petrology* 44, 1375-1400.

Dixon, J., Clague, D., Stolper, M., (1991). Degassing history of water, sulfur and carbon in submarine lavas from Kilauea volcano, Hawaii. *The Journal of Geology* **99**, 371-394.

Dostal, J., Dupuy, C., Carron, J.P., Dekerneizon, M.L. and Maury, R.C. (1983). Partition-Coefficients of Trace-Elements - Application to Volcanic-Rocks of St-Vincent, West-Indies. *Geochimica et Cosmochimica Acta* **47**(3): 525-533.

Edmonds, M., A. Aiuppa, M. Humphreys, R. Moretti, G. Giudice, R. S. Martin, R. A. Herd, and T. Christopher (2010), Excess volatiles supplied by mingling of mafic magma at an

andesite arc volcano, *Geochem. Geophys. Geosyst.*, 11, Q04005, doi:10.1029/2009GC002781

Eichelberger, J. C. (1975). Origin of andesite and dacite: Evidence of mixing at Glass Mountain in California and at other circum-Pacific volcanoes. *Geological Society of America Bulletin* **86**, 1381-1391.

Eichelberger, J. C. (1980). Vesiculation of mafic magma during replenishment of silicic magma reservoirs. *Nature* **288**, 446-450.

Esawi, E.K., (2004). Amph-class: An excel spreadsheet for the classification and nomenclature of amphiboles based on the 1997 recommendations of the international mineralogical association. *Computers and Geosciences* **30**, 753-760

Ewart, A., Bryan, W. B., and Gill, J.B. (1973). Mineralogy and geochemistry of the younger volcanic islands of Tonga, S.W. Pacific, *Journal of Petrology* **14:** 429–465.

Ewart, A. and Griffin, W.L. (1994). Application of Proton-Microprobe Data to Trace-Element Partitioning in Volcanic-Rocks. *Chemical Geology* **117**(1-4): 251-284.

Feeley, T.C., Wilson, L.F., Underwood, S.J. (2008) Distribution and compositions of magmatic inclusions in the Mount Helen dome, Lassen Volcanic Center, California: Insights into magma chamber processes. Lithos 106:173-189.

Govindaraju, K. (1994). 1994 compilation of working values and sample description for 383 geostandards. *Geostandards Newsletter* **18**, 1-158.

Green, T.H., Adam, J., Site, S.H. (1993). Proton microprobe determined trace element partition coefficients between pargasite, augite and silicate or carbonatitic melts. EOS, Transactions of the American Geophysical Union 74: 340.

Green, T., Blundy, J., Adam, J. and Yaxley, G. (2000). SIMS determination of trace element partition coefficients between garnet, clinopyroxene and hydrous basaltic liquids at 2-7.5 GPa and 1080-1200C. *Lithos* **5**3, 165-187.

Halama, R., Boudon, G., Villemant, B., Joron, J.L., Le Friant, A., Komorowski, J.C. (2006). Pre-eruptive crystallization conditions of mafic and silicic magmas at the Plat Pays volcanic complex, Dominica (Lesser Antilles). Journal of Volcanology and Geothermal Research 153:200-220.

Harford, C. L., Pringle, M. S., Sparks, R. S. & Young, S. R. (2002). The volcanic evolution of Montserrat using $^{40}Ar/^{39}Ar$ geochronology. In: Druitt, T. H. & Kokelaar, B. P. (eds.) The eruption of Soufrière Hills volcano, Montserrat, from 1995 to 1999. London, *Memoirs: Geological Society of London*, 93-113.

Harford, C. L., Sparks, R. S. J. & Fallick, A. E. (2003). Degassing at the Soufrière Hills Volcano, Montserrat, Recorded in Matrix Glass Compositions. *Journal of Petrology* **44**, 1503-1523.

Higuchi, H. and Nagasawa, H. (1969). Partition of trace elements between rock-forming minerals and the host volcanic rocks. *Earth and Planetary Science Letters* **7**, 281-287.

Hilyard, M., Nielsen, R.L., Beard, J.S., Patino-Douce, A. and Blencoe, J. (2000). Experimental determination of the partitioning behavior of rare Earth and high field strength elements between paragasitic amphibole and natural silicate melts. *Geochimica et Cosmochimica Acta* **64**: 1,103-1,120.

Holland, T., and Blundy, J., 1994, Non-ideal interactions in calcic amphiboles and their bearing on amphibole-plagioclase thermometry. *Contributions to Mineralogy and Petrology* **116**, 433-447.

Humphreys, M., Christopher, T. & Hards, V. (2008). Microlite transfer by disaggregation of mafic inclusions following magma mixing at Soufrière Hills volcano, Montserrat. *Contributions to Mineralogy and Petrology* **5**, 609-624.

Humphreys, M., Edmonds, M., Christopher, T. and Hards, V. (2010). Magma hybridization and diffusive exchange recorded in heterogeneous glasses from Soufrière Hills, Volcano, Montserrat. *Geophysical. Research Letters* **37**, L00E06.

Huppert, H. E., Sparks, R. S. J. & Turner, J. S. (1982). Effects of volatiles on mixing in calc-alkaline magma systems. *Nature* **297**, 554-557.

Kent, A.J.R., Darr, C., Koleszar, A.M., Salisbury, M.J., & Cooper, K.M. (2010) Preferential eruption of andesitic magmas through recharge filtering. Nature Geoscience 3,631-635.

Langmuir, C.H., Bender, J.F., Bence, A.E., Hanson, G.N., Taylor, S.R. (1977). Petrogenesis of basalts from the FAMOUS area: Mid Atlantic Ridge. *Earth and Planetary Science Letter*s **36**, 133-156.

Leake, B., Woolley, A. R., Arps, C., Birch, W., Gilbert, M. C., Grice, J., Hawthorne, F., Kato, A., Kisch, H., Krivovichev, V., Linthout, K., Laird, J., Mandarino, J., Maresch, W., Nickel, E., Rock, N., Schumacher, J., Smith, D., Stephenson, N., Ungaretti, L., Whittaker, E. & Youzhi, G. (1997). Nomenclature of amphiboles: report of the subcommittee on amphiboles of the international mineralogical association, commission on new minerals and mineral names. *The Canadian Mineralogist* **35**, 219-246.

Le Bas, M. J., LeMaitre, R. W., Streckeisen, A. & Zanettin, B. (1986). A chemical classification of volcanic rocks based on the total alkali-silica diagram. *Journal of Petrology* **27**, 745-750.

Lemarchand, F., Villemont, B, and Calais, G. (1987). Trace element distribution coefficients in alkaline series. *Geochimica et Cosmochimica Acta* **51**, 1,071-1,081.

Lepage, L.D., 2003, ILMAT: an Excel worksheet for ilmenite-magnetite geothermometry and geobarometry. *Computers and Geosciences* **29**, 673-678.

Luhr, J.F. and Carmichael, I.S.E. (1980). The Colima volcanic complex, Mexico. I: post-caldera andesites from Volcan Colima. *Contributions to Mineralogy and Petrology* **71***: 343-372.*

Macdonald, R., Hawkesworth, C. J. & Heath, E. (2000). The Lesser Antilles volcanic chain: a study in arc magmatism. *Earth-Science Reviews* **49**, 1-76.

Martin, V. M., Pyle, D. M. & Holness, M. B. (2006). The role of crystal frameworks in the preservation of enclaves during magma mixing. *Earth and Planetary Science Letters* **248**, 787-799.

Matsui, Y., Onuma, N., Nagasawa, H., Higuchi, H. and Banno, S. (1977). Crystal structure control in trace element partition between crystal and magma. *Tectonics* **100**, 315-324.

Mattson, S. R., Vogel, T. A. & Wilband, J. T. (1986). Petrochemistry of the silicic-mafic complexes at Vesturhorn and Austurhorn, Iceland: evidence for zoned/stratified magma. *Journal of Volcanology and Geothermal Research* **28**, 197-223.

McKenzie D., O'Nions R. K. (1991). Partial melt distribution from inversion of rare earth element concentrations. *Journal of Petrology* 32:1021–1091.

Murphy, M.D., Sparks, R.S.J., Barclay, J., Carroll, M.R., Lejeune, A-M., Brewer, T.S., Macdonald, R., Black, S., Young, S. (1998) The role of magma mixing in triggering the current eruption at the Soufrière Hills volcano, Montserrat, West Indies. Geophysical Research Letters 25, 3433-3436.

Murphy, M. D., Sparks, R. S. J., Barclay, J., Carroll, M. R. & Brewer, T. S. (2000). Remobilization of Andesite Magma by Intrusion of Mafic Magma at the Soufrière Hills Volcano, Montserrat, West Indies. *Journal of Petrology* **41**, 21-42.

Nielsen, R.L. (1992). BIGD: a FORTRAN program to calculate trace-element partition coefficients for natural mafic and intermediate composition magmas. *Computers and Geosciences* **18***: 773-788*

Okamoto, K. (1979). Geochemical study on magmatic differentiation of Asama Volcano, Central Japan, *Journal of the Geoogical. Society of Japan* **85**, 525–535.

Pallister, J.S., Hoblitt, R.P., Meeker, G.P., Knight, R.J., Siems, D.F. (1996) Magma Mixing at Mount Pinatubo: Petrographic and Chemical Evidence from the 1991 Deposits. Fire and Mud: Eruptions and Lahars of Mount Pinatubo, Phillippines Eds Newhall, C.G. and Punongbayan R.S. **(PAGES)**

Philpotts, J.A. and Schnetzler, C.C. (1970). Phenocryst-matrix partition coefficients for K, Rb, Sr and Ba, with applications to anorthosite and basalt genesis. *Geochimica et Cosmochimica Acta* **34**(3), 307-322.

Reid, F. (1983). Origin of the Rhyolitic Rocks of the Taupo Volcanic Zone, New-Zealand. *Journal of Volcanology and Geothermal Research* **15**(4), 315-338.

Rollinson, H., (1993) Using geochemical data; evaluation, presentation, interpretation, by Hugh R. Rollinson. Harlow: Longman Publishing Group.


Rutherford, M. J. & Devine, J. D. (2003). Magmatic Conditions and Magma Ascent as Indicated by Hornblende Phase Equilibria and Reactions in the 1995-2002 Soufrière Hills Magma. *Journal of Petrology* **44**, 1433-1453.

Rutherford, M. J. & Hill, P. M. (1993). Magma ascent rates from amphibole breakdown: An experimental study applied to the 1980-1986 Mount St. Helens eruptions. *Journal of Geophysical Research* **98**, 19667-19685.

Schiano, P., Monzier, M., Eissen, J.-P., Martin, H., Koga, K.T. (2010). Simple mixing as the major control of the evolution of volcanic suites in the Ecuadorian Andes. Contributions to Mineralogy and Petrology 160, 297-312.

Sisson, T.W. (1994). Hornblende-Melt Trace-Element Partitioning Measured by Ion Microprobe. *Chemical Geology* **117**(1-4), 331-344.

Sisson, T. W. & Bacon, C. R. (1999). Gas-driven filter pressing in magmas. *Geology* **27**, 613-616.

Snyder, D. & Tait, S. (1995). Replenishment of magma chambers: comparison of fluid-mechanic experiments with field relations. *Contributions to Mineralogy and Petrology* **122**, 230-240.

Sparks, R. S. J. & Marshall, L. A. (1986). Thermal and mechanical constraints on mixing between mafic and silicic magmas. *Journal of Volcanology and Geothermal Research* **29**, 99-124.

Sparks, S. R. J., Sigurdsson, H. & Wilson, L. (1977). Magma mixing: a mechanism for triggering acid explosive eruptions. *Nature* **267**, 315-318.

Stix, J., Gauthier, G., and Ludden, J. (1995). A critical look at the quantitative laser-ablation ICP-MS analysis of natural and synthetic glasses. *The Canadian Mineralogist* **33**, 435-444.

Wiebe, R. A. (1974). Coexisting Intermediate and Basic Magmas, Ingonish, Cape Breton Island. *The Journal of Geology* **82**, 74-87.

Wiebe, R. A. (1994). Silicic Magma Chambers as Traps for Basaltic Magmas: The Cadillac Mountain Intrusive Complex, Mount Desert Island, Maine. *The Journal of Geology* **102**, 423-437.

Zellmer, G. F., Hawkesworth, C. J., Sparks, R. S. J., Thomas, L. E., Harford, C. L., Brewer, T. S. & Loughlin, S. C. (2003). Geochemical Evolution of the Soufrière Hills Volcano, Montserrat, Lesser Antilles Volcanic Arc. *Journal of Petrology* **44**, 1349-1374.

Table 1:  Field texture and rock name

| Enclave Type | Composition | Size | shape | margin texture |
|---|---|---|---|---|
| Type 1 (T1) | Basaltic to basaltic andesite | up to 15 cm | spherical | glassy |
| Type 2 (T2) | Basaltic to basaltic andesite | up to 28 cm | angular | crenulate |
| Type 3 (T3) | Basaltic andesite | up to 15 cm | angular | crenulate |

Table 2: Representative whole-rock compositions of mafic enclaves and andesite lavas

| Rock type | Enclave | Enclave | Enclave | Enclave | Enclave | Enclave | Enclave | Enclave | Enclave | Enclave | Enclave | Enclave |
|---|---|---|---|---|---|---|---|---|---|---|---|---|
| Sample no. | CM26 | CM28 | CM36 | CM37 | CM38 | CM41 | CM51 | CM52 | CM56 | CM58 | CM62 | CM64 |
| Year erupted | 2002 | 2002 | 1997 | 1997 | 1997 | 2002 | 2002 | 2002 | 2002 | 2002 | 2002 | 2002 |
| Enclave type | T1 | T1 | T2 | T3 | T2 | T1 | T2 | T2 | T1 | T2 | T2 | T3 |
| wt.% | | | | | | | | | | | | |
| $SiO_2$ | 52.53 | 54.60 | 50.10 | 53.79 | 53.58 | 51.44 | 52.68 | 50.79 | 50.69 | 53.44 | 52.85 | 52.38 |
| $TiO_2$ | 0.80 | 0.74 | 0.86 | 0.79 | 0.76 | 0.85 | 0.80 | 0.85 | 0.87 | 0.84 | 0.81 | 0.80 |
| $Al_2O_3$ | 19.79 | 19.13 | 20.19 | 19.15 | 19.50 | 19.91 | 19.61 | 20.07 | 20.02 | 19.07 | 19.37 | 19.60 |
| $Fe_2O_3$ | 9.28 | 8.69 | 10.20 | 9.54 | 9.20 | 9.46 | 9.33 | 9.97 | 9.92 | 9.79 | 9.46 | 9.36 |
| MnO | 0.19 | 0.19 | 0.19 | 0.21 | 0.20 | 0.19 | 0.19 | 0.19 | 0.20 | 0.21 | 0.20 | 0.23 |
| MgO | 4.48 | 4.01 | 4.79 | 3.61 | 4.14 | 4.94 | 4.34 | 4.86 | 5.00 | 3.73 | 4.45 | 4.38 |
| CaO | 10.00 | 9.24 | 10.64 | 9.40 | 9.55 | 10.42 | 9.83 | 10.54 | 10.38 | 9.54 | 9.69 | 10.04 |
| $Na_2O$ | 2.95 | 3.09 | 2.84 | 3.25 | 3.01 | 2.83 | 2.98 | 2.72 | 2.86 | 3.02 | 3.03 | 3.39 |
| $K_2O$ | 0.49 | 0.73 | 0.46 | 0.62 | 0.57 | 0.47 | 0.53 | 0.60 | 0.39 | 0.66 | 0.52 | 0.38 |
| $P_2O_5$ | 0.12 | 0.14 | 0.14 | 0.15 | 0.14 | 0.13 | 0.13 | 0.13 | 0.12 | 0.13 | 0.15 | 0.11 |
| LOI | <d/l | <d/l | 0.15 | <d/l | <d/l | <d/l | <d/l | <d/l | <d/l | <d/l | <d/l | <d/l |
| | | | | | | | | | | | | |
| Total | 100.62 | 100.56 | 100.13 | 100.50 | 100.65 | 100.63 | 100.42 | 100.72 | 100.45 | 100.43 | 100.50 | 100.66 |
| | | | | | | | | | | | | |
| *ppm* | | | | | | | | | | | | |
| BaO | 110 | 142 | 75 | 154 | 113 | 98 | 108 | 85 | 65 | 155 | 102 | 97 |
| $Cr_2O_3$ | <d.l. | 25 | <d.l. | 18 | 25 | 26 | 16 | <d.l. | 23 | <d.l. | 20 | <d.l. |
| Ni | 19 | 10 | 10 | 6 | 11 | 26 | 9 | 12 | 15 | 7 | 11 | 8 |
| V | 209 | 182 | 215 | 184 | 188 | 220 | 208 | 219 | 226 | 212 | 205 | 174 |
| Ga | 18.5 | 17.5 | 19 | 18 | 19 | 19 | 18 | 19 | 18 | 18 | 19 | 18 |
| Nb | 1.40 | 2.10 | 1.5 | 2.5 | 2.6 | 1.1 | 1.6 | 1.6 | 1.3 | 1.7 | 2.0 | 2.6 |
| Pb | 1.60 | 1.60 | 1.0 | <d.l. | 1.1 | <d.l. | <d.l | <d.l. | <d.l. | <d.l | <d.l. | <d.l. |
| Rb | 9.80 | 13.20 | 8 | 17 | 11 | 9 | 10 | 12 | 7 | 13 | 12 | 7 |
| Sr | 276 | 269.6 | 275.9 | 295.1 | 274.9 | 270.6 | 273.4 | 271.7 | 273.1 | 284.6 | 268 | 302.1 |
| Y | 19.55 | 20.06 | 20.84 | 28.03 | 19.93 | 21.53 | 18.57 | 19.84 | 21.08 | 20.98 | 21.52 | 32.27 |
| Zr | 65.60 | 78.60 | 62 | 57 | 72 | 69 | 72 | 63 | 70 | 78 | 62 | 51 |
| | | | | | | | | | | | | |
| *ppm* | | | | | | | | | | | | |
| La | 6.60 | 7.91 | 5.64 | 9.82 | 7.40 | 6.36 | 6.91 | 5.86 | 6.19 | 8.35 | 7.03 | 7.91 |
| Ce | 14.56 | 17.09 | 13.17 | 22.57 | 16.27 | 14.36 | 15.32 | 13.41 | 14.04 | 18.13 | 15.62 | 19.93 |
| Pr | 2.04 | 2.32 | 1.94 | 3.26 | 2.25 | 2.07 | 2.11 | 1.94 | 2.01 | 2.48 | 2.20 | 3.19 |
| Nd | 9.37 | 10.48 | 9.40 | 15.27 | 10.34 | 9.88 | 9.97 | 9.36 | 9.74 | 11.35 | 10.31 | 16.02 |
| Sm | 2.47 | 2.47 | 2.64 | 3.96 | 2.68 | 2.73 | 2.60 | 2.60 | 2.63 | 2.95 | 2.73 | 4.55 |
| Eu | 0.90 | 0.92 | 0.95 | 1.25 | 0.95 | 0.96 | 0.94 | 0.93 | 0.97 | 1.06 | 0.97 | 1.38 |
| Gd | 3.00 | 3.24 | 3.37 | 4.81 | 3.23 | 3.48 | 3.33 | 3.30 | 3.32 | 3.61 | 3.43 | 5.80 |
| Tb | 0.47 | 0.49 | 0.51 | 0.73 | 0.49 | 0.53 | 0.49 | 0.51 | 0.51 | 0.55 | 0.51 | 0.88 |
| Dy | 3.13 | 3.25 | 3.39 | 4.87 | 3.31 | 3.48 | 3.32 | 3.37 | 3.41 | 3.66 | 3.46 | 5.89 |
| Ho | 0.65 | 0.69 | 0.71 | 1.03 | 0.69 | 0.73 | 0.70 | 0.70 | 0.71 | 0.78 | 0.73 | 1.23 |
| Er | 1.95 | 2.07 | 2.10 | 3.11 | 2.08 | 2.20 | 2.10 | 2.10 | 2.14 | 2.35 | 2.18 | 3.76 |
| Tm | 0.29 | 0.31 | 0.31 | 0.47 | 0.31 | 0.32 | 0.31 | 0.32 | 0.31 | 0.35 | 0.33 | 0.56 |
| Yb | 1.97 | 2.15 | 2.10 | 3.27 | 2.13 | 2.23 | 2.12 | 2.11 | 2.15 | 2.43 | 2.22 | 3.90 |
| Lu | 0.31 | 0.33 | 0.32 | 0.50 | 0.33 | 0.34 | 0.33 | 0.32 | 0.32 | 0.36 | 0.34 | 0.59 |
| Th | 1.41 | 1.81 | 0.99 | 1.94 | 1.57 | 1.21 | 1.41 | 1.07 | 1.13 | 1.78 | 1.47 | 1.05 |
| U | 0.42 | 0.59 | 0.30 | 0.58 | 0.48 | 0.37 | 0.43 | 0.33 | 0.37 | 0.53 | 0.44 | 0.32 |

<d.l. = below detection limit; n.d. = not determined.

Table 2: continued

| Rock type | Enclave | Enclave | Enclave | Enclave | Enclave | Host | Host | Host |
|---|---|---|---|---|---|---|---|---|
| Sample no. | CM65 | CM66 | CM75A | CM77 | MVO1448 | CM44 | CM25 | CM1448 |
| Year erupted | 2002 | 2002 | 2002 | 2002 | 2006 | 2002 | 2002 | 2006 |
| Enclave type | T1 | T2 | T3 | T3 | T1 | | | |
| wt.% | | | | | | | | |
| $SiO_2$ | 49.59 | 51.31 | 55.87 | 55.68 | 52.44 | 59.27 | 59.00 | 58.69 |
| $TiO_2$ | 0.90 | 0.86 | 0.70 | 0.74 | 0.79 | 0.62 | 0.62 | 0.63 |
| $Al_2O_3$ | 20.28 | 19.57 | 18.63 | 18.71 | 19.43 | 18.19 | 18.36 | 18.46 |
| $Fe_2O_3$ | 10.16 | 9.99 | 8.90 | 8.82 | 9.03 | 7.32 | 7.36 | 7.21 |
| MnO | 0.20 | 0.20 | 0.21 | 0.20 | 0.19 | 0.18 | 0.18 | 0.18 |
| MgO | 5.33 | 4.88 | 3.29 | 3.21 | 4.72 | 2.95 | 2.98 | 3.05 |
| CaO | 10.79 | 10.12 | 8.48 | 8.47 | 10.03 | 7.71 | 7.78 | 7.87 |
| $Na_2O$ | 2.72 | 2.81 | 3.47 | 3.63 | 2.92 | 3.54 | 3.49 | 3.51 |
| $K_2O$ | 0.49 | 0.54 | 0.73 | 0.75 | 0.50 | 0.83 | 0.81 | 0.86 |
| $P_2O_5$ | 0.12 | 0.15 | 0.16 | 0.15 | 0.12 | 0.15 | 0.14 | 0.14 |
| LOI | <d.l | <d.l. | <d.l. | <d.l. | <d.l. | <d.l. | <d.l. | <d.l. |
| | | | | | | | | |
| Total | 100.58 | 100.43 | 100.44 | 100.36 | 100.17 | 100.76 | 100.72 | 100.60 |
| | | | | | | | | |
| *ppm* | | | | | | | | |
| BaO | 63 | 115 | 168 | 196 | 107 | 228 | 209 | 212 |
| $Cr_2O_3$ | <d.l. | <d.l. | 17 | 17 | 17 | 20 | 24 | 23 |
| Ni | 13 | 12 | 6 | 6 | 14 | 6 | 8 | 9 |
| V | 247 | 233 | 128 | 146 | 219 | 130 | 130 | 141 |
| Ga | 17.30 | 17.6 | 17.9 | 18.0 | 16.7 | 17.4 | 16.8 | 17.2 |
| Nb | 1.60 | 1.60 | 2.6 | 2.8 | 2.1 | 2.50 | 2.5 | 2.6 |
| Pb | <d.l. | 1.20 | 1.9 | 1.8 | 2.0 | 1.90 | 1.2 | 1.9 |
| Rb | 11.50 | 10.20 | 15.0 | 14.4 | 11.6 | 16.9 | 16.5 | 16.6 |
| Sr | 268.90 | 261.50 | 287.10 | 278.00 | 263.90 | 267.10 | 265.10 | 265.50 |
| Y | 20.34 | 21.40 | 25.73 | 31.70 | 20.21 | 20.12 | 20.07 | 21.20 |
| Zr | 61.60 | 71.10 | 73.50 | 76.30 | 78.20 | 99.70 | 98.70 | 97.70 |
| | | | | | | | | |
| *ppb* | | | | | | | | |
| La | 5.44 | 6.30 | 10.75 | 11.17 | 6.81 | 10.60 | 10.40 | n.d. |
| Ce | 12.81 | 14.29 | 23.76 | 24.89 | 14.93 | 21.97 | 21.40 | n.d. |
| Pr | 1.91 | 2.06 | 3.27 | 3.50 | 2.09 | 2.87 | 2.79 | n.d. |
| Nd | 9.36 | 9.89 | 14.88 | 16.38 | 9.73 | 12.43 | 12.09 | n.d. |
| Sm | 2.65 | 2.72 | 3.70 | 4.32 | 2.55 | 2.89 | 2.83 | n.d. |
| Eu | 0.96 | 0.95 | 1.18 | 1.27 | 0.89 | 0.97 | 0.96 | n.d. |
| Gd | 3.51 | 3.39 | 4.38 | 5.29 | 3.18 | 3.39 | 3.28 | n.d. |
| Tb | 0.53 | 0.53 | 0.67 | 0.80 | 0.49 | 0.50 | 0.50 | n.d. |
| Dy | 3.52 | 3.49 | 4.40 | 5.27 | 3.26 | 3.39 | 3.24 | n.d. |
| Ho | 0.74 | 0.74 | 0.92 | 1.10 | 0.69 | 0.71 | 0.69 | n.d. |
| Er | 2.19 | 2.22 | 2.81 | 3.35 | 2.07 | 2.18 | 2.11 | n.d. |
| Tm | 0.32 | 0.33 | 0.44 | 0.50 | 0.31 | 0.33 | 0.32 | n.d. |
| Yb | 2.21 | 2.24 | 3.00 | 3.38 | 2.11 | 2.32 | 2.26 | n.d. |
| Lu | 0.33 | 0.34 | 0.46 | 0.52 | 0.32 | 0.36 | 0.36 | n.d. |
| Th | 0.91 | 1.14 | 2.24 | 2.22 | 1.42 | 2.58 | 2.50 | n.d. |
| U | 0.27 | 0.36 | 0.67 | 0.67 | 0.44 | 0.77 | 0.75 | n.d. |

<d.l. = below detection limit; n.d. = not determined.

Table 3: Mineral summary of the three enclave types

| Enclave Type | Xenocrysts (vol %) | Phenocrysts (vol %) | Microphenocrysts (vol %) | Microlites (vol %) | Glass (vol %) | Void Space | Plagioclase type | Plagioclase size (mm) | Plagioclase shape | Plagioclase Core XAn | Plagioclase Rim XAn | Sieve textures | Amphibole Composition | Amphibole shape | Amphibole size (mm) | Pyroxene | Quartz | Groundmass |
|---|---|---|---|---|---|---|---|---|---|---|---|---|---|---|---|---|---|---|
| T1 | 0 - 15 | | 45 - 65 | 5 - 10 | < 5 | 10 - 15 | 1 | 0.7 - 3 | sub - anhedral | 47 - 67 | 71 - 84 | core-rim boundary | Magnesiohb | prismatic | 0.5 - 6 | yes | yes | |
| T2 | | 0 - 15 | 50 - 70 | 5 - 10 | < 5 | 5 - 10 | 2 | 0.65 - 1 | sub - anhedral | 75 - 87 | 61 - 81 | core extensive | Tschermakite | acicular | 0.1 - 1.5 | yes | no | |
| T2 & T3 | | | | | | | 3 | < 0.65 | tabular | 69 - 79 | 70 - 83 | none | | | | | | Rhyolitic composition; diktytaxitic |
| T3 | | 0 - 15 | 60 - 70 | < 10 | < 5 | <10 | 4 | 0.1 - 1.5 | sub - anhedral | 49 - 90 | 49 - 62 | none | Magnesiohb | anhedral | 0.4 - 1 | no | no | Ryolitic composition; diktytaxitic |

Table 4: Representative plagioclase analyses

| Sample | Enclave Type | n[1] | SiO$_2$ | Al$_2$O$_3$ | Fe$_2$O$_3$ | MgO | CaO | Na$_2$O | K$_2$O | BaO | Total | An[2] |
|---|---|---|---|---|---|---|---|---|---|---|---|---|
| *CM41* | T1 | | | | | | | | | | | |
| *Ph1* rim | | 1 | 46.69 | 33.33 | 0.59 | 0.15 | 17.25 | 1.67 | 0.03 | 0.00 | 99.71 | 83.55 |
| core | | 12 | 54.85 | 28.20 | 0.44 | 0.09 | 11.28 | 5.01 | 0.15 | 0.01 | 100.01 | 52.19 |
| *Ph2* rim | | 2 | 46.61 | 33.35 | 0.63 | 0.08 | 17.40 | 1.64 | 0.02 | 0.00 | 99.73 | 84.00 |
| core | | 7 | 54.84 | 30.00 | 0.32 | 0.03 | 11.93 | 4.76 | 0.11 | 0.00 | 100.22 | 55.27 |
| *Ph3* rim | | 3 | 54.41 | 28.30 | 0.59 | 0.05 | 11.40 | 5.05 | 0.12 | 0.03 | 99.96 | 52.38 |
| core | | 11 | 54.35 | 28.57 | 0.35 | 0.02 | 11.52 | 4.95 | 0.11 | 0.02 | 99.88 | 53.25 |
| *MPh1* rim | | 2 | 47.00 | 33.29 | 0.70 | 0.30 | 17.14 | 1.85 | 0.02 | 0.00 | 100.30 | 82.03 |
| core | | 4 | 48.57 | 32.46 | 0.39 | 0.01 | 15.95 | 2.57 | 0.04 | 0.00 | 100.00 | 75.32 |
| *ML* core | | 1 | 47.57 | 32.60 | 0.68 | 0.07 | 16.60 | 2.14 | 0.02 | 0.00 | 99.69 | 79.27 |
| core | | 2 | 47.97 | 32.83 | 0.66 | 0.08 | 16.68 | 2.01 | 0.03 | 0.02 | 100.28 | 80.26 |
| core | | 2 | 47.65 | 32.56 | 0.67 | 0.07 | 16.54 | 2.03 | 0.03 | 0.00 | 99.55 | 80.12 |
| core | | 4 | 49.14 | 31.76 | 0.75 | 0.11 | 15.71 | 2.57 | 0.03 | 0.02 | 100.10 | 75.32 |
| *Ph1* rim | | 4 | 49.78 | 31.14 | 0.68 | 0.08 | 15.00 | 2.97 | 0.04 | 0.01 | 99.71 | 71.32 |
| core | | 9 | 54.29 | 28.56 | 0.33 | 0.03 | 11.52 | 4.89 | 0.12 | 0.02 | 99.75 | 54.52 |
| *CM26* | | | | | | | | | | | | |
| *ML* core | T1 | 1 | 49.93 | 31.28 | 0.63 | 0.07 | 14.79 | 2.97 | 0.045 | 0.00 | 99.73 | 71.05 |
| core | | 1 | 48.66 | 31.53 | 0.72 | 0.09 | 15.59 | 2.52 | 0.046 | 0.00 | 99.17 | 75.20 |
| core | | 1 | 48.60 | 32.12 | 0.74 | 0.09 | 15.88 | 2.34 | 0.019 | 0.00 | 99.78 | 77.09 |
| core | | 1 | 49.10 | 31.78 | 0.73 | 0.08 | 15.37 | 2.69 | 0.044 | 0.01 | 99.73 | 74.22 |
| core | | 1 | 49.25 | 31.36 | 0.74 | 0.09 | 15.35 | 2.66 | 0.06 | 0.00 | 99.51 | 73.83 |
| core | | 1 | 48.87 | 31.76 | 0.71 | 0.11 | 15.54 | 2.48 | 0.055 | 0.04 | 99.56 | 75.25 |
| core | | 1 | 48.77 | 31.73 | 0.65 | 0.11 | 15.99 | 2.48 | 0.033 | 0.00 | 99.76 | 76.09 |
| *MPh1* rim | | 3 | 48.59 | 32.11 | 0.70 | 0.08 | 15.91 | 2.46 | 0.027 | 0.00 | 99.89 | 76.16 |
| core | | 3 | 49.10 | 31.99 | 0.72 | 0.09 | 15.66 | 2.50 | 0.05 | 0.02 | 100.12 | 75.44 |
| *Ph2* rim | | 5 | 47.34 | 33.12 | 0.57 | 0.08 | 17.07 | 1.70 | 0.01 | 0.01 | 99.97 | 83.26 |
| core | | 12 | 48.44 | 32.43 | 0.65 | 0.08 | 16.13 | 2.16 | 0.03 | 0.02 | 99.95 | 78.60 |
| *Ph3* rim | | 2 | 55.39 | 28.06 | 0.35 | 0.02 | 10.85 | 5.20 | 0.12 | 0.01 | 100.00 | 50.50 |
| core | | 7 | 48.95 | 31.91 | 0.72 | 0.09 | 15.87 | 2.46 | 0.03 | 0.00 | 100.03 | 76.15 |
| *MPh2* rim | | 2 | 55.71 | 27.76 | 0.33 | 0.01 | 10.55 | 5.31 | 0.11 | 0.02 | 99.81 | 49.24 |
| Core | | 2 | 49.12 | 32.52 | 0.68 | 0.08 | 15.95 | 2.33 | 0.03 | 0.02 | 100.73 | 78.89 |
| *Ph3* rim | | 2 | 51.60 | 30.23 | 0.53 | 0.06 | 13.74 | 3.56 | 0.06 | 0.01 | 99.77 | 65 |
| core | | 7 | 55.71 | 27.76 | 0.33 | 0.01 | 10.55 | 5.31 | 0.11 | 0.02 | 99.81 | 49 |
| *Ph2* rim | | 2 | 50.57 | 31.30 | 0.73 | 0.19 | 14.66 | 3.03 | 0.05 | 0.00 | 100.53 | 73 |
| core | | 8 | 55.28 | 28.70 | 0.30 | 0.02 | 11.25 | 5.02 | 0.12 | 0.01 | 100.70 | 55 |
| *MPh2* rim | | 2 | 49.12 | 32.52 | 0.68 | 0.08 | 15.95 | 2.33 | 0.03 | 0.02 | 100.73 | 79 |
| core | | 2 | 49.31 | 32.30 | 0.66 | 0.10 | 15.74 | 2.42 | 0.04 | 0.00 | 100.56 | 78 |
| *MPh3* core | | 2 | 49.23 | 32.05 | 0.64 | 0.10 | 15.67 | 2.46 | 0.03 | 0.04 | 100.21 | 78 |
| *ML* core | | 3 | 49.55 | 32.09 | 0.67 | 0.09 | 15.49 | 2.51 | 0.03 | 0.00 | 100.45 | 77 |

[1]n= number of analyses per single grain; [2]mol % An; Ph=phenocryst; MPh=microphenocryst; ML=microlite

Table 4: Representative plagioclase analyses

| Sample | Enclave Type | n[1] | SiO$_2$ | Al$_2$O$_3$ | Fe$_2$O$_3$ | MgO | CaO | Na$_2$O | K$_2$O | BaO | Total | An[2] |
|---|---|---|---|---|---|---|---|---|---|---|---|---|
| **MVO119** | T2 | | | | | | | | | | | |
| *Ph1* rim | | *4* | *51.32* | 30.30 | 0.53 | 0.05 | 13.73 | 3.60 | 0.06 | 0.01 | 99.60 | 65 |
| core | | *4* | *46.42* | 33.54 | 0.51 | 0.02 | 17.40 | 1.53 | 0.02 | 0.00 | 99.45 | 85 |
| *Ph2 rim* | | *2* | *50.21* | 31.26 | 0.55 | 0.02 | 14.59 | 3.16 | 0.05 | 0.00 | 99.83 | 70 |
| *core* | | *7* | *48.90* | 32.34 | 0.44 | 0.03 | 15.78 | 2.44 | 0.08 | 0.02 | 100.01 | 76 |
| *MPh1* rim | | *2* | *46.53* | 33.35 | 0.59 | 0.03 | 17.58 | 1.48 | 0.02 | 0.02 | 99.60 | 85 |
| core | | *4* | *46.59* | 33.68 | 0.50 | 0.02 | 17.59 | 1.42 | 0.03 | 0.01 | 99.84 | 86 |
| *ML* core | | *1* | *49.22* | 31.95 | 0.65 | 0.09 | 17.59 | 2.67 | 0.05 | 0.00 | 99.96 | 74 |
| **CM52** | T2 | | | | | | | | | | | |
| *Ph1* rim | | 3 | 48.37 | 32.33 | 0.54 | 0.04 | 16.20 | 2.30 | 0.02 | 0.00 | 99.80 | 78 |
| core | | 2 | 47.10 | 33.28 | 0.57 | 0.04 | 17.28 | 1.67 | 0.04 | 0.03 | 100.01 | 83 |
| *Ph2* rim | | 2 | 47.50 | 32.82 | 0.61 | 0.03 | 16.85 | 1.93 | 0.02 | 0.00 | 99.78 | 81 |
| core | | 3 | 46.37 | 33.35 | 0.64 | 0.06 | 17.54 | 1.51 | 0.01 | 0.00 | 99.49 | 85 |
| *Ph3* rim | | 2 | 47.16 | 33.10 | 0.62 | 0.07 | 17.26 | 1.72 | 0.02 | 0.00 | 99.95 | 83 |
| Core | | 4 | 52.11 | 29.54 | 0.74 | 0.05 | 14.15 | 2.81 | 0.41 | 0.01 | 99.82 | 69 |
| *MPh1 rim* | | 1 | 47.61 | 33.10 | 0.66 | 0.07 | 17.15 | 1.78 | 0.01 | 0.00 | 100.38 | 83 |
| *core* | | 12 | 47.61 | 32.93 | 0.66 | 0.07 | 16.91 | 1.92 | 0.02 | 0.00 | 100.11 | 81 |
| **CM66E** | T2 | | | | | | | | | | | |
| *Ph1* rim | | 3 | 47.52 | 33.00 | 0.55 | 0.04 | 16.71 | 1.95 | 0.02 | 0.01 | 99.80 | 81 |
| core | | 6 | 47.58 | 33.11 | 0.51 | 0.03 | 16.77 | 1.73 | 0.09 | 0.01 | 99.84 | 82 |
| *Ph2* rim | | 2 | 47.08 | 33.33 | 0.62 | 0.05 | 17.00 | 1.79 | 0.03 | 0.02 | 99.92 | 82 |
| core | | 4 | 47.24 | 33.16 | 0.53 | 0.03 | 16.89 | 1.74 | 0.06 | 0.01 | 99.67 | 82 |
| *Ph3* rim | | 4 | 47.50 | 33.13 | 0.53 | 0.04 | 16.70 | 1.86 | 0.02 | 0.01 | 99.79 | 82 |
| core | | 5 | 48.26 | 32.78 | 0.62 | 0.05 | 16.49 | 1.71 | 0.16 | 0.01 | 100.08 | 81 |
| *Ph4* rim | | 4 | 52.70 | 29.70 | 0.44 | 0.03 | 12.57 | 4.20 | 0.02 | 0.01 | 99.75 | 59 |
| core | | 3 | 53.53 | 29.35 | 0.64 | 0.07 | 13.84 | 2.46 | 0.35 | 0.01 | 100.24 | 71 |
| *Ph5* rim | | 3 | 46.71 | 33.64 | 0.56 | 0.04 | 17.25 | 1.60 | 0.02 | 0.01 | 99.83 | 84 |
| Core | | 2 | 51.10 | 30.45 | 0.78 | 0.06 | 14.26 | 2.74 | 0.51 | 0.01 | 99.92 | 69 |
| **CM107** | T2 | | | | | | | | | | | |
| *Ph1* rim | | 1 | 46.53 | 33.49 | 0.60 | 0.05 | 17.11 | 1.74 | 0.12 | 0.00 | 99.91 | 51 |
| core | | 2 | 49.55 | 31.37 | 0.92 | 0.05 | 14.98 | 2.94 | 0.10 | 0.00 | 99.75 | 60 |
| *Ph2* rim | | 2 | 51.30 | 30.21 | 0.57 | 0.06 | 13.98 | 3.15 | 0.03 | 0.00 | 99.81 | 90 |
| Core | | 3 | 48.79 | 32.05 | 0.57 | 0.04 | 15.90 | 2.09 | 0.13 | 0.00 | 99.64 | 49 |
| *Ph3* core | | 4 | 46.53 | 33.92 | 0.46 | 0.00 | 17.28 | 1.50 | 0.04 | 0.05 | 99.56 | 76 |
| rim | | 4 | 47.06 | 33.43 | 0.58 | 0.05 | 16.81 | 1.71 | 0.11 | 0.04 | 99.77 | 52 |

[1]n = number of analyses per single grain; [2] mol % An; Ph=phenocryst; MPh=microphenocryst; ML=microlite

Table 4: Representative plagioclase analyses

| Sample | Enclave Type | n[1] | SiO$_2$ | Al$_2$O$_3$ | Fe$_2$O$_3$ | MgO | CaO | Na$_2$O | K$_2$O | BaO | Total | An[2] |
|---|---|---|---|---|---|---|---|---|---|---|---|---|
| *CM73* | T3 | | | | | | | | | | | |
| *Ph1* rim | | 2 | 49.45 | 32.08 | 0.35 | 0.03 | 14.96 | 2.77 | 0.03 | 0.02 | 99.56 | 83 |
| core | | 2 | 47.83 | 33.19 | 0.34 | 0.01 | 16.35 | 2.07 | 0.04 | 0.01 | 99.86 | 72 |
| *Ph2* rim | | 3 | 55.04 | 28.50 | 0.44 | 0.02 | 10.95 | 5.03 | 0.24 | 0.03 | 99.53 | 68 |
| core | | 3 | 55.39 | 28.26 | 0.33 | 0.01 | 10.65 | 5.20 | 0.18 | 0.01 | 99.63 | 78 |
| *Ph3* rim | | 5 | 55.05 | 28.41 | 0.35 | 0.02 | 10.78 | 5.03 | 0.03 | 0.01 | 99.72 | 85 |
| core | | 5 | 54.98 | 28.41 | 0.35 | 0.02 | 10.95 | 5.01 | 0.02 | 0.03 | 99.68 | 83 |
| *CM64* | T3 | | | | | | | | | | | |
| *Ph1* rim | | 4 | 55.35 | 27.98 | 0.34 | 0.02 | 10.52 | 5.24 | 0.04 | 0.01 | 99.68 | 73 |
| core | | 5 | 53.74 | 29.20 | 0.30 | 0.01 | 11.84 | 4.56 | 0.03 | 0.00 | 99.82 | 80 |
| *Ph2* rim | | 6 | 55.70 | 27.86 | 0.44 | 0.02 | 10.34 | 5.37 | 0.12 | 0.02 | 100.12 | 52 |
| core | | 4 | 45.84 | 34.53 | 0.36 | 0.02 | 17.93 | 1.27 | 0.13 | 0.02 | 99.99 | 50 |
| *Ph3* rim | | 4 | 55.51 | 27.91 | 0.33 | 0.03 | 10.47 | 5.28 | 0.13 | 0.02 | 99.80 | 51 |
| core | | 4 | 45.44 | 34.96 | 0.39 | 0.01 | 18.25 | 1.05 | 0.14 | 0.02 | 99.88 | 52 |
| *MPh1* rim | | 4 | 54.87 | 28.60 | 0.44 | 0.03 | 11.07 | 5.01 | 0.13 | 0.03 | 99.62 | 49 |
| core | | 4 | 55.54 | 27.92 | 0.31 | 0.02 | 10.42 | 5.38 | 0.11 | 0.01 | 99.77 | 56 |
| *MPh2* rim | | 3 | 55.02 | 28.39 | 0.57 | 0.03 | 10.83 | 5.05 | 0.14 | 0.01 | 99.89 | 49 |
| core | | 3 | 54.83 | 28.41 | 0.36 | 0.03 | 11.03 | 4.97 | 0.02 | 0.01 | 99.96 | 87 |
| *MPh3* rim | | 3 | 52.25 | 30.31 | 0.36 | 0.02 | 13.03 | 3.86 | 0.13 | 0.02 | 99.69 | 49 |
| core | | 3 | 50.23 | 31.67 | 0.35 | 0.02 | 14.54 | 3.02 | 0.01 | 0.00 | 100.11 | 89 |
| *MPh4* rim | | 3 | 56.11 | 27.68 | 0.33 | 0.01 | 10.09 | 5.38 | 0.13 | 0.02 | 100.17 | 52 |
| core | | 2 | 46.37 | 34.35 | 0.34 | 0.01 | 17.50 | 1.39 | 0.13 | 0.03 | 99.75 | 49 |
| *MPh5* rim | | 3 | 55.07 | 28.47 | 0.44 | 0.02 | 10.86 | 5.13 | 0.13 | 0.03 | 100.06 | 51 |
| core | | 3 | 55.21 | 28.44 | 0.36 | 0.02 | 10.81 | 5.06 | 0.12 | 0.02 | 99.77 | 52 |
| *MPh6* rim | | 3 | 52.93 | 29.89 | 0.31 | 0.02 | 12.51 | 4.11 | 0.08 | 0.00 | 99.91 | 63 |
| core | | 3 | 47.11 | 33.93 | 0.35 | 0.01 | 16.93 | 1.73 | 0.05 | 0.01 | 99.89 | 70 |
| *CM61* | T3 | | | | | | | | | | | |
| *Ph1* rim | | 3 | 53.48 | 29.51 | 0.38 | 0.02 | 12.09 | 4.44 | 0.13 | 0.01 | 99.74 | 48 |
| core | | 3 | 55.13 | 28.39 | 0.31 | 0.02 | 10.87 | 5.07 | 0.01 | 0.00 | 99.98 | 86 |
| *Ph2* rim | | 3 | 52.71 | 29.72 | 0.38 | 0.02 | 12.62 | 4.16 | 0.13 | 0.00 | 100.12 | 51 |
| core | | 3 | 45.40 | 34.79 | 0.34 | 0.01 | 18.24 | 1.01 | 0.12 | 0.03 | 100.05 | 51 |
| *MPh1* rim | | 1 | 55.44 | 27.89 | 0.39 | 0.04 | 10.45 | 5.31 | 0.10 | 0.02 | 99.87 | 60 |
| core | | 1 | 48.44 | 32.42 | 0.39 | 0.01 | 15.82 | 2.39 | 0.03 | 0.01 | 100.10 | 83 |
| *MPh2* rim | | 1 | 54.97 | 28.42 | 0.33 | 0.03 | 10.94 | 4.94 | 0.10 | 0.01 | 100.05 | 57 |

n[1]= number of analyses per single grain; 2mol % An; Ph=phenocrysts

Table 5: Representative amphibole analyses

| Rock Type<br>Enclave type<br>Sample Name<br>Crystal Size<br>n[1] | Mafic<br>Enclave<br>T1<br>CM41<br>Ph | Mafic<br>Enclave<br>T1<br>CM41<br>MPH<br>8 | Mafic<br>Enclave<br>T1<br>CM41<br>ML<br>7 | Mafic<br>Enclave<br>T1<br>CM26<br>PH<br>4 | Mafic<br>Enclave<br>T2<br>CM52<br>PH<br>9 | Mafic<br>Enclave<br>T2<br>Cm52<br>MPH<br>8 | Mafic<br>Enclave<br>T2<br>CM52<br>Inclusion*<br>1 | Host Lava<br>CM41H_2<br>PH<br>10 |
|---|---|---|---|---|---|---|---|---|
| *Wt %* | | | | | | | | |
| $SiO_2$ | | 40.99 | 40.88 | 47.05 | 40.50 | 40.07 | 40.81 | 47.59 |
| $TiO_2$ | | 1.88 | 1.88 | 1.39 | 1.79 | 1.86 | 1.88 | 1.40 |
| $Al_2O_3$ | | 14.38 | 14.72 | 6.61 | 13.60 | 14.60 | 13.93 | 7.01 |
| $FeO^2$ | | 10.86 | 10.74 | 14.35 | 12.28 | 11.52 | 11.59 | 14.50 |
| MnO | | 0.14 | 0.14 | 0.47 | 0.20 | 0.14 | 0.17 | 0.48 |
| MgO | | 15.02 | 14.86 | 14.49 | 13.26 | 14.28 | 14.80 | 14.37 |
| CaO | | 11.62 | 11.63 | 10.92 | 11.44 | 11.54 | 11.37 | 10.83 |
| $Na_2O$ | | 2.20 | 2.24 | 1.25 | 2.15 | 2.24 | 2.27 | 1.26 |
| $K_2O$ | | 0.23 | 0.25 | 0.18 | 0.23 | 0.22 | 0.17 | 0.21 |
| F | | 0.01 | 0.02 | 0.08 | 0.01 | 0.02 | 0.00 | 0.05 |
| Cl | | 0.02 | 0.02 | 0.10 | 0.03 | 0.01 | 0.01 | 0.11 |
| | | | | | | | | |
| Total | | 97.35 | 97.38 | 96.91 | 95.50 | 96.52 | 96.99 | 97.81 |
| | | | | | | | | |
| *Cations[3]* | | | | | | | | |
| $Si^{4+}$ | | 6.02 | 6.00 | 6.98 | 6.11 | 5.97 | 6.04 | 6.98 |
| $Ti^{4+}$ | | 0.21 | 0.21 | 0.16 | 0.20 | 0.21 | 0.21 | 0.15 |
| $Al^{IV}$ | | 2.14 | 2.15 | 1.13 | 2.02 | 2.19 | 2.14 | 1.18 |
| $Al^{VI}$ | | 0.28 | 0.33 | 0.14 | 0.35 | 0.30 | 0.22 | 0.00 |
| $Fe^{2+}$ | | 0.11 | 0.13 | 0.57 | 0.47 | 0.20 | 0.07 | 0.57 |
| $Fe^{3+}$ | | 1.19 | 1.16 | 1.16 | 1.05 | 1.20 | 1.32 | 1.16 |
| $Mn^{2+}$ | | 0.02 | 0.17 | 0.06 | 0.03 | 0.02 | 0.02 | 0.06 |
| $Mg^{2+}$ | | 3.29 | 3.25 | 3.20 | 2.97 | 3.09 | 3.26 | 3.14 |
| $Ca^{2+}$ | | 1.83 | 1.83 | 1.73 | 1.85 | 1.83 | 1.80 | 1.70 |
| $Na^B$ | | 0.22 | 0.23 | 0.31 | 0.19 | 0.21 | 0.25 | 0.34 |
| $Na^A$ | | 0.39 | 0.40 | 0.04 | 0.43 | 0.42 | 0.38 | 0.02 |
| $K^A$ | | 0.04 | 0.05 | 0.03 | 0.04 | 0.04 | 0.03 | 0.04 |

[1]n = number of analyses per grain; [2]Ferrous and ferric iron calculated on the bases of 15 cations (Esawi 2004); [3]Structural formulae for all hornblendes calculated on the bases of 23 oxygens (Esawi 2004); Ph= phenocryst, MPh=microphenocryst, ML=microlite.

Table 6: Representative pyroxene analyses

| Mafic Enclaves Sample name | CM41 | | | | | | CM26 | T1 | CM52 | |
|---|---|---|---|---|---|---|---|---|---|---|
| Enclave Type | T1 | | | | | | T1 | | T2 | |
| Crystal Type | opx | cpx | cpx MPh | opx MPh | cpx MPh | cpx MPh | cpx MPH | opx MPh | cpx MPh Pigeonite[2] | cpx MPh Pigeonite[2] |
| Thermometer | Phc | Phr | Cpx/liq | n.a. | Cpx/liq | Cpx/liq | Cpx/liq | n.a. | | |
| | n.a. | n.a. | | | | | | | | |
| *Wt %* | | | | | | | | | | |
| $SiO_2$ | 51.79 | 48.68 | 50.34 | 52.60 | 52.25 | 51.84 | 51.19 | 52.06 | 50.72 | 51.20 |
| $TiO_2$ | 0.11 | 0.83 | 0.66 | 0.23 | 0.29 | 0.56 | 0.39 | 0.26 | 0.45 | 0.30 |
| $Al_2O_3$ | 0.61 | 6.55 | 3.58 | 1.84 | 1.52 | 1.67 | 2.81 | 2.59 | 2.29 | 2.18 |
| $FeO^T$ | 24.08 | 8.04 | 11.02 | 18.62 | 10.54 | 15.10 | 10.93 | 17.75 | 19.88 | 17.14 |
| MnO | 1.65 | 0.21 | 0.50 | 0.79 | 0.72 | 0.66 | 0.55 | 0.60 | 1.29 | 1.14 |
| MgO | 20.39 | 14.07 | 14.36 | 22.43 | 13.86 | 17.04 | 13.60 | 24.12 | 14.14 | 15.95 |
| CaO | 1.01 | 21.28 | 19.43 | 3.20 | 20.29 | 12.78 | 19.87 | 2.08 | 10.87 | 11.59 |
| $Na_2O$ | 0.02 | 0.20 | 0.26 | 0.02 | 0.24 | 0.22 | 0.27 | 0.00 | 0.19 | 0.15 |
| $K_2O$ | 0.01 | 0.01 | 0.02 | 0.02 | 0.01 | 0.02 | 0.02 | 0.01 | 0.02 | 0.03 |
| Total | 99.67 | 99.88 | 100.18 | 99.73 | 99.72 | 99.89 | 99.63 | 99.47 | 99.85 | 99.70 |
| Mg# | 0.63 | 0.78 | 0.72 | 0.70 | 0.72 | 0.69 | 0.71 | 0.73 | 0.58 | 0.65 |
| P (kbar) | n.a | n.a. | 4.5 | n.a. | 4.0 | 4.4 | n.a. | n.a. | 4.0 | 4.0 |
| T(°C)* | n.a. | n.a. | 1092 | n.a. | 1084 | 1109 | n.a. | n.a. | 1062.87 | 1096.06 |

Each column represents the average of a single crystal. The calculated temperatures and pressures are given where appropriate; Pressures determined by cpx/liq thermometry used for Pigeonite calculations. Ph=phenocryst, Phr = phenocryst rim; Phc = phenocryst core; Ph=phenocryst; MPh=microphenocrysts; n.a = not applicable

Table 7: Representative Fe-Ti oxide analyses.

| Rock Type | Mafic Enclave | Mafic Enclave | Mafic Enclave | Mafic Enclave | Mafic Enclave | Mafic Enclave | Mafic Enclave | Mafic Enclave | Mafic Enclave | Host Andesite |
|---|---|---|---|---|---|---|---|---|---|---|
| Sample Name | MVO119 | MVO119 | CM105 | CM105 | CM52 | CM52 | CM107 | CM117 | CM117 | CM119H |
| Enclave Type | T1 | T1 | T1 | T1 | T2 | T2 | T2 | T3 | T3 | T1 |
| Crystal Type | Ph | MPh | Ph | MPh | Ph | MPh | MPh | MPh | MPh | Ph |
| Number of Analyses | 5 | 1 | 3 | 4 | 5 | 2 | 2 | 3 | 2 | 3 |
| *Wt %* | | | | | | | | | | |
| $SiO_2$ | 0.02 | 0.28 | 0.04 | 0.06 | 0.05 | 0.09 | 0.07 | 0.00 | 0.04 | 0.02 |
| $TiO_2$ | 7.83 | 7.53 | 7.34 | 6.72 | 6.00 | 5.82 | 5.74 | 42.37 | 8.83 | 8.22 |
| $Al_2O_3$ | 2.92 | 3.58 | 3.40 | 3.85 | 4.82 | 4.23 | 4.66 | 0.27 | 2.78 | 2.72 |
| FeO* | 82.32 | 81.47 | 82.64 | 82.95 | 82.17 | 81.56 | 83.81 | 51.51 | 81.20 | 82.84 |
| MnO | 0.57 | 0.51 | 0.43 | 0.41 | 0.55 | 0.44 | 0.59 | 0.73 | 0.54 | 0.55 |
| MgO | 1.76 | 1.43 | 1.36 | 1.33 | 1.27 | 1.08 | 1.40 | 2.71 | 1.48 | 1.67 |
| CaO | 0.06 | 0.23 | 0.06 | 1.33 | 0.00 | 0.02 | 0.00 | 0.01 | 0.01 | 0.01 |
| $Cr_2O_3$ | 0.00 | 0.02 | 0.00 | 0.01 | 0.01 | 0.02 | 0.04 | 0.02 | 0.01 | 0.01 |
| ZnO | 0.03 | 0.16 | 0.12 | 0.11 | 0.02 | 0.03 | 0.02 | 0.01 | 0.13 | 0.00 |
| $V_2O_3$ | 0.35 | 0.33 | 0.34 | 0.40 | 0.19 | 0.20 | 0.20 | 0.09 | 0.36 | 0.34 |
| $Nb_3O_5$ | 0.01 | 0.01 | 0.00 | 0.01 | 0.02 | 0.00 | 0.02 | 0.02 | 0.01 | 0.00 |
| NiO | 0.00 | 0.00 | 0.00 | 0.00 | 0.00 | 0.00 | 0.00 | 0.00 | 0.00 | 0.00 |
| Total | 95.80 | 95.54 | 95.73 | 95.89 | 95.11 | 93.47 | 96.55 | 97.72 | 95.49 | 96.39 |
| $Si^{4+}$ | 0.00 | 0.00 | 0.00 | 0.00 | 0.00 | 0.00 | 0.00 | 0.00 | 0.00 | 0.00 |
| $Mg^{2+}$ | 0.10 | 0.08 | 0.20 | 0.19 | 0.07 | 0.06 | 0.07 | 0.15 | 0.08 | 0.09 |
| $Cr^{3+}$ | 0.00 | 0.00 | 0.00 | 0.00 | 0.00 | 0.00 | 0.00 | 0.00 | 0.00 | 0.00 |
| $Ti^{4+}$ | 0.22 | 0.23 | 0.20 | 0.19 | 0.17 | 0.16 | 0.16 | 1.20 | 0.25 | 0.23 |
| $Fe^{2+}$ | 1.15 | 1.18 | 1.17 | 1.16 | 1.15 | 1.16 | 1.13 | 1.62 | 1.19 | 1.16 |
| $Fe^{3+}$ | 1.39 | 1.37 | 1.39 | 1.40 | 1.38 | 1.41 | 1.41 | n.a | 1.34 | 1.39 |
| $Al^{3+}$ | 0.13 | 0.12 | 0.15 | 0.17 | 0.20 | 0.19 | 0.20 | 0.01 | 0.12 | 0.12 |
| $Mn^{2+}$ | 0.02 | 0.02 | 0.01 | 0.01 | 0.02 | 0.01 | 0.02 | 0.02 | 0.01 | 0.02 |
| $Ca^{2+}$ | 0.00 | 0.00 | 0.00 | 0.00 | 0.00 | 0.00 | 0.00 | 0.00 | 0.00 | 0.00 |
| Total | 3 | 3 | 3 | 3 | 3 | 3 | 3 | 3 | 3 | 3 |
| Mg# | 0.04 | 0.04 | 0.03 | 0.03 | 0.03 | 0.03 | 0.03 | 0.09 | 0.03 | 0.04 |
| T°C | n.a | n.a. | n.a. | n.a. | n.a | n.a. | n.a. | 897 ± 16°C | 897 ± 16°C | n.a. |

Each column represents the average of a single crystal. ; Temperatures are reported as an average of techniques used in the ILMAT program; PH=phenocryst, MPH=microphenocryst

Table 8: Representative glass analyses of mafic enclaves and host lavas

| Rock type | mafic enclave | Mafic enclave | Mafic enclave | Mafic enclave | Mafic enclave | Mafic enclave | Mafic enclave | Mafic enclave | Mafic enclave | Mafic enclave | Mafic Enclave | Host lava | Host lava |
|---|---|---|---|---|---|---|---|---|---|---|---|---|---|
| Sample number | MVO 105 | MVO 107 | MVO 113 | MVO1 19E | CM2 | CM4 | CM5 | CM5 | CM5 | MVO1 237 | CM52 1 | CM4 1H | MVO1 19H |
| Number of analyses | 24 | 10 | 6 | 19 | 6 | 1 | 2 | 2 | 6 | 5 | Devitrified | 16 | 8 |
| Enclave Type | 1 | 2 | 1 | 1 | 191 | 121 | 92 | 12 | 111 | 2 | | 1 | |
| **Wt %** | | | | | | | | | | | | | |
| $SiO_2$ | 72.07 | 73.34 | 73.74 | 73.08 | 73.31 | 72.47 | 76.10 | 78.13 | 77.67 | 74.49 | 79.09 | 75.77 | 75.33 |
| $TiO_2$ | 0.57 | 0.48 | 0.48 | 0.47 | 0.47 | 0.60 | 0.32 | 0.24 | 0.33 | 0.26 | 0.26 | 0.64 | 0.33 |
| $Al_2O_3$ | 12.83 | 12.90 | 12.10 | 13.11 | 12.97 | 12.88 | 11.71 | 11.82 | 10.91 | 12.05 | 11.21 | 11.75 | 11.50 |
| $FeO^*$ | 2.71 | 2.38 | 2.36 | 2.28 | 2.30 | 2.91 | 1.60 | 0.47 | 1.86 | 1.94 | 0.48 | 1.76 | 1.99 |
| MgO | 0.11 | 0.21 | 0.19 | 0.18 | 0.18 | 0.22 | 0.10 | 0.04 | 0.12 | 0.07 | 0.02 | 0.12 | 0.41 |
| MnO | 0.06 | 0.09 | 0.00 | 0.07 | 0.08 | 0.06 | 0.01 | 0.00 | 0.02 | 0.00 | 0.09 | 0.03 | 0.06 |
| CaO | 1.02 | 1.59 | 1.44 | 1.36 | 1.45 | 1.37 | 0.49 | 2.59 | 0.31 | 0.65 | 2.65 | 0.65 | 1.00 |
| $Na_2O$ | 4.66 | 4.31 | 4.18 | 4.34 | 4.27 | 4.61 | 3.52 | 4.86 | 3.97 | 3.41 | 4.34 | 4.09 | 3.59 |
| $K_2O$ | 4.24 | 3.12 | 3.04 | 3.37 | 3.31 | 3.99 | 5.37 | 0.75 | 4.18 | 4.48 | 0.57 | 3.94 | 4.07 |
| $P_2O_5$ | 0.07 | 0.11 | 0.11 | 0.12 | 0.11 | 0.12 | 0.00 | 0.08 | 0.10 | 0.06 | 0.06 | 0.08 | 0.05 |
| Total | 98.34 | 98.55 | 97.64 | 98.38 | 98.45 | 99.24 | 99.22 | 98.99 | 99.47 | 97.69 | 98.81 | 99.00 | 98.31 |
| **ppm** | | | | | | | | | | | | | |
| Ba | 700 | 500 | 630 | 600 | 540 | 490 | 260 | 0.00 | 500 | 915 | 320 | 510 | 540 |
| Cl | 1480 | 2090 | 3420 | 2560 | 2770 | 1780 | 2082 | 420 | 580 | 3268 | 230 | 1190 | 1540 |
| S | b.d. | b.d. | b.d. | n.d. | b.d. | n.d. | n.d. | n.d. | n.d. | n.d. | n.d. | n.d. | n.d. |

Reported values are based on one thinsection; b.d. is below detection; n.d. is not determined

Table 9: Magma mixing calculations

| Test | | | Test 1 – T1 | | Test 2 – T1 | | Test 1 – T2 | | Test 2 – T2 | |
|---|---|---|---|---|---|---|---|---|---|---|
| Sample | Basalt end member CM65 | Andesite end member CM25 | Basaltic Andesite CM28 | Calculated Hybrid | Basaltic Andesite CM1448 | Calculated Hybrid | Basaltic Andesite CM107 | Calculated Hybrid | Basaltic Andesite CM38 | Calculated Hybrid |
| Wt % | | | | | | | | | | |
| $SiO_2$ | 49.81 | 59.01 | 54.77 (0.27) | 54.73 | 52.83 (0.26) | 52.63 | 54.88 (0.27) | 54.79 | 53.73 (0.53) | 53.67 |
| $TiO_2$ | 0.90 | 0.62 | 0.74 (0.00) | 0.75 | 0.80 (0.08) | 0.81 | 0.74 (0.00) | 0.75 | 0.77 (0.07) | 0.78 |
| $Al_2O_3$ | 20.37 | 18.36 | 19.19 (0.19) | 19.30 | 19.57 (0.19) | 19.76 | 19.08 (0.18) | 19.29 | 19.55 (0.19) | 19.53 |
| $FeO^T$ | 9.18 | 6.62 | 7.84 (0.07) | 7.82 | 8.18 (0.08) | 8.40 | 8.28 (0.08) | 7.80 | 8.30 (0.08) | 8.11 |
| MnO | 0.20 | 0.18 | 0.19 (0.00) | 0.19 | 0.19 (0.01) | 0.19 | 0.20 (0.00) | 0.19 | 0.20 (0.02) | 0.19 |
| MgO | 5.35 | 2.98 | 4.02 (0.04) | 4.09 | 4.75 (0.04) | 4.63 | 3.61 (0.03) | 4.07 | 4.15 (0.04) | 4.36 |
| CaO | 10.84 | 7.78 | 9.27 (0.09) | 9.21 | 10.10 (0.01) | 9.91 | 9.20 (0.09) | 9.19 | 9.58 (0.09) | 9.56 |
| $Na_2O$ | 2.73 | 3.49 | 3.10 (0.03) | 3.14 | 2.94 (0.02) | 2.96 | 2.99 (0.03) | 3.14 | 3.02 (0.03) | 3.05 |
| $K_2O$ | 0.49 | 0.81 | 0.73 (0.00) | 0.66 | 0.50 (0.05) | 0.59 | 0.87 (0.00) | 0.66 | 0.57 (0.05) | 0.63 |
| $P_2O_5$ | 0.12 | 0.14 | 0.14 (0.00) | 0.13 | 0.12 (0.01) | 0.13 | 0.15 (0.00) | 0.13 | 0.14 (0.01) | 0.13 |
| $\Sigma r^2$ | | | | 0.02 | | 0.13 | | 0.52 | | 0.09 |
| % Basalt | | | | 46.6 | | 69.5 | | 45.9 | | 58.1 |
| % Andesite | | | | 53.4 | | 30.5 | | 54.1 | | 41.9 |
| ppm | | | | | | | | | | |
| Ba | 56 | 187 | 127 | 126 | 96 | 96 | 158 | 127 | 101 | 111 |
| Ni | 13 | 8 | 10 | 10.3 | 14 | 11.5 | 16 | 10 | 11 | 11 |
| V | 247 | 130 | 182 | 184.5 | 219 | 211.3 | 171 | 184 | 188 | 198 |
| Rb | 11.5 | 16.5 | 13.2 | 14.2 | 11.6 | 13 | 15 | 14.2 | 11 | 14 |
| Sr | 268.9 | 265.1 | 269.6 | 266.9 | 263.9 | 267.8 | 274 | 267 | 275 | 267 |
| Y | 20.34 | 20.07 | 21.1 | 21 | 21 | 21 | 21 | 21 | 21 | 21 |
| Zr | 61.60 | 98.7 | 78.6 | 81.4 | 77.8 | 72.9 | 81 | 82 | 72 | 77 |
| ppb | | | | | | | | | | |
| La | 5.4 | 10.4 | 7.9 | 8.1 | 6.8 | 6.9 | 8.5 | 8.1 | 7.4 | 7.5 |
| Ce | 12.8 | 21.4 | 17.1 | 17.4 | 14.9 | 15.4 | 18.2 | 17.5 | 16.3 | 16.4 |
| Nd | 9.4 | 12.1 | 10.5 | 10.8 | 9.7 | 10.2 | 11 | 10.9 | 10.3 | 10.5 |
| Sm | 2.7 | 2.8 | 2.7 | 2.8 | 2.5 | 2.7 | 2.7 | 2.8 | 2.7 | 2.7 |
| Eu | 1.0 | 1.0 | 0.9 | 1.0 | 0.9 | 1.0 | 0.9 | 1.0 | 0.9 | 1.0 |
| Gd | 3.5 | 3.3 | 3.2 | 3.4 | 3.2 | 3.4 | 3.3 | 3.4 | 3.2 | 3.4 |
| Dy | 3.5 | 3.2 | 3.3 | 3.3 | 3.3 | 3.4 | 3.3 | 3.3 | 3.3 | 3.4 |
| Er | 2.2 | 2.1 | 2.1 | 2.1 | 2.1 | 2.2 | 2.1 | 2.1 | 2.1 | 2.2 |
| Yb | 2.2 | 2.3 | 2.2 | 2.3 | 2.1 | 2.2 | 21.3 | 2.3 | 2.1 | 2.2 |

Error reported for major elements is based on analytical precision (see text for details).

Table 10: Partition coefficients used for modeling

| | Plagioclase | *Reference | Orthopyroxene | *Reference | Amphibole | *Reference | Magnetite | *Reference |
|---|---|---|---|---|---|---|---|---|
| Ba | 0.60 | 1 | 0.02 | 7 | 0.44 | 14 | 0.12 | 20 |
| Ni | 0.12 | 4 | 8.00 | 6 | 7.00[1] | 11 | 31.00 | 16 |
| V | 0.27 | 4 | 0.60 | 6 | 1.49 | 12 | 6.85 | 16 |
| Rb | 0.15 | 1 | 0.02 | 6 | 0.16 | 13 | 0.15 | 19 |
| Sr | 1.74 | 2 | 0.00 | 8 | 0.35 | 10 | 0.11 | 19 |
| Y | 0.01 | 2 | 0.10 | 5 | 1.62[†] | 9 | 0.00 | 16 |
| Zr | 0.00 | 2 | 0.03 | 5 | 0.81[†] | 9 | 0.38 | 16 |
| La | 0.06 | 2 | 0.00 | 5 | 0.28[†] | 9 | 0.02 | 17 |
| Ce | 0.05 | 2 | 0.01 | 5 | 0.30 | 10 | 0.02 | 17 |
| Nd | 0.04 | 3 | 0.01 | 5 | 0.70 | 10 | 0.03 | 17 |
| Sm | 0.08 | 4 | 0.02 | 5 | 1.32[†] | 9 | 0.03 | 17 |
| Eu | 0.97 | 4 | 0.03 | 5 | 0.88 | 8 | 0.03 | 17 |
| Gd | 0.05 | 4 | 0.03 | 5 | 2.10[†] | 9 | 0.02 | 17 |
| Dy | 0.02 | 1 | 0.07 | 5 | 0.78 | 8 | 0.30 | 18 |
| Er | 0.05 | 2 | 0.12 | 5 | 0.68 | 8 | 0.00 | - |
| Yb | 0.08 | 2 | 0.22 | 5 | 0.59 | 8 | 0.02 | 17 |

*references: (1) Philpotts J.A. and Schnetzler (1970), (2) Aigner-Torres et al. (2007), (3) Higuchi and Nagasawa (1969), (4) Bindeman et al. (1998), (5) Green et al. (2000); (6) Ewart et al. (1973); (7) Okamoto (1979), (8) McKenzie and O'Nions (1991), (9) Hilyard et al. (2000), (10) Ronov and Yaroshevskiy (1976), (11) Dostal et al. (1983), (12) Sisson (1994), (13) Green et al. (1993), (14) Matsui et al. (1977), (16) Nielsen (1992), (17) Lemarchand et al. (1987), (18) Reid (1983), (19) Ewart and Griffin (1994), (20) Luhr and Carmichael (1980)

† pargasite

Table 11: Crystal fractionation calculations

| Test Sample | Plag | Amph | Mt | Test 1 Calculated Step 1- T1 CM65 to CM28 | Calculated Step 2 – T1 CM28 to CM25 | Test 2 Calculated Step 1 – T2 CM65 to MVO107 | Calculated Step 2 – T2 MVO107 to CM25 | Test 3 Calculated Fractionate T2 CM52 – CM107 |
|---|---|---|---|---|---|---|---|---|
| **Wt %** | | | | | | | | |
| $SiO_2$ | 46.37 | 40.50 | 0.02 | 50.60 | 55.17 | 50.81 | 55.10 | 51.56 |
| $TiO_2$ | nd | 1.79 | 7.62 | 0.98 | 0.81 | 0.97 | 0.83 | 0.92 |
| $Al_2O_3$ | 33.35 | 13.60 | 2.88 | 20.23 | 19.32 | 20.00 | 19.40 | 19.93 |
| $FeO^T$ | 0.64 | 12.25 | 91.24 | 9.22 | 7.86 | 9.24 | 8.28 | 9.03 |
| MnO | nd | 0.20 | 0.00 | 0.17 | 0.17 | 0.17 | 0.17 | 0.17 |
| MgO | 0.06 | 13.26 | 1.58 | 5.28 | 4.02 | 5.22 | 3.65 | 4.79 |
| CaO | 17.54 | 11.44 | 0.02 | 10.79 | 9.17 | 10.88 | 9.04 | 10.56 |
| $Na_2O$ | 1.51 | 2.15 | nd | 2.07 | 2.70 | 1.94 | 2.75 | 2.15 |
| $K_2O$ | 0.01 | 0.23 | nd | 0.53 | 0.65 | 0.62 | 0.66 | 0.67 |
| $P_2O_5$ | nd | 0.00 | nd | 0.09 | 0.11 | 0.10 | 0.11 | 0.11 |
| | | | | | | | | |
| $\Sigma r^2$ | | | | 0.56 | 0.21 | 0.86 | 0.17 | 0.43 |
| F | | | | 67 | 77 | 65 | 79 | 72 |
| % Plag. | | | | 42.5 | 44.0 | 39.0 | 50.4 | 41.3 |
| % Amph | | | | 51.4 | 49.6 | 57.3 | 38.9 | 54.6 |
| % Mt | | | | 6.0 | 6.4 | 3.8 | 10.7 | 4.1 |
| | | | | | | | | |
| **ppm** | | | | | | | | |
| Ba | | | | 102 | 163 | 125 | 165 | 133 |
| Ni | | | | 59 | 25 | 96 | 26 | 60 |
| V | | | | 326 | 192 | 256 | 235 | 236 |
| Rb | | | | 11.5 | 13 | 11 | 14 | 12 |
| Sr | | | | 262 | 262 | 260 | 267 | 266 |
| Y | | | | 20 | 20 | 21 | 19 | 21 |
| Zr | | | | 63 | 85 | 65 | 85 | 68 |
| | | | | | | | | |
| **ppb** | | | | | | | | |
| La | | | | 5.66 | 8.39 | 5.98 | 8.48 | 6.49 |
| Ce | | | | 12.30 | 17.30 | 12.80 | 17.50 | 13.90 |
| Nd | | | | 8.18 | 10.3 | 8.55 | 10.20 | 9.03 |
| Sm | | | | 2.40 | 2.58 | 2.46 | 2.52 | 2.49 |
| Eu | | | | 0.84 | 0.96 | 0.84 | 0.95 | 0.85 |
| Gd | | | | 3.33 | 3.35 | 3.63 | 3.18 | 3.49 |
| Dy | | | | 2.62 | 2.75 | 2.62 | 2.74 | 2.75 |
| Er | | | | 1.63 | 1.78 | 1.63 | 1.77 | 1.72 |
| Yb | | | | 1.80 | 2.01 | 1.81 | 1.99 | 1.88 |

n.d. = not determined; For bulk compositions refer to Table 12. CM65, CM25 and CM28

Figure 1. Generalized geologic map of Montserrat (after Harford et al., 2002). The current

activity is at located at the Soufriere Hills volcano (red star). Sampling location for the 8

December 2002 block and ash flow is at Whites Ghaut. The inset shows the tectonic setting of

the Lesser Antilles volcanic chain

**Figure 1**
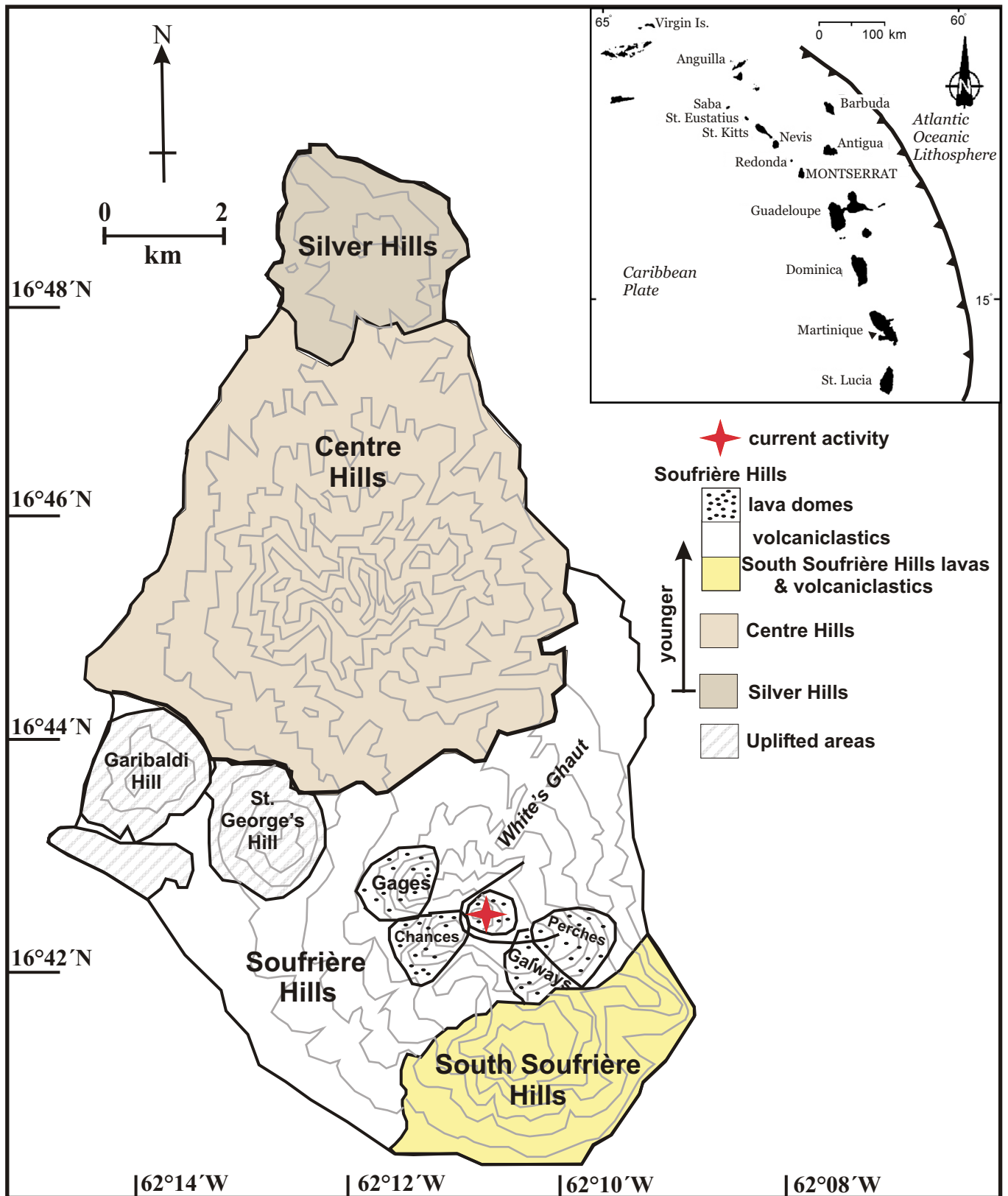
Figure 2. Field photos of enclave textures. A) White circles highlight enclaves in an andesitic host. B) A T2 enclave with multiple discrete enclaves at the margin (white circles highlight smaller enclaves). The black dashed lines outline the plagioclase enriched zones at the enclave margins. The white dashed line is the same white dashed line in Fig. 3C. C) Example of a Type 1 enclave with a glassy margin. Note the plagioclase crystals. Coin is ~ 2 cm for scale. D) A T1 enclave showing decreasing vesicularity from the center towards the rim. Pen is ~ 15 cm long for scale.

**Figure 2**



(a)

(b)

(c) glassy margin — plagioclase

(d) decreasing vesicularity
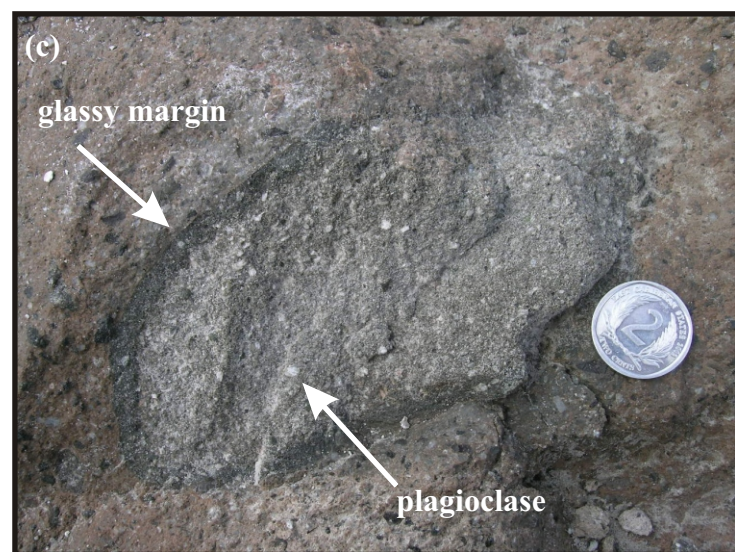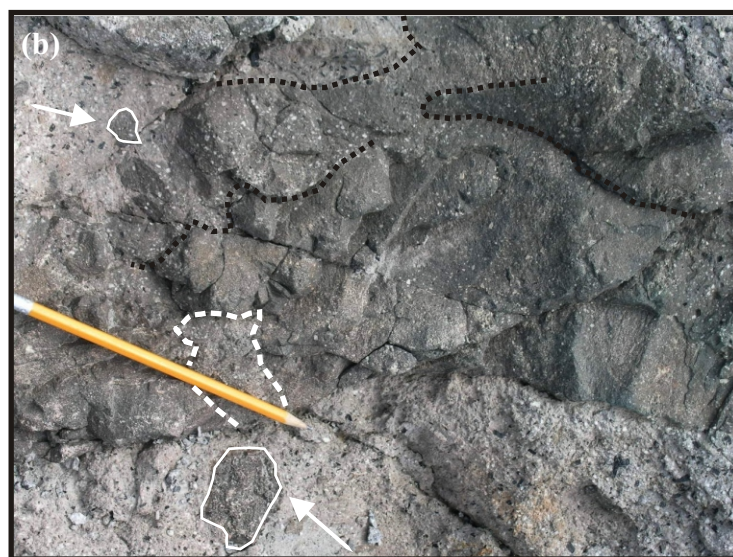
Figure 3. Field photos of enclave textures. A) A T2 enclave with crenulate margins and a fracture across the middle. B) The contact zone between a T2 enclave and andesitic host. White arrows point to an amphibole rich layer at the base of the enclave and to a plagioclase rich layer on the host side of the contact. C) Mafic fingers propagating towards the andesitic host on the margins of the T2 enclave. D) Partial fracture in the T2 enclave filled by crystal rich material (outlined by the white dashed line).

**Figure 3**
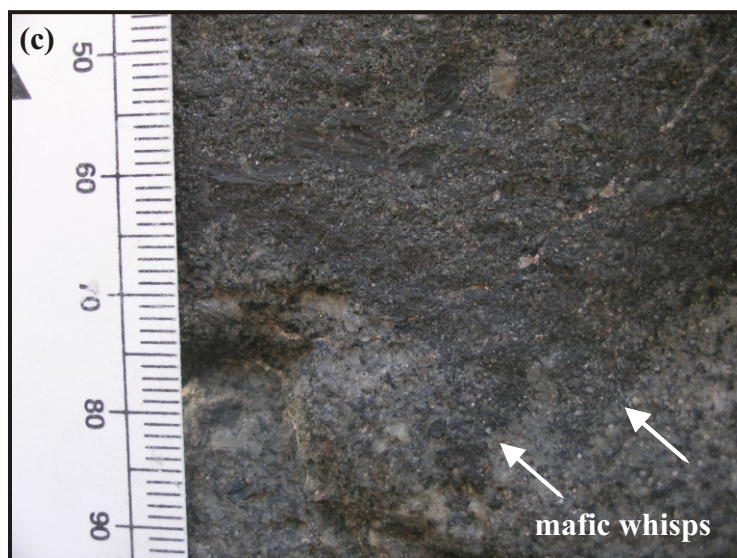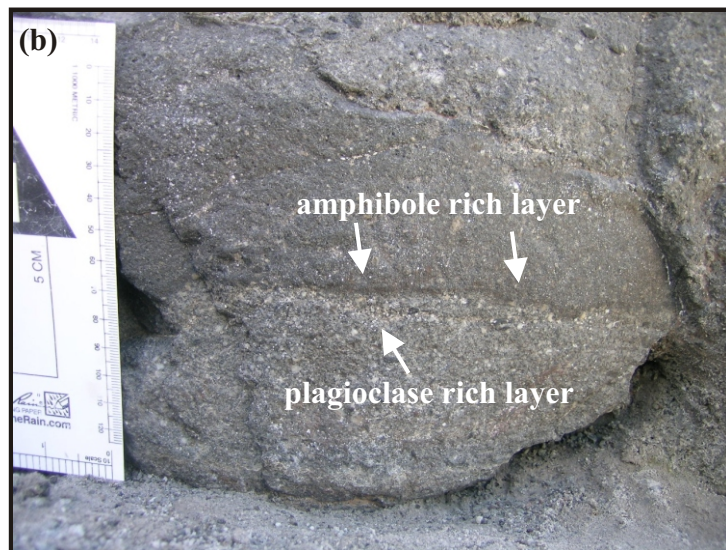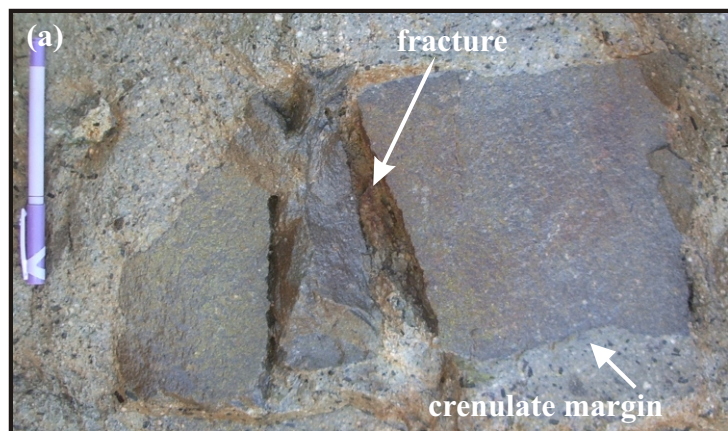
Figure 4. Whole-rock major element contents of enclaves and host rock. A) $SiO_2$ wt. % vs $Al_2O_3$ wt. %; B) $SiO_2$ wt. % vs $K_2O$ wt. % (Le Bas et al., 1986); C) $SiO_2$ wt. % vs MgO wt. %; D) $SiO_2$ wt. % vs $TiO_2$ wt. %. The enclave and host andesite compositions are similar from 1996 to 2002. *Grey symbols are SHV whole rock compositions from previous studies (Murphy et al. (2000); Harford et al. (2003); Zellmer et al. (2003); Barclay et al. (2010)).

**Figure 4**
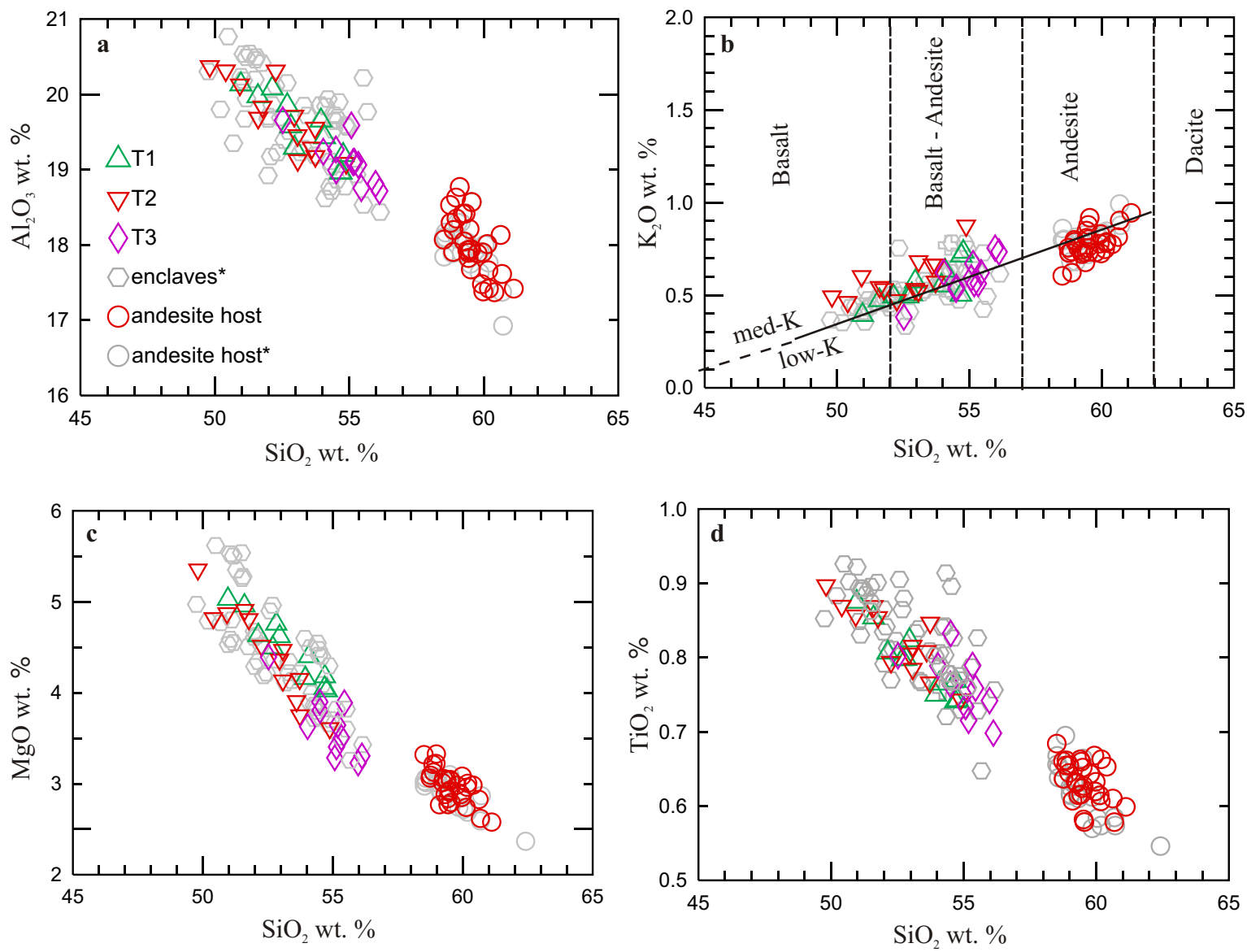
Figure 5. Whole-rock trace element contents of enclaves and host rock. A) Ni is slightly higher

in T1 enclaves relative to T2 and T3 enclaves; B) Y is higher for T3 enclaves relative to T1 and

T2 enclaves; C) Sr is buffered in all enclaves although T2 is slightly higher; D) Zr increases with

silica content although T3 is lower in Zr relative to T1 and T2. *Grey symbols are SHV whole

rock compositions from previous studies (Murphy et al. (2000); Harford et al. (2003); Zellmer et

al. (2003); Barclay et al., (2010))

**Figure 5**
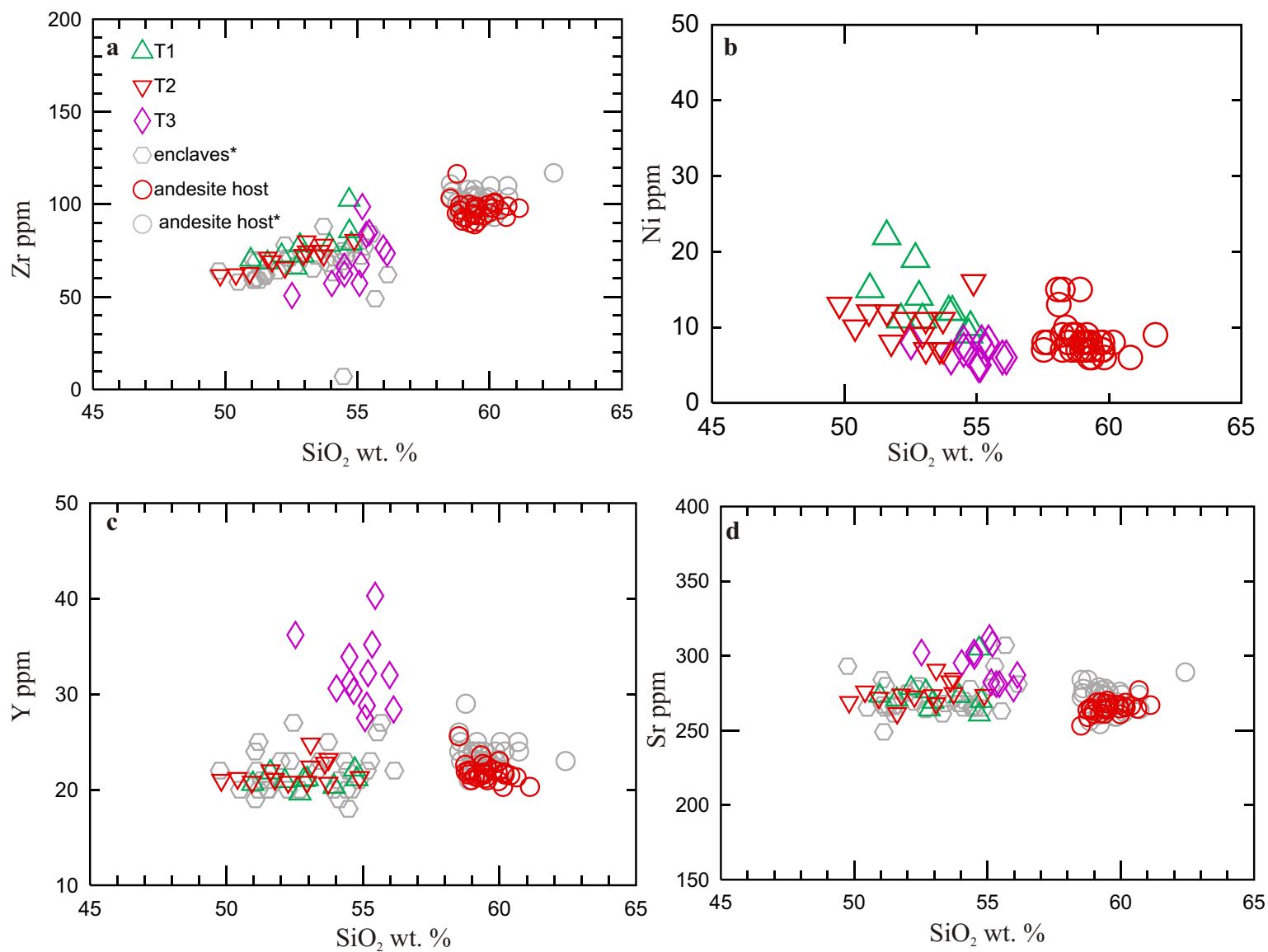
Figure 6. REE contents of enclaves. A) T1 enclaves; B) T2 enclaves; C) T3 enclaves.

**Figure 6**
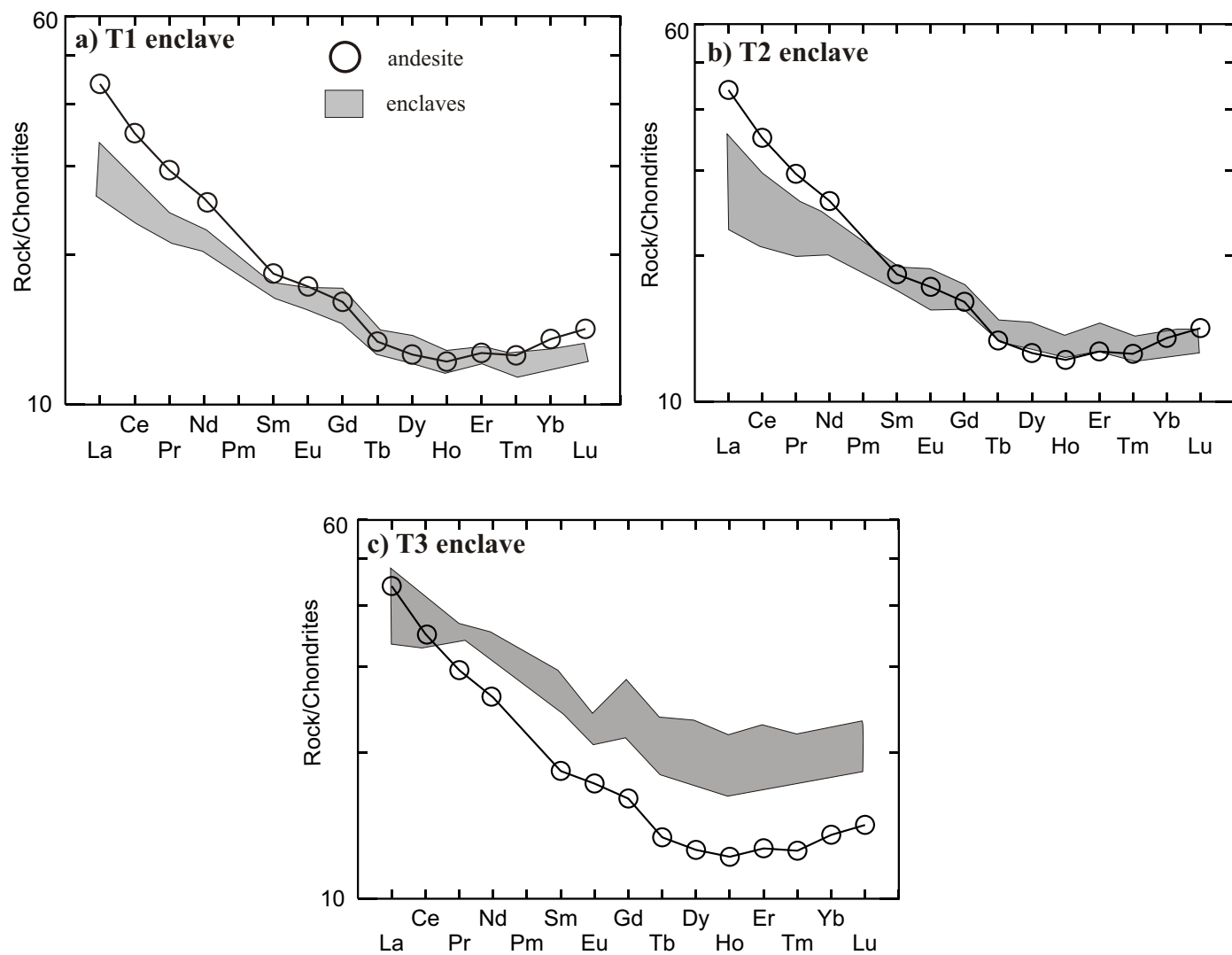
Figure 7. Microphotographs of minerals and groundmass textures observed in T1 enclaves. A) Reversely zoned plagioclase crystal in which the sodic core and more calcic edge are separated by a sieved zone. B) Prismatic magnesiohornblende crystal with an overgrowth rim. C) Orthopyroxene crystal with an overgrowth rim of clinopyroxene. D) Quartz crystal with an overgrowth rim of clinopyroxene. E) T1 groundmass with a framework of plagioclase and pyroxene microphenocrysts and microphenocrysts. White dashed line outlines angular void spaces (diktytaxitic texture). F) The contact between a T1 enclave and host andesite. Note the rigid framework with no decrease in grain size towards the contact; dashed white box indicates a broken plagioclase crystal.

**Figure 7**
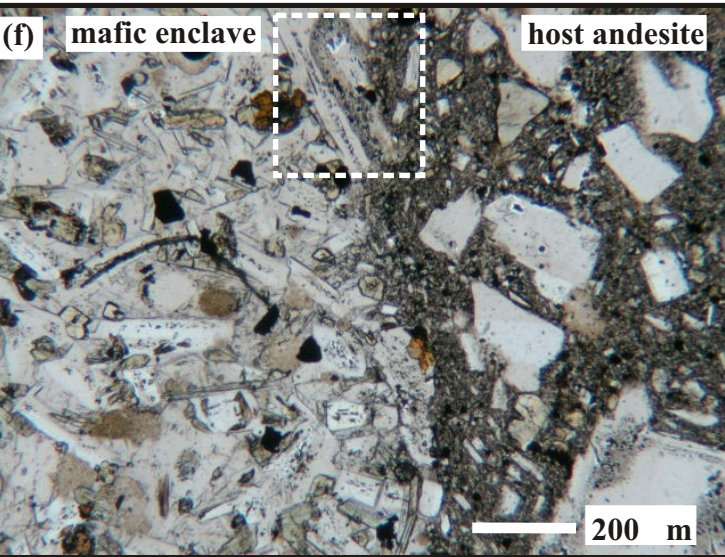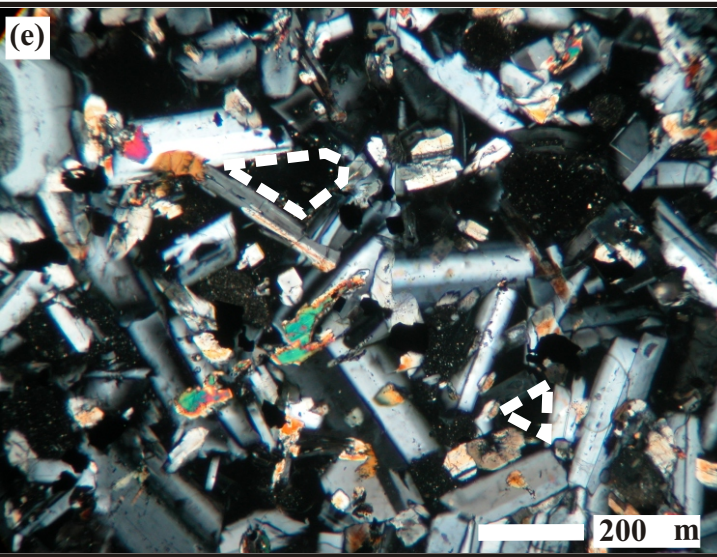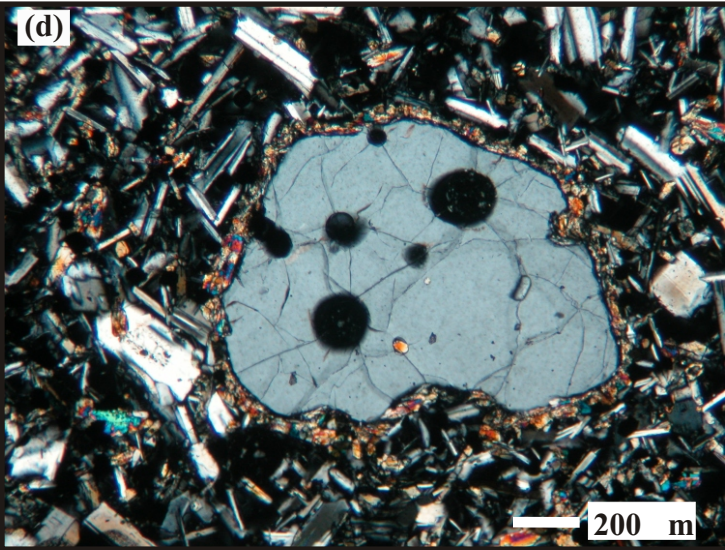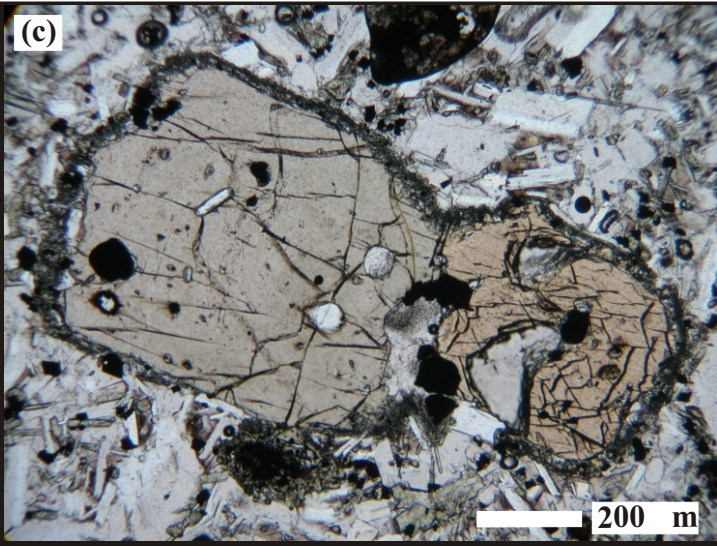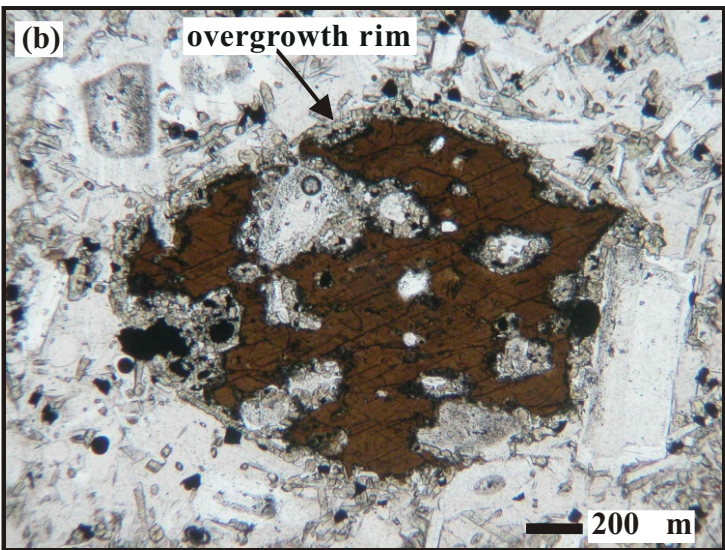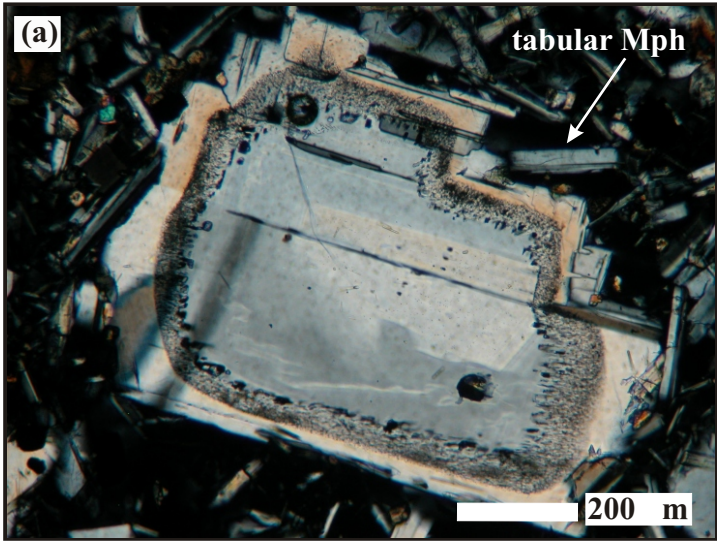
Figure 8. Plagioclase compositions as a function of An content. black circle = rim compositions;

white squares = core compositions; white triangles = microlites; Ph= phenocryst;

MPh=microphenocryst; ML=microlites.

**Figure 8**
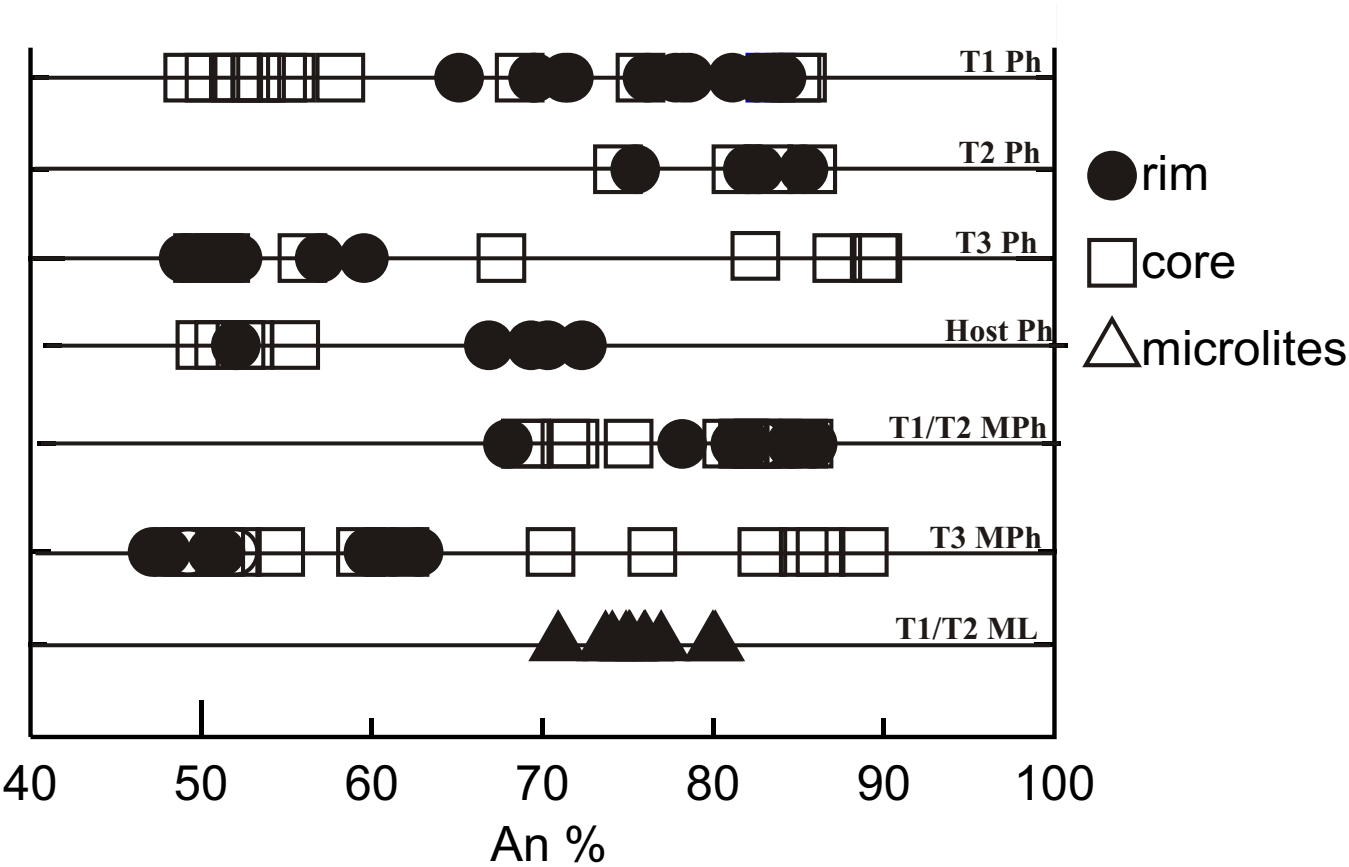
Figure 9. Microphotographs of notable minerals and microphenocrysts in T2 and T3 enclaves. A) High calcium, normally zoned plagioclase crystal with a sieve textured core observed in a T2enclave. B) Framework minerals of acicular amphibole and tabular plagioclase microphenocrysts observed in a T2 enclave. C) Magnesiohornblende microphenocrysts with an overgrowth rim and embayed plagioclase microphenocrysts observed in a T3 enclave.
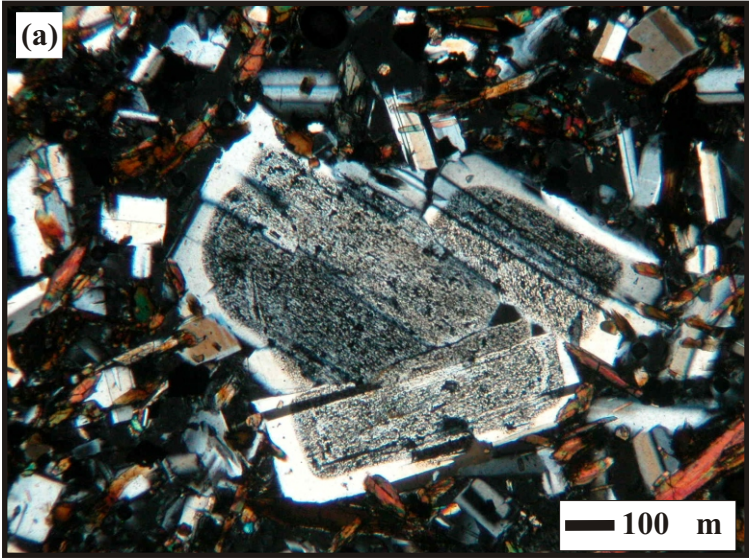
**Figure 9**
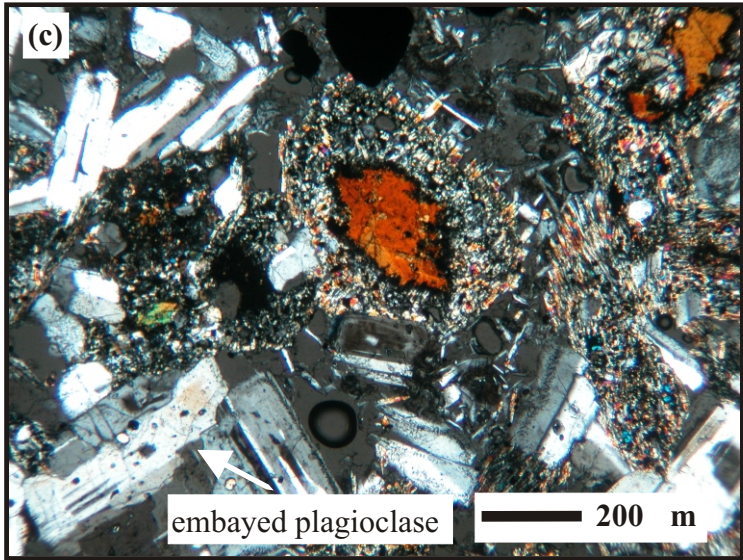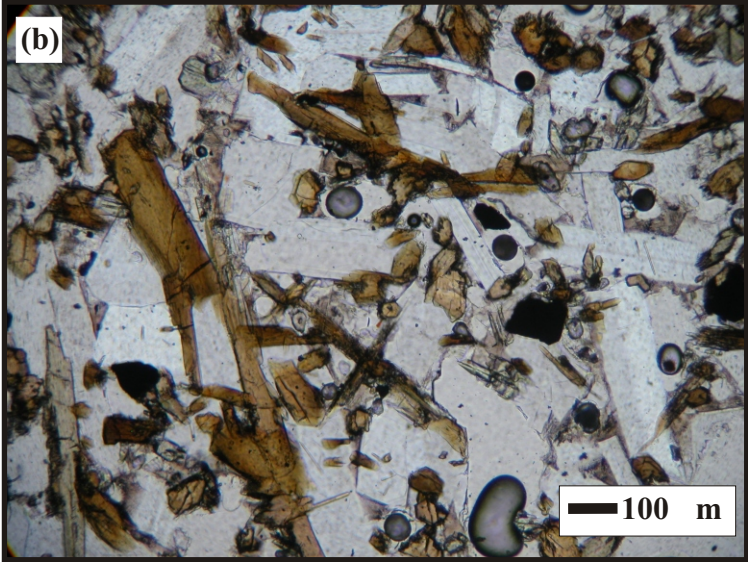
Figure 10. Amphibole compositions as a function of Si and Mg number. Ph= phenocryst;

MPh=microphenocryst; ML=microlites. Open green triangles = T1 phenocrysts; closed green

triangles = T1 microphenocryts and microlites; open red triangles = T2 phenocrysts,

microphenocrysts and microlites; open pink diamonds = T3 phenocrysts, microphenocrysts and

microlites; open red circle = andesite phenocrysts.
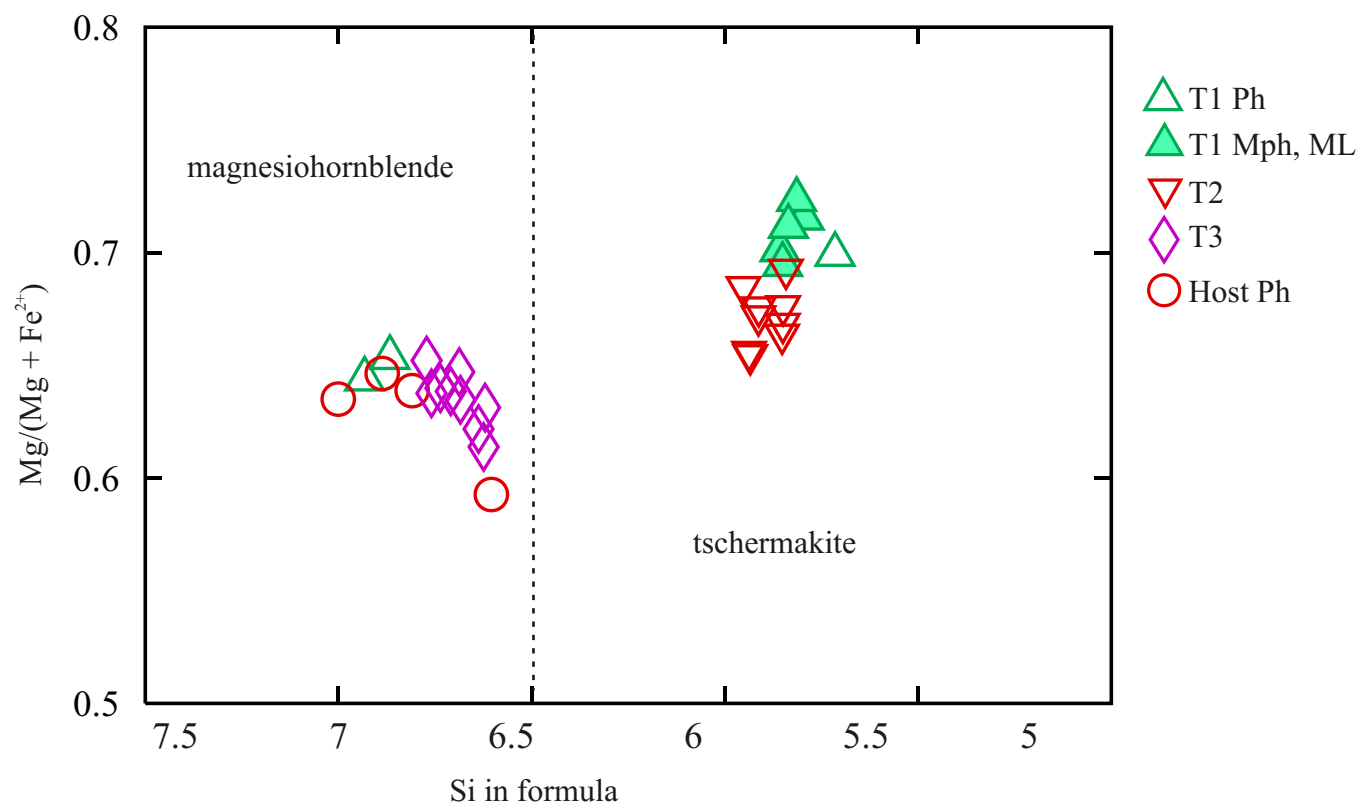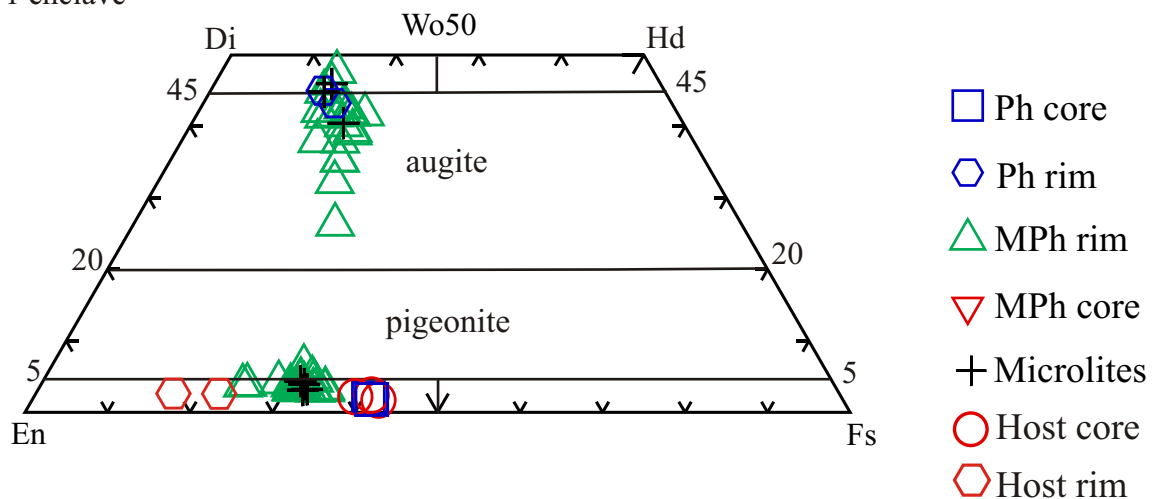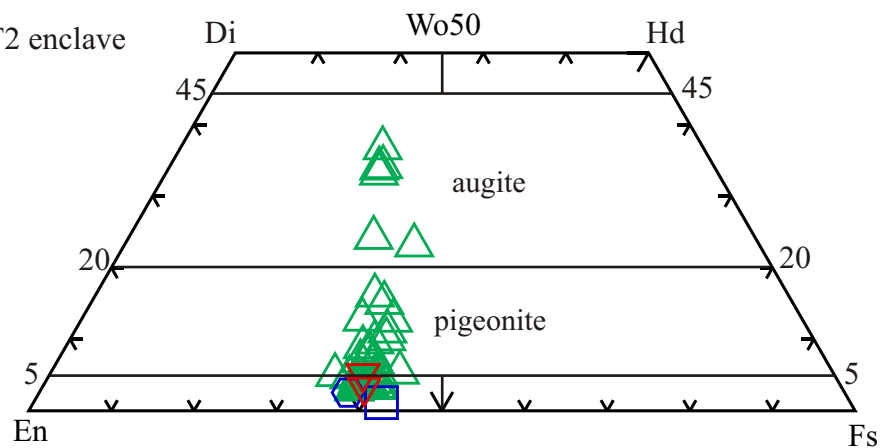
**Figure 10**

Figure 11. Pyroxene compositions. A) Type 1 enclave compositions; B) Type 2 enclave

compositions; C) Type 3 enclave compositions. Ph= phenocryst; MPh=microphenocryst;

ML=microlites. Open blue squares = phenocryst cores; open blue circles = phenocryst rims;

open green triangles = microphenocryst rims; open red triangles = microphenocryst cores; black

crosses = microlites; open red circles = andesite cores; open red hexagon = andesite rims.

**Figure 11**

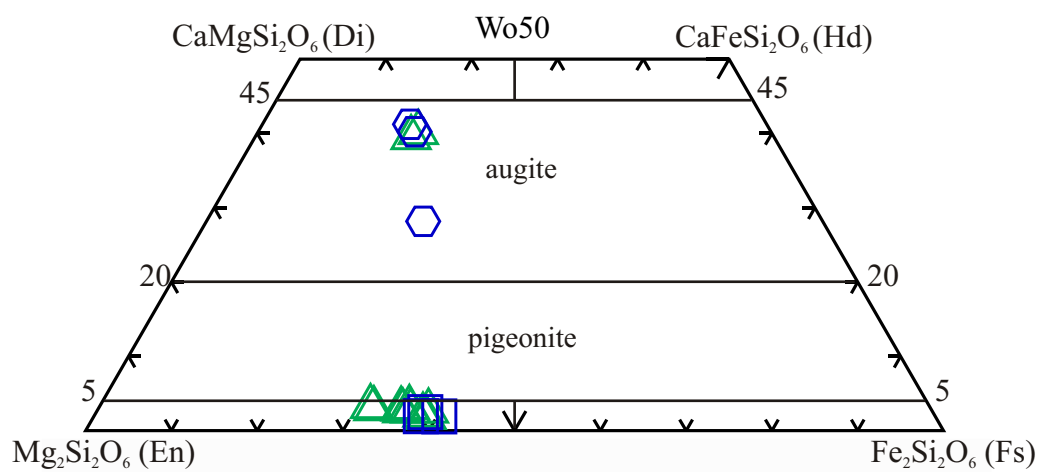A) T1 enclave



B) T2 enclave



C) T3 enclave

Figure 12. Fe – Ti oxide ternary compositions. Open green triangles = Type 1 enclave; open red triangles = Type 2 enclaves; open pink triangles = Type 3 enclaves; open red circle = andesite composition.
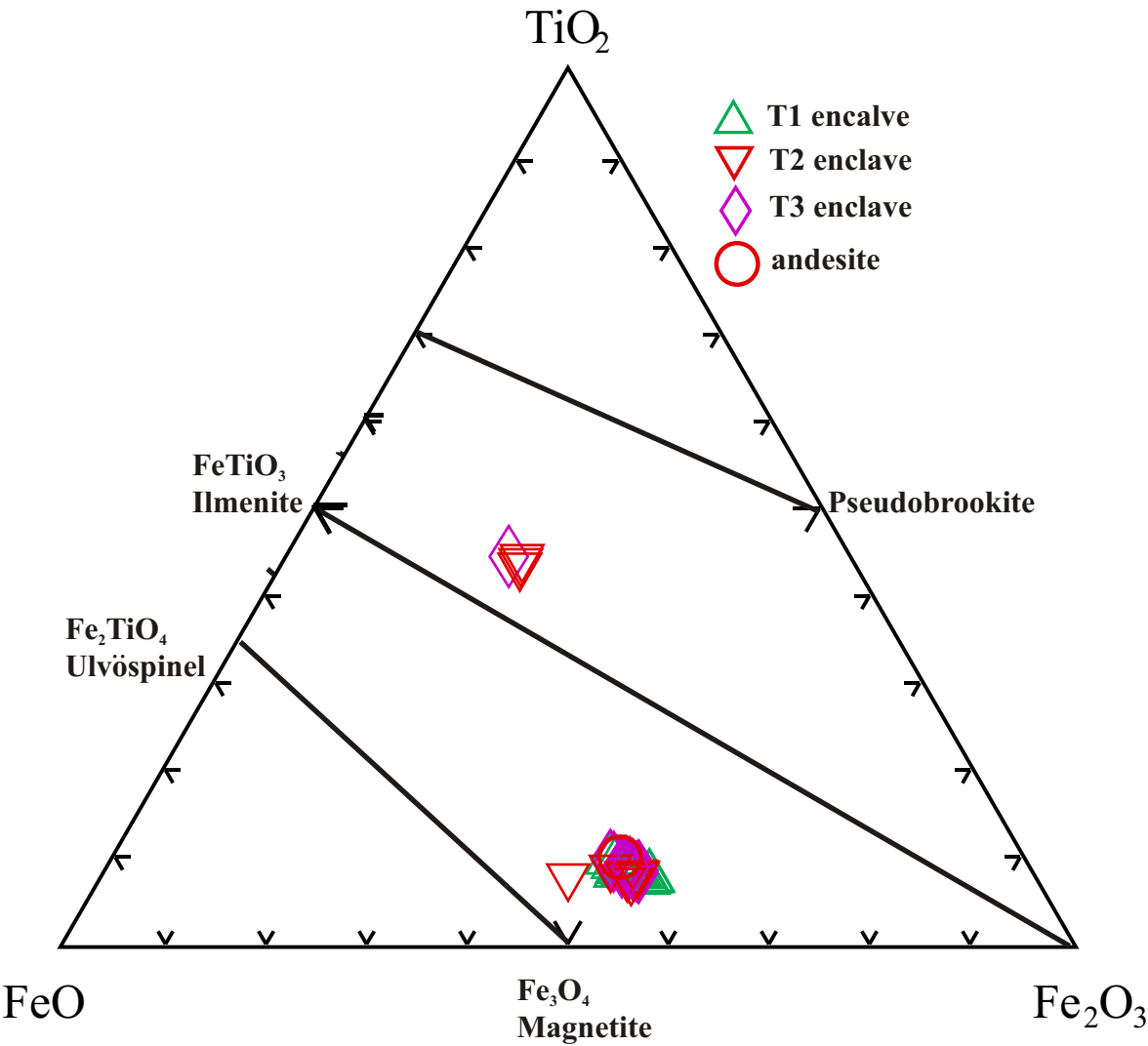
**Figure 12**

Figure 13. Bulk rock and matrix glass compositions for T1 and T2 enclaves. A) $SiO_2$ wt. % vs $K_2O$ wt. %; B) $SiO_2$ wt. % vs $TiO_2$ wt. %. The matrix glass compositions of the enclave matrix glass overlap those of the andesite. Black lines connect bulk rock with glass from same sample.
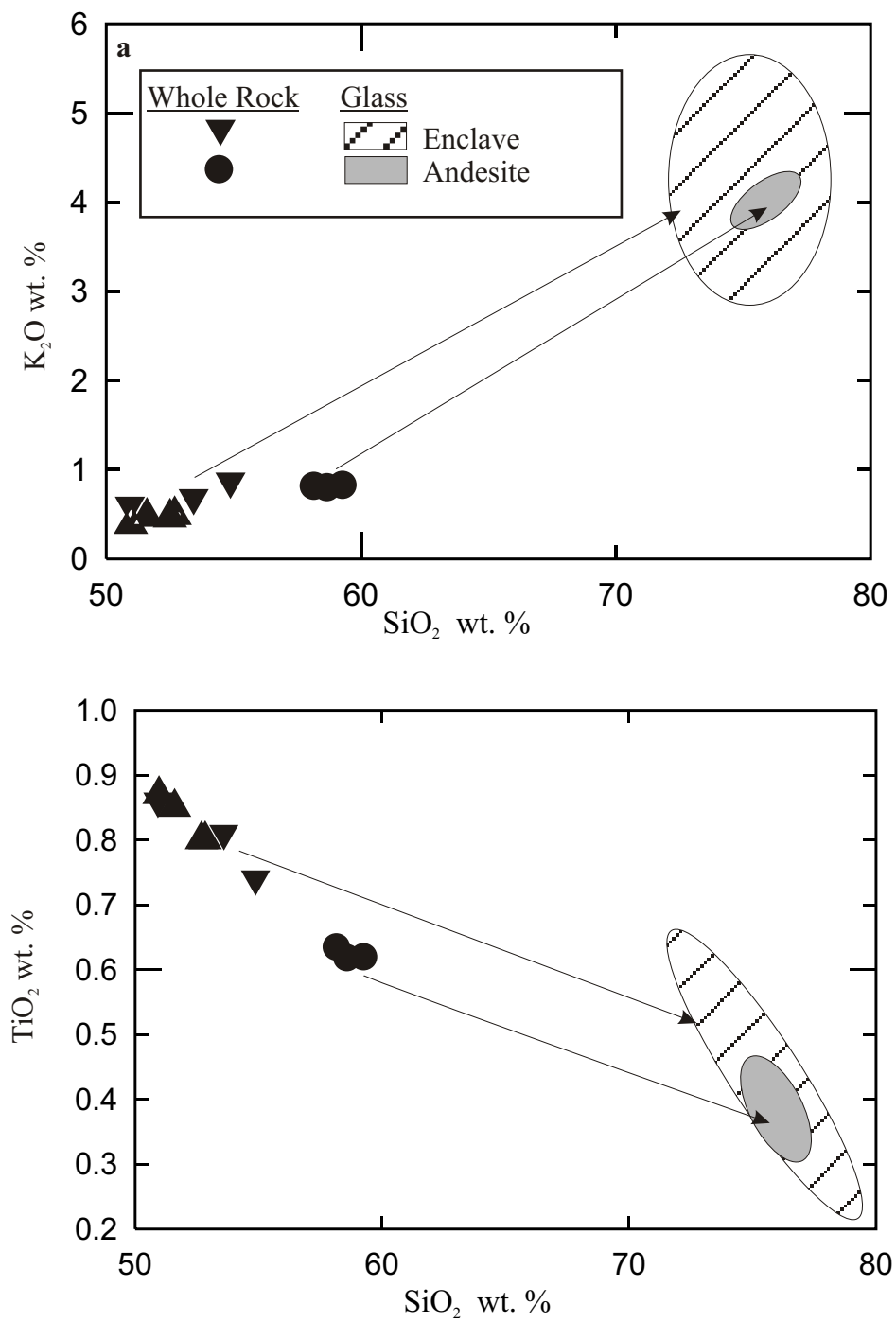
**Figure 13**

Figure 14. Enclave and host rock glass compositions of a T1 enclave. Each compositional pair (i.e. matrix glass and andesite glass) represent analysis at the enclave/andesite contact.

**Figure 14**
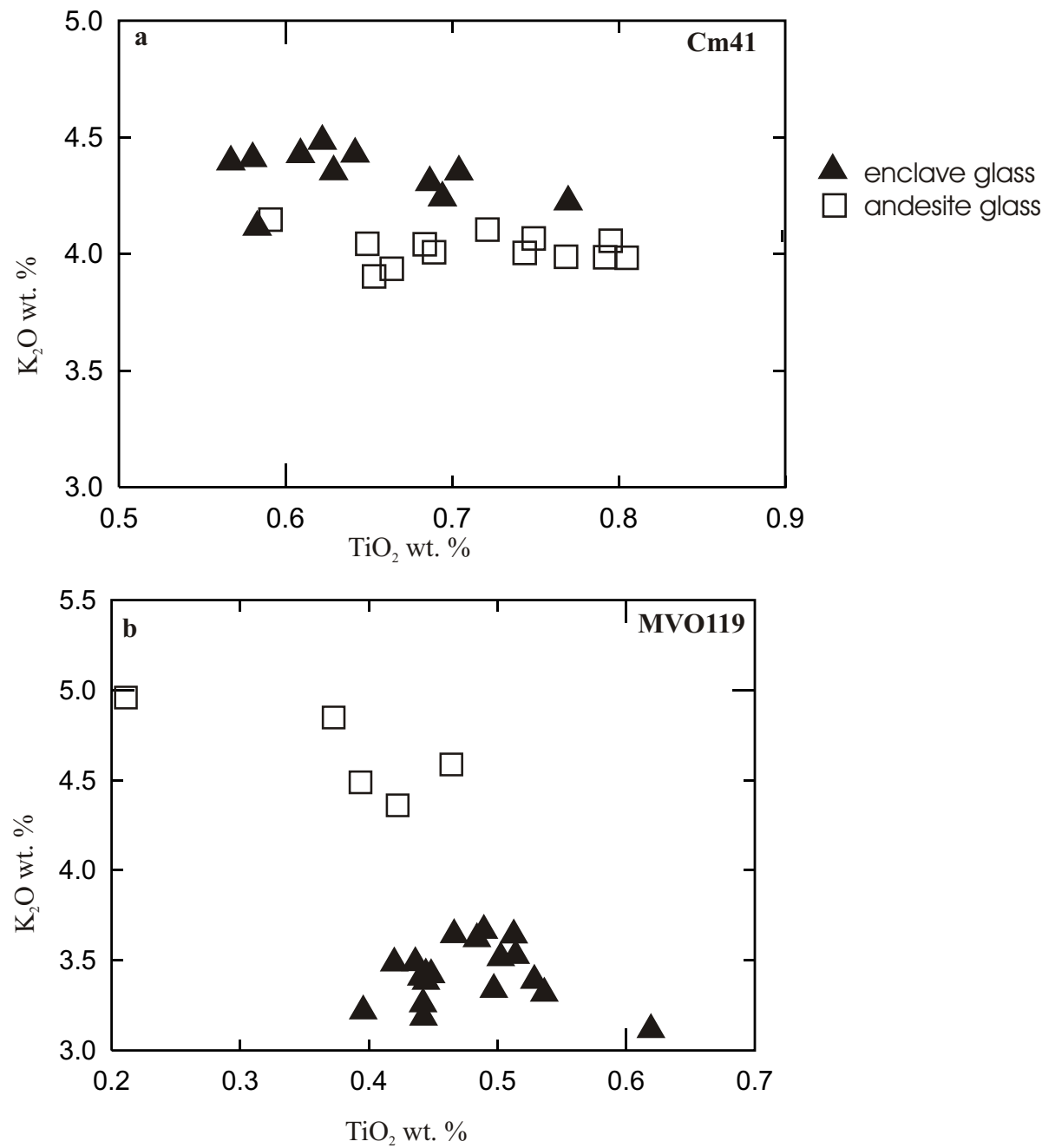
Figure 15. Magma mixing models for trace elements in the T1 and T2 enclaves. A) T1; B) T2.

The numbers represent the percentage of mafic magma relative to the andesite. Green triangles =

T1; red triangles = T2; red circles = andesite.
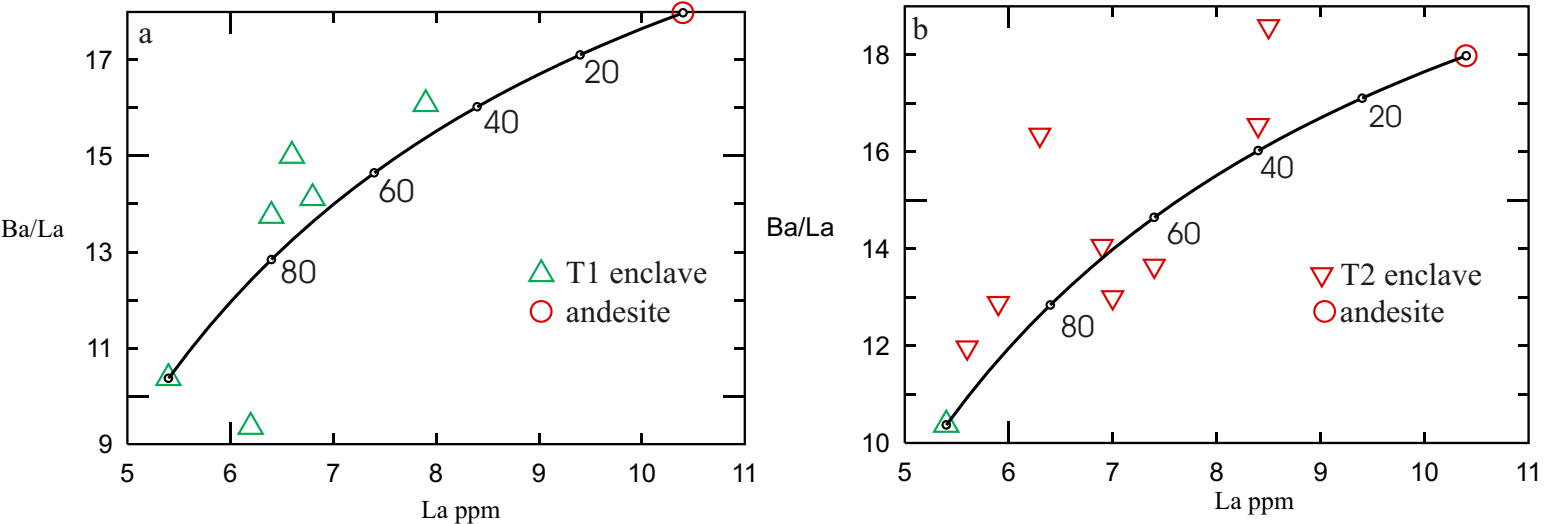
Figure 14

Figure 16. Trace element ratios to discriminate between garnet and amphibole fractionation. A) La/Yb vs $SiO_2$ wt. %; B) Dy/Yb vs. $SiO_2$ wt. % ; C) Dy/Yb vs La/Yb. Qualitative scale for comparison.
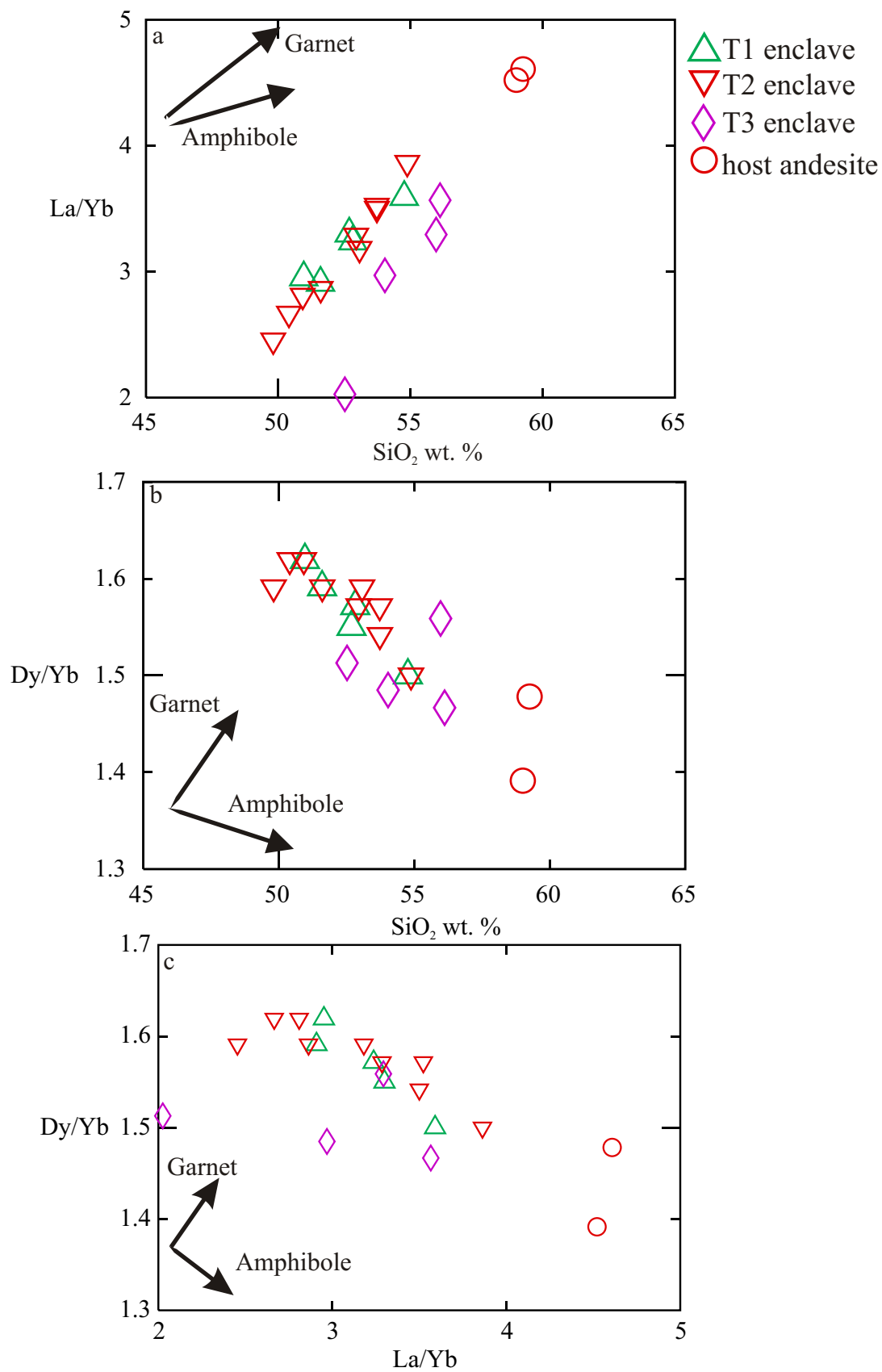
**Figure 16**

Figure 17. Model of mafic magma petrogenesis and enclave formation at the SHV.

A) 1) Upon ascent from the mantle wedge the basalt undergoes differentiation, fractionating amphibole at mid to deep crustal levels. As multiple diapers of differentiated basaltic liquid ascends towards the surface some 2) pond at the mid crust fractionating plagioclase and others 3) are intercepted by the andesitic magma reservoir A hydrous, high-alumina, plagioclase bearing basaltic magma intrudes into the base of an andesitic magma chamber. The basalt which ponds in the mid crust fractionating plagioclase forms the T3 enclave, while the differentiated basalt which intercepts the andesitic reservoir undergoes mixing forming the T1 and T2 enclaves. B) Upon intrusion the higher temperature basalt cools against portions of the andesitic host and begins to crystallize as the andesitic host heats. When the viscosities and densities are similar mixing takes place and crystallization of amphibole and plagioclase microphenocrysts ensues. During crystallization, volatiles become supersaturated forming bubbles which rise into the uppermost part of the mixing horizon. With enough bubbles they upper layer becomes buoyant and diapir of the bubble-rich crystallized framework form detaching from the mixing horizon, forming the T1 enclaves. B) The T2 enclaves represent hybrid magma just below the bubble horizon. Discrete enclaves are rigid and most likely form when subsequent intrusions disturb the mixing horizon causing overturn.

**Figure 17**



a

0 km

andesite magma reservoir

~5 km

~15 km

basaltic magma
reservoir crystallizing
mostly plagioclase

basaltic intrusion

② ③

deep crust

basaltic magma reservoir
crystallizing amphibole

①

b

T1 enclaves

mixing horizon

○○ bubbles ⦂⦂ crystals ▮ cooler
basalt temperature

c

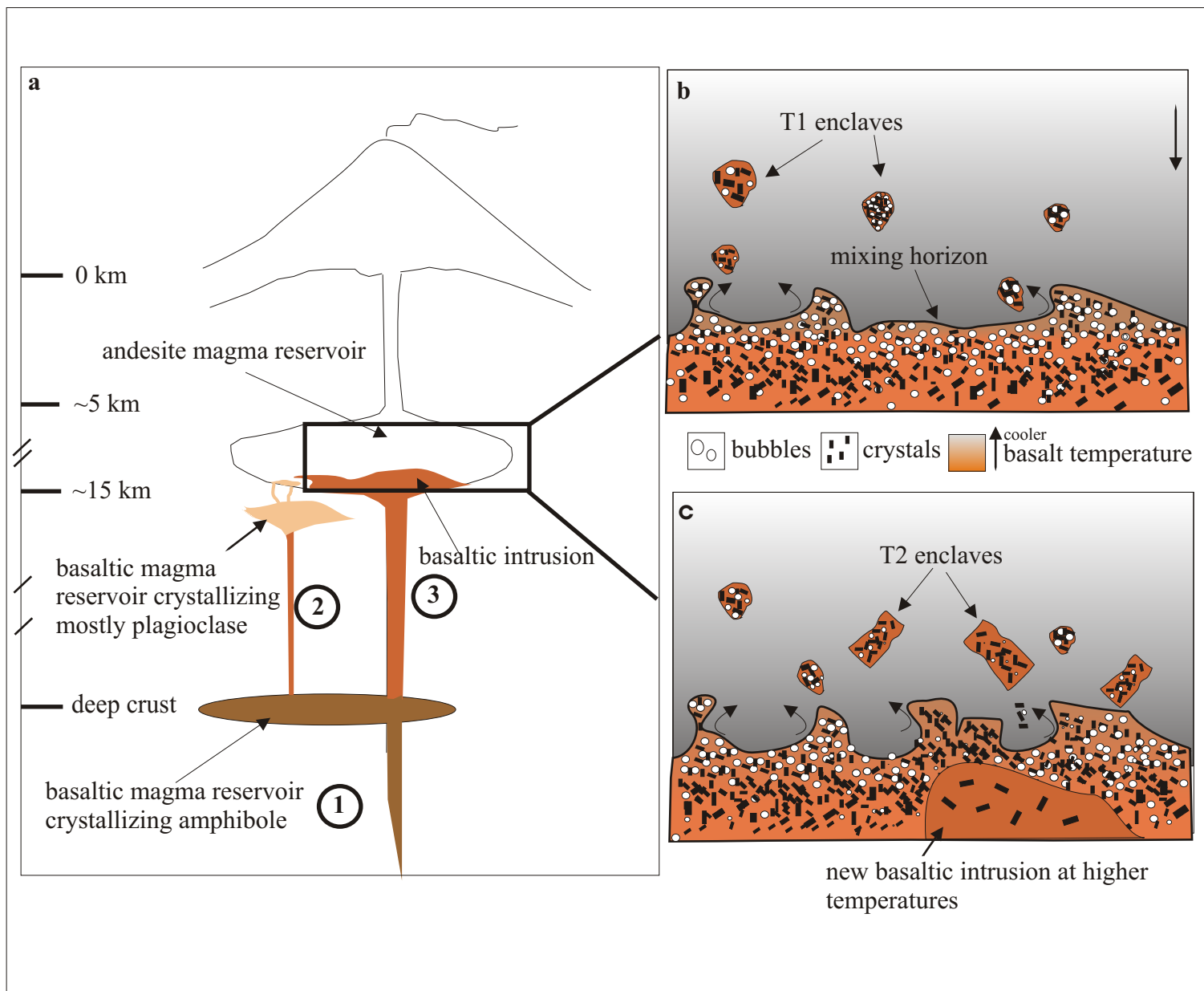T2 enclaves

new basaltic intrusion at higher
temperatures

Table 1: Comparison of accepted and observed values for whole-rock reference materials.

| Standard *References | UTR2 1 | UTR2 this study | SR7 2 | SR7 this study | MVO107 3 | MVO107 this study |
|---|---|---|---|---|---|---|
| *Wt %* | | | | | | |
| $SiO_2$ | 74.16 | 73.51 | 52.59 | 52.69 | 53.56 | 54.58 |
| $TiO_2$ | 0.24 | (0.51) | (0.23) | (0.29) | 0.71 | 0.74 |
| $Al_2O_3$ | 10.44 | 0.24 | 0.96 | 0.95 | 18.76 | 18.98 |
| $FeO^T$ | 4.43 | (0.01) | (0.01) | (0.00) | 8.37 | 8.23 |
| MnO | 0.09 | 10.66 | 14.09 | 14.06 | 0.19 | 0.19 |
| MgO | 0.05 | (0.36) | (0.03) | (0.11) | 3.74 | 3.60 |
| CaO | 0.18 | 4.09 | 7.67 | 7.79 | 9.33 | 9.15 |
| $Na_2O$ | 5.52 | (0.14) | (0.20) | (0.08) | 2.92 | 2.97 |
| $K_2O$ | 4.39 | 0.09 | 0.15 | 0.16 | 0.77 | 0.87 |
| $P_2O_5$ | 0.01 | (0.00) | (0.01) | (0.00) | 0.14 | 0.15 |
| | | 0.09 | 7.46 | 8.03 | | |
| Total | 99.51 | (0.06) | (0.08) | (0.33) | 99.51 | 100.4 |
| | | 0.31 | 8.26 | 7.95 | | |
| *ppm* | | (0.22) | (0.08) | (0.42) | | |
| Ba | n.d. | 5.51 | 2.81 | 2.84 | 127 | 158 |
| Cr | n.d. | (0.10) | (0.11) | (0.04) | <2 | 15 |
| Ni | 3 | 4.34 | 3.15 | 3.21 | 7 | 16 |
| V | n.d. | (0.20) | (0.02) | (0.02) | 142 | 171 |
| Ga | n.d. | 0.02 | 0.45 | 0.47 | n.d. | 18 |
| Nb | 91 | (0.00) | (0.02) | (0.00) | n.d. | 2 |
| Rb | 137 | | | | 14 | 15 |
| Sr | 1.4 | 98.86 | 97.59 | 98.15 | 278 | 274 |
| Zr | 1174 | | | | 73 | 81 |
| | | n.d. | 1395 | 1436 | | |
| | | 66 (6) | (51) | (132) | | |
| | | 6 (1) | 332 (13) | 420 | | |
| | | 3 (3) | 99 (9) | (119) | | |
| | | 31 (1) | 182 (4) | 111 (2) | | |
| | | 74 (6) | n.d. | 187 (1) | | |
| | | 130 (7) | 10 (1) | 16 (1) | | |
| | | 13 (25) | 78 (1) | 8 (1) | | |
| | | 1102 | 709 (3) | 77 (1) | | |
| | | (75) | 141 (7) | 694 (6) | | |
| | | | | 143 (5) | | |
| n | | 8 | 4 | 8 | 1 | 1 |

*References = (1) Stix et al., 1995; (2) Don Francis, personal communication; (3) Murphy et al., 2000.
Error is reported as 1σ; n = number of analyses; n.d. = not determined

Table 2: Statistical precision of glass standards used for electron microprobe analysis (EMPA).

| Session Date | 2 March 2006 | 2 April 2006 | 8 Dec. 2007 | 31 Dec. 2007 | 15 Jan. 2008 | 2 March 2006 | 8 Dec. 2007 | 31 Dec. 2007 | 15 Jan. 2008 | †Pooled dates | †Pooled dates |
|---|---|---|---|---|---|---|---|---|---|---|---|
| Standard | UTR2 | UTR2 | UTR2 | UTR2 | UTR2 | BMAK | BMAK | BMAK | BMAK | UTR2 | BMAK |
| *Wt %* | | | | | | | | | | | |
| SiO2 | 74.63 | 74.16 | 73.94 | 74.31 | 74.29 | 50.81 | 50.61 | 49.89 | 50.36 | 74.16 | 50.45 |
| TiO2 | (0.44) | (0.51) | (0.19) | (0.43) | (0.66) | 4.06 | (0.04) | (0.65) | (0.74) | (0.45) | (0.39) |
| Al2O3 | 0.22 | 0.22 | 0.22 | 0.22 | 0.21 | 12.10 | 4.04 | 4.13 | 4.11 | 0.22 | 4.08 |
| FeOT | (0.01) | (0.03) | (0.02) | (0.03) | (0.04) | 13.75 | (0.09) | (0.01) | (0.04) | (0.03) | (0.07) |
| MnO | 10.42 | 10.37 | 10.35 | 10.33 | 10.39 | 0.00 | 12.28 | 12.21 | 12.07 | 10.37 | 12.20 |
| MgO | (0.17) | (0.07) | (0.06) | (0.03) | (0.11) | 5.08 | (0.12) | (0.12) | (0.18) | (0.08) | (0.11) |
| CaO | 4.33 | 4.35 | 4.28 | 4.25 | 4.26 | 9.07 | 14.12 | 13.50 | 13.72 | 4.29 | 13.73 |
| Na2O | (0.06) | (0.12) | (0.11) | (0.14) | (0.12) | 3.16 | (0.26) | (0.28) | (0.23) | (0.12) | (0.22) |
| K2O | 0.01 | 0.08 | 0.07 | 0.05 | 0.08 | 0.82 | 0.21 | 0.10 | 0.18 | 0.058 | 0.18 |
| P2O5 | (0.02) | (0.03) | (0.05) | (0.02) | (0.03) | 0.35 | (0.02) | (0.00) | (0.08) | (0.03) | (0.01) |
| Total | 0.00 | 0.00 | 0.00 | 0.00 | 0.00 | | 5.13 | 5.12 | 5.16 | 0.00 | 5.15 |
| | (0.00) | (0.00) | (0.00) | (0.00) | (0.00) | | (0.03) | (0.02) | (0.04) | (0.00) | (0.03) |
| *ppm* | 0.18 | 0.22 | 0.18 | 0.15 | 0.19 | | 9.32 | 9.27 | 9.42 | 0.18 | 9.35 |
| Cl | (0.01) | (0.08) | (0.06) | (0.01) | (0.06) | 230 | (0.04) | (0.15) | (0.10) | (0.06) | (0.09) |
| | 5.79 | 5.79 | 5.83 | 6.01 | 5.85 | | 3.11(0.07) | 3.63 | 3.33 | 5.86 | 3.26 |
| | (0.01) | (0.23) | (0.13) | (0.15) | (0.13) | | 0.84 | (0.07) | (0.11) | (0.16) | (0.08) |
| | 4.33 | 4.44 | 4.33 | 4.39 | 4.34 | | (0.02) | 0.84 | 0.83 | 4.37 | 0.83 |
| | (0.03) | (0.05) | (0.05) | (0.05) | (0.07) | | 0.38 | (0.01) | (0.03) | (0.05) | (0.02) |
| | 0.00 | 0.00 | 0.00 | 0.00 | 0.00 | | (0.01) | 0.38 | 0.30 | 0.00 | 0.39 |
| | (0.00) | (0.00) | (0.00) | | (0.00) | | | (0.01) | (0.01) | (0.00) | (0.01) |
| | 2080 | 2078 | 2053 | 2017 (69) | 2156 | | 227 (12) | 197 | 265 | 2077 | 223 |
| | (26) | (58) | (78) | | (40) | | | (23) | (35) | (63) | (34) |
| N | 3 | 8 | 9 | 6 | 5 | 1 | 3 | 4 | 2 | 31 | 10 |

Note: We report the data as an average of repeat analysis on standards throughout individual analytical sessions. For published standard analysis see Dixon et al., 1991 (BMAK as A99) and Stix et al., 1995 (UTR2). Sulfur was analyzed but below detection limits and therefore not reported.

†All sessions are combined and a pooled error is calculated at 1σ; n = number of analyses; n.d. = not determined.

The pooled standard deviation is calculated according to,

$$S_p = \left( \frac{(n_1-1){s_1}^2 + (n_2-1){s_2}^2 + ...(n_k-1){s_k}^2}{n_1 + n_2 + ...n_k - k} \right)^{1/2}$$

where $S_p$ is the pooled standard deviation, $n_1$ is the sample size of the first sample, $s_1$ is the standard deviation of the first sample, and $k$ is the number of samples being comb

Table 3: Representative plagioclase analyses in host andesite lava.

| Sample Name | n | SiO$_2$ | Al$_2$O$_3$ | Fe$_2$O | MgO | CaO | Na$_2$O | K$_2$O | BaO | Total | An† |
|---|---|---|---|---|---|---|---|---|---|---|---|
| *CM119 (HPh2)* | | | | | | | | | | | |
| rim | 2 | *55.02* | 28.36 | 0.33 | 0.01 | 10.97 | 5.91 | 0.12 | 0.00 | 99.91 | 51 |
| core | 4 | *55.33* | 27.93 | 0.30 | 0.03 | 10.87 | 5.23 | 0.13 | 0.02 | 99.84 | 50 |
| *CM119 (HPh3)* | | | | | | | | | | | |
| rim | 2 | *50.00* | 31.31 | 0.64 | 0.04 | 14.95 | 2.92 | 0.06 | 0.00 | 99.93 | 72 |
| core | 6 | *54.05* | 28.36 | 0.35 | 0.02 | 11.67 | 4.71 | 0.10 | 0.00 | 99.29 | 55 |
| *CM119 (HPh4)* | | | | | | | | | | | |
| rim | 2 | *50.47* | 30.93 | 0.64 | 0.08 | 14.60 | 3.13 | 0.07 | 0.00 | 99.93 | 70 |
| core | 8 | *44.76* | 28.35 | 0.31 | 0.02 | 11.17 | 5.01 | 0.12 | 0.02 | 99.78 | 52 |
| *CM37 (HPh1)* | | | | | | | | | | | |
| rim | 3 | 51.16 | 30.53 | 0.52 | 0.08 | 13.83 | 3.44 | 0.09 | 0.03 | 99.69 | 66 |
| core | 5 | 54.79 | 28.07 | 0.31 | 0.02 | 10.94 | 5.04 | 0.13 | 0.02 | 99.32 | 52 |

n = number of analyses per single grain; † mol % An; HPh = host phenocryst

Diagram A) Determination of matrix glass devitrification
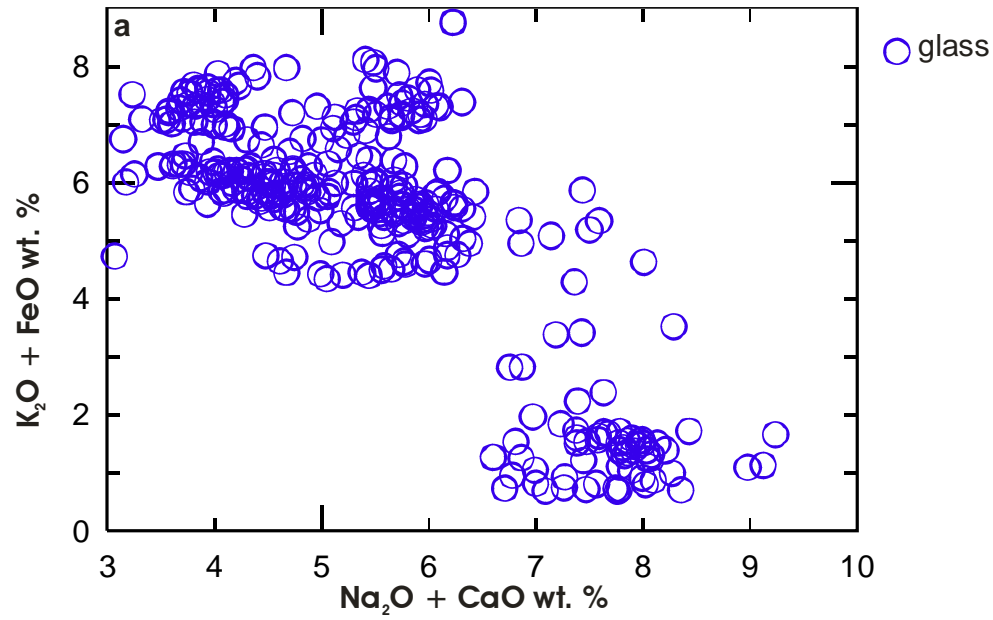


A) Mafic matrix glass populations. Non-devitrified glass (real glass) is high in K2O and FeO while the devitrified glass is high in Na2O and CaO.

**Link to Chapter 2**

In Chapter 1 we established the significance of the mafic enclaves and their petrogenesis. We determined that the mafic magma undergoes significant fractionation of amphibole at deep crustal levels. As the fractionated basaltic liquid rises from depth, some batches pond at shallower levels and undergo fractionation of plagioclase, while other batches intrude the andesitic reservoir. Once the mafic magma intrudes the shallow reservoir, it interacts with the andesitic magma at a mixing horizon. The enclaves form and detach from this horizon due to volatile driven buoyancy and subsequent intrusions of more mafic magma, while the shallowly ponded magma intrudes the reservoir but demonstrates only mass transfer of crystals. The mafic magma contributes heat and mass to the andesitic reservoir, but to understand the volatile contributions, we must also know the volatile contents of the host andesite. In Chapter 2 we measure volatile concentrations of the andesite magma. We analyze phenocryst hosted melt inclusions from vulcanian pumice to establish 1) which volatiles are present, 2) their concentrations, and 3) the model that best describes their entrapment.

**Chapter 2**

**Phenocryst hosted melt inclusions mirror conduit and upper magma reservoir conditions during vulcanian explosions, Soufrière Hills volcano, Montserrat, West Indies**

Crystal P. Mann, Paul Wallace and John Stix

**Submitted to Bulletin of Volcanology.**

## Abstract

The mechanics of explosive eruptions influence ascent pathways of magmas. Vulcanian explosions are a stop – start mechanism which recur on timescales of hours to days evacuating the uppermost portions of the conduit. During the repose time between explosions, magma rises from depth and refills the conduit and stalls until the overpressure is sufficient to generate another explosion. Aliquots of liquid trapped during crystal growth record melt compositions at the time of entrapment prior to eruption. We analyzed major elements, Cl, $H_2O$ and $CO_2$ in plagioclase-hosted melt inclusions, sampled from pumice erupted during four vulcanian events at Soufrière Hills volcano, Montserrat, to determine magma compositions prior to eruption. Using Fourier Transform Infrared Spectroscopy we measure up to 6.74 wt. % $H_2O$ and < 80 ppm $CO_2$. Of 42 melt inclusions, 81% cluster between 2.8 to 5.4 wt. % $H_2O$ (57 to 173 MPa or 2 – 7 km) representing lower conduit/upper magma reservoir conditions. We suggest two models to explain the magmatic conditions prior to eruption: Model 1: Melt inclusions are trapped during crystal growth in magma stalled in the lower conduit/upper magma reservoir undergoing closed system degassing with up to 1 wt. % vapor in the melt. Model 2: melt inclusions are originally trapped at deeper levels of the magma chamber recorded by the high chlorine contents (2520 – 3270 ppm). During vulcanian explosions, the magma ascends and undergoes multi-step decompression. During decompression the water diffusively re-equilibrates with the surrounding liquid. Hence the melt inclusions record re-equilibration depths within the lower conduit/upper magma reservoir.

**Introduction**

Dissolved volatiles ($H_2O$, $CO_2$, S, Cl and F) comprise only several weight percent of magma, yet volatile exsolution and expansion of the vapor phase provides the major driving force for magma ascent and explosive eruptions. Differences in eruptive style are controlled by the exsolution of dissolved volatiles and crystallization due to undercooling of the liquid, which when coupled have a major effect on magma rheology. Modeling these coupled mechanisms with gas escape places constraints on the main parameters that control these different processes and the transitions between eruptive styles (Eichelberger et al. 1986; Jaupart and Allègre 1991). However, a large number of parameters cannot be measured directly in natural systems (e.g., viscosity, kinetics of crystallization, conduit diameter, magma reservoir overpressure and magma reservoir depth, to cite several). Therefore, knowing the concentration of dissolved volatiles and their associated liquid compositions provides useful information with respect to the magma's ascent path to the surface.

Quenched glassy melt inclusions trapped in phenocrysts provide reliable estimates of liquid (melt) evolution over time. These aliquots of liquid are trapped in phenocrysts during crystal growth recording liquid compositions and volatile contents at that time. Interpretation of melt inclusion compositions have associated difficulties and uncertainties, yet melt inclusions trapped at different times during evolution of a magma body can provide insight into the changing magma system (e.g., Lowenstern 1995;Wallace et al. 1999; Danyushevsky et al. 2002; Metrich and Wallace 2008).

The current eruption of the Soufrière Hills volcano (SHV), Montserrat, has exhibited a wide variety of eruptive styles and eruptive products: phreatic to phreatomagmatic explosions, lava dome extrusion, dome collapse and sub-plinian to vulcanian explosive eruptions (Robertson et al. 2000). Vulcanian explosions are common following a large dome collapse and can demonstrate

periodicity, with regular explosions on the orders of hours to days following the collapse (Druitt et al. 2002; Edmonds et al. 2006; Herd et al. 2005; Voight et al. 1999). Here, we present the volatile ($H_2O$, $CO_2$, Cl) and major element compositions of phenocryst-hosted melt inclusions from a suite of samples erupted from the SHV during vulcanian explosions from 1997 to 2004. We aim to use the variability observed in these volatiles to assess pre-eruptive magmatic conditions (i.e., pressure and depth). Based on our results, we present two models of magma storage appropriate for SHV.

**Explosive activity at the Soufriere Hills volcano**
The island of Montserrat, located in the northern section of the Lesser Antilles volcanic chain, comprises three volcanic massifs, the youngest of which is the South Soufrière Hills-Soufrière Hills complex beginning at ~230 ka (Harford et al. 2002). On 18 July 1995, after ~350 years of quiescence, phreatic explosions opened a new vent at the SHV (Young et al. 1998). The eruption is still ongoing at the time of writing (August 2010).

We focus on vulcanian explosions which took place immediately after dome collapse. In 1997, ~13 hours after dome collapse, a series of 13 vulcanian explosions occurred from 4 – 12 August 1997, and ~20 hours after dome collapse, another series of 75 vulcanian explosions took place from 22 September to 21 October 1997 (Druitt et al. 2002; Robertson et al. 2000). In 2003, a series of 5 vulcanian explosions took place from 13 – 15 July, the first during the final stages of dome collapse and the other four immediately afterwards (Edmonds et al. 2006). On 3 March 2004, one explosion occurred immediately after dome collapse followed by another smaller event on 5 March 2004 (G. Ryan, personal comm.).

*Working model of vulcanian explosions at the Soufrière Hills volcano*

Vulcanian explosions are short (seconds to minutes), discrete, small volume explosions ($<10^8$ $m^3$) (Morrissey and Mastin 2000), often occurring as pulsatory events. Vulcanian explosions occur when the conduit is suddenly decompressed, such as after dome collapse or when gas overpressure in a rising magma reaches a threshold value (Druitt et al. 2002; Robertson et al. 1998). During decompression, a fragmentation wave propagates down the conduit, tapping magma to depths of 0.5 to 2 km in a few tens of seconds and discharging an average volume of 3 x $10^5$ $m^3$ DRE (Clarke et al. 2007; Druitt et al. 2002; Melnik and Sparks 2002). Repetitive explosions are triggered when the critical gas overpressure (typically a few MPa at a few hundred meters depth) is exceeded within growing bubbles in [rapidly] rising magma between explosions (Melnik and Sparks 2002). After the initial explosion, the conduit refills and forms an impermeable plug at the top. Magmatic volatiles accumulate below this plug; when the conduit overpressure exceeds the strength of the surrounding rock, the plug fails resulting in another explosion (Druitt et al. 2002; Self et al. 1979; Voight et al. 1998). It is common to observe the eruption column collapse into a fountain to generate pumice flows (Druitt et al. 2002). Magmatic products from the explosions include ash, ballistic clasts, conduit rock and pumice, which vary in density and vesicularity.

## Methodology

*Sampling*

Due to their rapid cooling upon eruption, the pumice clasts are likely to preserve glassy phenocryst-hosted melt inclusions that are representative of the pre-ascent magma compared to samples from slowly-cooled dome rock. We chose a subset of pristine pumice clasts sampled from the four events described in the previous section: the 4-13 August 1997 series, 22

September to 21 October 1997 series, 12 -15 July 2003 series, and the 3 March 2004 series, for a

total of 5 samples (Fig 1a).

*Melt inclusion selection and preparation*
Melt inclusions from plagioclase and a single quartz phenocryst were analyzed for $H_2O$ and $CO_2$

by Fourier Transform Infrared Spectroscopy (FTIR) and for major elements, Cl, F and S by

Electron Microprobe Analysis (EPMA). Although the pumice phenocryst assemblage also

contains amphibole, orthopyroxene, and Fe-Ti oxides (Murphy et al. 2000), plagioclase was the

best choice for melt inclusion studies. Inclusions in the amphiboles were small (<10 um in

diameter) (Buckley et al. 2006), making them unsuitable for FTIR analysis, whereas

orthopyroxene, Fe-Ti oxides and quartz are present  in small quantities (< 5  %).

Sample preparation techniques for FTIR are described in detail by Wallace et al. (1999).

Samples were lightly crushed and sieved, and plagioclase phenocrysts were separated by hand

under a binocular microscope. The phenocrysts were hand picked in a refractive index liquid to

screen for cracks and re-entrant or hourglass features. Phenocrysts were mounted in Crystalbond

509 (an adhesive soluble in acetone) and polished on both sides. In the case of the smaller melt

inclusions, many of the plagioclase wafers were intersected on only one side. We do not consider

this to be a problem because the molecular $H_2O$ peak of interest (3550 $cm^{-1}$) is not overlapped by

any Si-O or Al-O peaks in plagioclase (1600 $cm^{-1}$, 1800 $cm^{-1}$). Inclusion thickness was measured

by mounting the edge of the doubly polished plagioclase wafer onto a needle using epoxy and

immersing the wafer in a pool of refractive index liquid. The crystal was then rotated and viewed

parallel to its flat side under a microscope with a calibrated eyepiece, allowing for a direct

measurement of thickness.

We chose melt inclusions that were wholly enclosed (i.e., no cracks or re-entrant features;

Blundy and Cashman 2005; Humphreys et al. 2008). The melt inclusion shapes range from

negative crystal shapes to ellipsoids ranging in size from 15 μm to 50 μm with an average size of

~ 30 μm (Fig 1b). We analyzed melt inclusions that were found both in the crystal core and

closer to the rim. Some phenocrysts contain more than one melt inclusion. The melt inclusions

were pristine, clear and glassy with the exception of one which was brown and glassy. All

plagioclase-hosted melt inclusions contained small shrinkage vapor bubbles (Fig 1b).

Following FTIR analyses, a subset of the plagioclase-hosted melt inclusions and one quartz-

hosted melt inclusion were analyzed by EMPA. To accomplish this, the plagioclase wafer was

mounted onto double-sided sticky tape and placed in epoxy (Araldite 502). Once hardened, the

mount was polished first with 6 μm and then 1 μm diamond paste to remove tape resin and

expose the melt inclusion.

*Fourier Transform Infrared Spectroscopy*
Transmission infrared spectra of the melt inclusions were obtained using a Thermo Nicolet

Nexus 670 Fourier-Transform Infrared Spectrometer (FTIR) interfaced with a Continuum IR

microscope at the University of Oregon. The FTIR has a globar source, an extended KBr

beamsplitter and a liquid nitrogen-cooled MCT-A detector. The infrared beam was directed

through an adjustable aperture and manually focused on the melt inclusion. Band assignments for

dissolved water and carbon dioxide in rhyolitic glass were taken from Newman et al. (1986) and

Newman et al. (1988), respectively. Water is present as molecular $H_2O$ at 5200 cm$^{-1}$, as OH$^-$ at

4500 cm$^{-1}$ and as total $H_2O$ at 3550 cm$^{-1}$. When observed, the molecular $CO_2$ peak at 2350 cm$^{-1}$

is distinct from the spectrum of peaks which indicate gaseous $CO_2$, as is sometimes found in

pressurized bubbles (Fine & Stolper, 1985). Absorption (peak heights) were measured using

Omnic software in all cases where the peak could be distinguished from background. As most of

the melt inclusions analyzed in this study were thin, molecular $H_2O$, OH$^-$ and $CO_2$ were difficult

to distinguish from spectral noise, and only the height of the total water peak at 3550 cm$^{-1}$ was

measured. Total amounts of dissolved water and $CO_2$ concentrations were calculated from peak heights using the Beer-Lambert Law: $C = (mw)(abs)/\rho d\varepsilon$, where C is the concentration in weight fraction of the absorbing species, mw is the molecular weight of the volatile species (18.02 for total $H_2O$ and 44.00 for $CO_2$), abs is the absorbance, $\rho$ is the density of the glass, d is the inclusion thickness (pathlength), and $\varepsilon$ is the molar absorptivity coefficient. Glass densities were calculated from the compositions of the melt inclusions (Skirius, 1990) starting with an anhydrous density of 2400 kg m$^3$ and the molar absorption coefficients were calculated for the 3550 cm$^{-1}$ peak starting with an absorptivity of 80 m$^3$mol$^{-1}$ (Leschik *et al.*, 2004). The molar absorption coefficient for $CO_2$ was taken from Behrens et al. 2004 (Behrens *et al.*, 2004)**.** The accuracy of the results from FTIR analysis is limited primarily by 1) the accuracy of the peak height measurement which decreases with decreasing inclusion thickness and 2) inclusion thickness measurements. For $H_2O$ we calculate a precision of better than 5 wt. % (1$\sigma$) based on a minimum of two repeat measurements on the same melt inclusion. For $CO_2$ we calculate a precision of better than 22 % ppm (1$\sigma$). Thickness measurements are considered accurate to $\pm$ 3 $\mu$m. We report a total error of $\pm$ 10% water and $\pm$ 28 % $CO_2$ for all melt inclusion analyses.

*Electron Microprobe Analyses*

A subset of the phenocryst-hosted melt inclusion glasses were analyzed by electron microprobe analyses (EPMA). We analyzed major elements, Cl, F and S at McGill University using a JEOL JXA-8900 electron microprobe with five wavelength dispersive spectrometers. Operating conditions were an accelerating voltage of 15 kV, a beam current of 10 nA and a beam diameter of 15 $\mu$m. For calibration, a series of glass standards were chosen which correspond closely to major element compositions of the melt inclusion glass. Silica, Al, Na and K were calibrated with a hydrous synthetic standard (M6N), Fe with UTR2, and Mg, Ca, Ti and P with BMAK. Mn was calibrated with spessartine, Ba with Ba-rich alkali feldspar, Cl with KN9 (3100

ppm Cl), S with a pyrrhotite standard (#507: 38.25 wt. % S) and F with fluorite (48.66 wt % F).

Analytical techniques were optimized to minimize loss of sodium while at the same time

ensuring good precision (Supplementary data A). Elements were analyzed in the same order and

for the same length of time for both standards and unknowns. For analysis of chlorine, fluorine

and sulfur, we increased the count times to improve statistical precision. The counting times for

S (100 seconds), Cl (100 seconds) and F (500 seconds) reduced detection limits to between 138

and 144 ppm for S, 67 to 69 ppm for Cl and 191 to 201 ppm for F. Each glass spot was analyzed

once and the ZAF correction model applied. For major elements, precision for Si is better than

0.3 %, Al, Ti, Ca, Mg and Fe are better than 0.5 %, K is better than 1 % Na is better than 5, P is

better than 6 % and precision for Ba is better than 1 %. Precision for Cl is better than 2 %. S and

F were close to detection.

Using detailed back-scattered electron imaging (BSE) we looked for signs of post entrapment

crystallization (PEC) (Humphreys et al. 2010). We observed no change in color contrast (i.e.

dark rind of sodic plagioclase or a lighter rind of calcic plagioclase) around the edge of the melt

inclusions and consider changes in melt composition due to PEC negligible.

## Results

*Dissolved $H_2O$ and $CO_2$ concentrations*

We report $H_2O$ and $CO_2$ concentrations from 42 melt inclusions analyzed by FTIR.

Dissolved $H_2O$ concentrations from the phenocryst-hosted melt inclusions (39 from plagioclase

and 3 from quartz) range from 1.2 wt. % to 6.7 wt. % $H_2O$ (Fig 2a). $CO_2$ concentrations are < 80

ppm as measured in a total of 4 melt inclusions and below detection in 38 melt inclusions (Fig

2b). Most melt inclusions (81%) have $H_2O$ contents between 2.8 and 5.4 wt. % $H_2O$. We

interpret the low $CO_2$ contents to reflect both partial degassing of the melts before inclusion

entrapment, which would affect low solubility $CO_2$ much more than $H_2O$ and Cl, and post-entrapment loss of $CO_2$ to shrinkage bubbles (e.g., Metrich and Wallace, 2008).

Devine et al. (1998) used the volatile-by-difference method (100 wt. % minus the analytical total equals the volatile content (VBD)) to estimate $H_2O$ contents from pumice explosively erupted in September of 1996. They report an average of 4.7 wt. % $H_2O$ for 26 plagioclase-hosted melt inclusions and 3.7 wt. % $H_2O$ for 2 quartz-hosted melt inclusions. Barclay et al. (1998) analyzed 6 quartz-hosted melt inclusions by FTIR and report an average of $4.3 \pm 0.5$ wt. % $H_2O$ and $CO_2$ contents of < 50 ppm $CO_2$ in 2 melt inclusions (total error of 12.5% which includes thickness measurements and background fitting procedure). Buckley et al. (2006) report VBD totals from 4 hornblende-hosted melt inclusions that range from 3.8 - 8.3 wt. % $H_2O$ in a sample which was erupted 1 on March 1999.

We compare volatile contents from different eruptions and include a sample from 17 September 1996 by Barclay et al. (1998). The highest $H_2O$ concentrations and the broadest range of $H_2O$ contents are observed in pumice from August 1997, but all the vulcanian events show overlap in water contents (Fig 3). The $H_2O$ and $CO_2$ contents we measure show good agreement with previous studies (Fig 2a, b; Supplementary data Table 1 and Table 2).

*Chlorine contents*

Chlorine was analyzed by EPMA in one quartz hosted melt inclusion and 10 plagioclase-hosted melt inclusions. (Supplementary data Table 3) Chlorine content of the quartz-hosted melt inclusion is 2520 ppm Cl, while the chlorine contents in the plagioclase-hosted melt inclusions cluster from 2855 ppm to 3270 ppm Cl (Figure 4). Fluorine and S were below detection.

*Major element compositions*

Plagioclase-hosted melt inclusion compositions range from 72.8 - 76.2 wt. % SiO2 (anhydrous). One analysis of a quartz-hosted melt inclusion indicates a composition of 78.7 wt. % SiO2 (anhydrous). Na2O, CaO, and Al2O3 decrease with increasing SiO2. TiO2 and FeO decrease slightly and MgO is nearly constant at ~ 0.3 wt. %. The quartz phenocryst contains the lowest values of $Al_2O_3$, CaO and $K_2O$ and one of the lowest $Na_2O$ concentrations. The role of $K_2O$ is complicated in the SHV magmatic system (Harford et al. 2003; Humphreys et al. 2010; Mann and Stix 2010). Due to the absence of a potassic phase in the crystallizing assemblage, $K_2O$ is considered an indicator of melt evolution as a result of crystallization. However, in this study we observe $K_2O$ as slightly compatible trending towards lower $K_2O$ in the quartz-hosted melt inclusion (Fig 5). Diffusive exchange of $K^+$ from the mafic enclave glass to the rhyolite is observed at the SHV, but the low $K_2O$ concentrations in this study are most similar to the endmember rhyolite which has not been enriched in $K_2O$ (Humphreys et al. 2010). $K_2O$ constitutes ~ 0.1 – 0.2 wt. % of plagioclase and ~ 0.1 - 0.2 wt. % of amphibole phenocrysts (Mann and Stix 2010; Murphy et al. 2000), therefore we follow Harford et al. (2002) and suggest that the slight compatibility comes from some incorporation of K into these phases.

**Discussion**

The phenocryst-hosted melt inclusions are $H_2O$- and Cl-rich rhyolitic melt inclusions (Supplementary data Table 3). The phenocryst hosted melt inclusions from 1996 to 2004 are rhyolitic in composition, with a significant cluster (81 %) having 2.8 - 5.4 wt. % $H_2O$, low $CO_2$ (4 of 42 melt inclusions), and high and similar chlorine contents from 2855 – 3270 ppm Cl.

*Post entrapment processes*

Before interpreting magmatic processes, we assess the melt inclusions in terms of post-entrapment modification. We consider diffusive re-equilibration to be the most important

(Metrich and Wallace 2008). Diffusive re-equilibration of $H^+$ can take place from the host crystal to the surrounding magma depending on 1) the species diffusion coefficient, 2) the partition coefficient of the species between the crystal and liquid, 3) the temperature, and 4) the ratio of melt inclusion size to host (Qin et al. 1992). Quartz hosted melt inclusions from the early-erupted stage of the Bishop Tuff with ~ 5.5 wt.% $H_2O$ were heated to 800ºC and 100 MPa for 4 to 1512 hours; after 24 hours water contents decreased by ~ 1 wt. % $H_2O$, after 48 hours by ~ 2 wt.% $H_2O$, and after 168 hours by ~ 3.5 wt.% $H_2O$ (Severs et al. 2007). Vapor bubbles in melt inclusions can form due to shrinkage during cooling or due to diffusive loss of molecular $H_2O$ (Severs et al. 2007). All of our plagioclase hosted melt inclusions have vapor bubbles; therefore, we cannot rule out diffusive re-equilibration.

*Pressure and depth determinations*

Volatile solubility is weakly dependent on temperature, hence we consider a range of temperatures determined for SHV magmas. Phase equilibrium studies place a minimum temperature of 780ºC for the magmatic system due to the observed absence of biotite in the crystallizing assemblage and a maximum temperature of 850 ºC based on the stability of amphibole at 130 MPa (Barclay et al. 1998; Couch et al. 2003a; Rutherford and Devine 2003). Mafic enclaves suggest the presence of a more mafic contribution and thus a localized increase in temperature to ~ 900 °C (Murphy et al. 2000; Mann et al. 2010). Therefore we calculate the effect of temperature at 780°C, 850° and 900°C (Supplementary data Table 4). We determine that an increase in temperature of 120 ºC has a relatively small effect on pressures calculated from measured volatile contents. For example, an increase in temperature from 780 to 900 ºC, at water contents of ~ 3 wt. % $H_2O$, only increases the calculated pressure from 55 to 66 MPa. At water contents of ~ 7 wt. % $H_2O$, calculated pressure increases from 231 to 251 MPa. The increase in pressure at greater temperatures is larger for higher water concentrations, but the overall effect is

insignificant for our interpretations. Therefore an intermediate temperature of 850 ºC is used for further calculations.

The pressure-dependence of $H_2O$ and $CO_2$ solubility in rhyolitic melts is well established (Liu et al. 2005), and the concentrations of these volatiles in each melt inclusion can therefore be used to calculate the pressures of the crystals at the time of inclusion entrapment (Burgisser et al. 2008; Newman and Lowenstern 2002; Wallace et al. 1999). For the SHV we calculate the vapor saturation pressures using *Volatilecalc* (Newman and Lowenstern 2002). The measured range of water contents from 1.2 - 6.7 wt. % $H_2O$ corresponds to entrapment pressures of 12 - 251 MPa. The bulk of the water contents from ~ 2.8 - 5.4 wt. % $H_2O$ correspond to pressures from ~ 57 - 173 MPa. The minimum pressure of 12 MPa corresponds to a depth of 0.5 km, and the maximum pressure of 251 MPa corresponds to a depth of ~ 10 km.  Our results show that most of our melt inclusions (81%) were trapped between ~2 and 7 km (57 to 173 MPa) (Supplementary data Table 4).

Geophysical data provide independent constraints on the location of the subsurface magma reservoir. Gardner and White (2002) estimate volcano-tectonic (VT) earthquake depths from 0 to ~5 km b.s.l. (August to September 1995). Aspinall et al. (1998) relocate hypocenters from 1995 to 1997, suggesting VT earthquake at depths from 0 to ~ 8 km b.s.l. Roman et al. (2008) used the same velocity model as Aspinall et al. (1998) to pick VT earthquakes from 1995 to 2007, but only considered VT earthquakes with high quality locations (i.e. vertical and horizontal location errors < 1.5 km, azimuthal gap <180 degrees and RMS <0.20). In their study, out of ~10,000 VT earthquakes considered, 1430 events had well constrained locations at depths from 1 to ~ 3 km b.s.l. Using a fixed latitude, longitude and radius, Global Positioning System geodetic data collected from October 1995 to July 1996 approximate a spherical deflating Mogi point source

located at ~ 6 km b.s.l. (Mattioli et al. 1998). Based on dilatometer data captured during the July 2003 dome collapse, Voight et al. (2006) suggest two possible reservoir scenarios: 1) a spherical pressure source at ~ 5.1 km b.s.l., and 2) an ellipsoid-shaped pressure source ranging from ~5.1 to 5.3 km b.s.l.

To summarize, the seismic data indicate movement of magma from 1 to ~ 8 km b.s.l., whereas deformation data suggest a pressure source between 4 and 6 km b.s.l. Volcano - tectonic earthquakes reflect the brittle response of the host rock possibly due to the movement of magma, although they provide little direct evidence of a magma body. The GPS and dilatometer data estimate a pressure source which is consistent with our data, although similar deformation fields can be produced with deep sources and large volume changes or shallower sources with a smaller volume change. The significant clustering of trapped melt inclusions at our calculated depths of 2 - 7 km overlap with seismic activity and correlate with estimates of reservoir depth from GPS studies, suggesting that the melt inclusions were trapped in the volcanic conduit and the upper magma reservoir with the reservoir top estimated at ~ 5 km.

*Volatile variability*

Either the melt inclusion volatile contents record conditions at the time of entrapment or, in the case of $H_2O$, they could represent conditions at the time of re-equilibration. We examine water contents as a function of increasing silica and consider two possibilities: 1) isobaric vapor-saturated crystallization involving an $H_2O$ -rich vapor phase and 2) decompression degassing and crystallization in the rhyolitic melt (Fig 6; Fig 7). Water contents observed in melt inclusions trapped in amphibole, plagioclase and quartz hosts appear to follow a general trend of isobaric vapor-saturated crystallization (i.e., similar water contents with increasing silica contents) (Fig 6). For isobaric vapor saturated crystallization with a more $CO_2$-rich vapor phase water contents

would increase with decreasing $CO_2$ as crystallization proceeds (Fig 7). The limited number of inclusions for which we have $CO_2$ data do not show evidence for this effect (Fig 7). The best fit to the data is a water saturated closed system degassing model with ~1 wt. % water vapor (Fig 7). This suggests that the melt contained variable amounts exolved gas when the melt inclusions were trapped in the conduit and upper magma reservoir.

*Chlorine contents*
We report relatively high chlorine contents for arc magmas (2520 ppm to 3270 ppm; Fig 4), a characteristic of the SHV magmas noted by previous studies (Edmonds et al. 2002). Signorelli and Carroll (2001) used a starting hydrous rhyolitic composition similar to the phenocryst-free pre-eruptive matrix of the SHV andesite and determined chlorine solubility in the melt of 0.48 to 0.68 wt. % Cl (25 to 250 MPa; 860 to 890ºC) in the presence of a vapor and/or brine. The Cl contents we determine are slightly lower (0.25 to 0.33 wt. % Cl), suggesting the melt was not saturated in both the vapor and brine. At 200 MPa the miscibility gap between $H_2O$ vapor and brine has disappeared. At this pressure, the melt is not saturated with both phases, whereas at pressures < 200 MPa both phases exist (Webster et al. 1997). The affinity of chlorine for a water-rich vapor phase is well documented (Metrich and Rutherford 1992; Webster and Holloway 1988) and provides a way for chlorine to leave the melt on ascent and crystallization of the SHV magma (Edmonds et al. 2001). The presence of the HCl species in the gas plume supports the presence of Cl in the vapor phase (Christopher et al. 2010; Edmonds et al. 2002).

Again we consider two paths the melt could have followed: isobaric vapor-saturated crystallization with a $H_2O$-rich vapor phase, decompression degassing and crystallization, or both (Fig 8). Isobaric vapor-saturated crystallization involving a $H_2O$-rich vapor phase would cause an increase in Cl with decreasing water concentration, as chloride has the higher solubility, whereas depending on the starting composition decompression degassing and crystallization

could cause 1) either a decrease in water with not much change in Cl or 2) a decrease in both

water and Cl (Webster et al. 1997) (Fig 8). The current models of degassing at SHV clearly

demonstrate that the SO2:HCl ratios are a function of depth, thus at deeper levels S is the

dominant volatile phase, where as at shallower depths Cl is the dominant volatile phase

(Edmonds et al. 2001). Therefore at pressures >200 MPa the melt was undergoing isobaric

vapor-saturated crystallization involving a water rich vapor phase and $SO_2$.

There appears to be a decoupling of the volatile data with the chlorine contents suggesting

higher entrapment conditions than the $H_2O$-$CO_2$ solubility model. The high chlorine contents

suggests that the melt inclusions are trapping liquid compositions at > 200 MPa, while the $H_2O$-

$CO_2$ data suggest pressures of 100-200 MPa.

**Models for magma ascent and degassing at Soufrière Hills volcano**

In this section we describe two models which we think explain the variable $H_2O$ contents, low

$CO_2$ and high chlorine contents presented in this study. The premise for model 1 is that melt

inclusions form during crystal growth recording pressures at the time of entrapment (Fig 9a).

Thus higher water contents were trapped at higher pressures and lower water contents were

trapped at lower pressures. The premise for model 2 is that melt inclusions are trapped during

crystal growth at deeper levels, but experience post-entrapment modification through diffusive

equilibrium of $H_2O$ in the melt inclusion with the matrix glass at shallower levels (Fig 9b). The

magma batch which transports the phenocrysts to the surface experiences stop-start

decompression, facilitating the diffusion of water from the host phenocryst to the matrix.

*Model 1: Melt inclusion entrapment during crystal growth*

We first explore a model in which the melt inclusions are trapped during crystal growth.

Thus, their water contents are representative of conditions at the time of entrapment such that the

lower water contents were trapped in the conduit at lower pressure, and the higher water contents trapped in the upper magma reservoir at higher pressure. We explore this model based on, (1) a general decrease in water contents with increasing silica content observed in plagioclase hosted melt inclusions (Fig 6) and (2) the lack of $CO_2$ which indicates that the melt was relatively degassed prior to formation of the melt inclusions. The $H_2O$-$CO_2$ solubility model supports a melt undergoing closed system degassing with ~ 1 wt. % of exsolved vapor. This suggests that the magma stalls in the lower conduit/upper magma reservoir long enough to trap melt inclusions during crystal growth.

Couch et al. (2003a) ran a series of decompression experiments on materials analogous to SHV bulk compositions and determined crystal growth during decompression to be on the order of $10^{-8}$ mm/s at 125 MPa. At this rate a plagioclase phenocryst 500 µm in length would take ~2 years to form, or a growth rim of 50 µm (the minimum we observe) would take ~ 20 days to form. Thus, the minimum amount of time the phenocrysts need to form and trap a melt inclusion in the conduit/upper reservoir would be on the order of tens of days. Couch et al. (2003b) suggest a conduit configuration which is more narrow at a depth of >1 km, stalling the ascending magma for several days to account for extensive crystallization of microlites in the dome lavas. Prior to vulcanian explosions, extrusion of magma to the surface is continuous for up to ~2.5 year intervals at rates of up to 9 $m^3$/s (Sparks et al. 1998). If we assume that the magma rises to the surface from the uppermost portions of the shallow magma reservoir, the magma may stall on ascent at a narrow chokepoint for tens of days forming melt inclusions.

There is abundant evidence that indicates that the SHV is a long lived magmatic system possibly formed by diapers of andesite rising through the crust and amalgamating (Annen 2009; Annen et al. 2006; Bachmann and Bergantz 2008; Murphy et al. 2000). SHV magmas erupted

over the last 18 ka have similar mineral chemistry and a small range in bulk composition (Murphy et al. 2000). Mass balance calculations between phenocryst compositions and glass compositions indicate a high crystallinity prior to eruption and a reservoir temperature well below the experimentally determined water-saturated temperature. Based on these observations Murphy et al. (2000) suggest that the magma has experienced a protracted cooling history, which together with the similar mineral and bulk chemistry suggests that the eruptions are tapping the same magma body. Harford et al. (2002) found xenocrystic plagioclase with apparent ages of at least 400 ka from $^{40}$Ar/$^{39}$Ar analysis of phenocryst separates. Zellmer et al. (2003) examined Sr and Ba profiles in plagioclase and observed complex zoning patterns, with relatively flat Sr zonation. They conclude that crystal growth was relatively fast and occurred early followed by residence times of ~ 15 to ~320 years at magmatic temperatures of ~850°C. Therefore the phenocrysts which comprise the andesitic pumice are a mixture of old crystals from a partially to fully solidified roof rock/roof mush that became incorporated into the current batches of magma and new crystals. In support of this, we note two melt inclusions of a different melt composition (Fig 5). This could explain why we see an abundance of plagioclase-hosted melt inclusions recording low pressures indicative of upper reservoir conditions.

Model 1 suggests that majority of the melt inclusion contents are trapped during crystal growth at lower conduit/upper magmatic reservoir conditions (Fig 9a). To account for the presence of melt inclusions formed at low pressures erupted for almost a decade, the phenocrysts could be a mixture of older crystals and newer crystals.

**Model 2: Melt inclusions re-equilibrate with the surrounding liquid**

In order for diffusive re-equilibration to take place, there must be a change in the chemical potential of water surrounding the phenocryst host (Qin et al. 1992). This could occur by ascent and degassing of magma or by the transport of phenocrysts to a different region of the magma reservoir through convection or gravitational settling. We have established that a major portion of melt inclusions between ~ 2.8 and 5.4 wt. % $H_2O$ reflect a conduit/upper reservoir environment. If the phenocrysts were settling out due to gravity, we would expect more phenocrysts with higher water contents. Convection or convective self-mixing (Couch et al. 2001) may play a role in moving the phenocrysts from regions of higher pressure to regions of lower pressure. Here we discuss pumice erupted during vulcanian explosions, resulting in ascent due to the sudden decrease of pressure as the primary method of phenocryst transport.

Decompression styles vary and are best quantified by density and texture of groundmass crystals. Single step decompression is a single decompression event which brings magma from an initial pressure to a final pressure in one step, such as during a plinian eruption. Multi-step decompression starts with an initial pressure, bringing the magma to a final pressure in multiple increments of decompression. During slower decompression, tiny crystals < 100 μm in length (microlites) develop in the groundmass of the pumice as magma ascends from the magma reservoir to the surface (Cashman 1992). Couch et al. (2003b) use an analogue composition equivalent to the groundmass composition of the Soufrière Hills lava to determine the effects of degassing-induced crystallization ranging from 130 MPa to 50 MPa. Experimental results for single step decompression indicate that large changes in temperature or large degrees of undercooling (ΔT) result in nucleation-dominated crystallization, while smaller changes in ΔT, such as multi-step decompression, result in growth-dominated crystallization. For larger ΔT, microlite morphology will vary from tabular through swallowtail to dendritic (Hammer and

Rutherford, 2002). Our pumice samples have low percentages of microlites; those observed are tabular in shape consistent with multi-step decompression (Clarke et al. 2007; Couch et al. 2003b).

During episodes of vulcanian activity as observed at the SHV, the ascending magma undergoes multiple decompression events on its way to the surface. During each explosion, the non-erupted magma undergoes decompression approximately equal to the explosion magnitude (~24 MPa) (Clarke et al. 2007; Jaquet et al. 2006; Couch et al. 2003b). Jaquet et al. (2006) apply a statistical study of the explosion time series from the 22 September to 21 October 1997 series and suggest that each batch of magma experienced 6 to 8 episodic decompressions recording 60 - 87 hours of eruptive history. This would be equal to an overall decompression of 144 - 192 MPa. The repose interval between explosions for the 4-13 August 1997 series varies from ~ 10 – 63 hours (Druitt et al. 2002). A plagioclase hosted melt inclusion rising from deeper regions in the magma reservoir during a series of vulcanian explosions (such as the 1997 series) would have time to undergo diffusive equilibrium and lose as much as 2 wt. % water in 48 hours (Severs et al. 2007). Multi-step decompression acting as a catalyst for diffusive re-equilibration also explains the significant cluster of $H_2O$ concentrations corresponding to the lower conduit and upper magma reservoir. This model suggests that the melt inclusions record not the pressure of entrapment but instead the pressure of melt inclusion re-equilibration.

The decompression style and melt composition is remarkably different between plinian eruptions and vulcanian eruptions. A plinian eruption is a good example of a single step decompression event in which the melt ascent from a higher pressure to the surface in one explosion. Water contents from phenocryst-hosted melt inclusions sampled from the18 May 1980 plinian phase of the Mt. St. Helens eruption demonstrate a decrease in water content (6.7 to

~ 1.4 wt. % $H_2O$) with a negligible changes in silica content (cluster at ~ 72 wt. % $SiO_2$) (Blundy and Cashman 2005; Blundy et al. 2007). This variation in melt inclusion composition is attributed to the rapid, continuous extraction of the plinian magma tapping relatively deep into the magma reservoir (Blundy et al. 2007). The mechanism of vulcanian explosions is a start-stop mechanism with varying amounts of repose time between explosions. We report variable water contents (1.2 – 6.7 wt. % $H_2O$) with a range of silica contents (~72 – 82 wt. % $SiO_2$), thus a broader range of silica contents relative to the plianian phase, but a similar range of water contents. We suggest that the melt inclusion compositions observed in pumice from plinian eruptions provide a better record of the magma chamber conditions at the time of eruption, while melt inclusion compositions observed in pumice from vulcanian explosions provides information about the path of magma ascent.

In this model we argue that the re-equilibration of water takes place during the repose intervals between the vulcanian explosions (Fig 9b). We suggest that the melt inclusions are first trapped at deeper levels at higher pressures; upon ascent, water diffusively re-equilibrates with the surrounding matrix melt as the magma moves towards the surface. Multi-step batch decompression during vulcanian explosions provides a reasonable decompression style for the re-equilibration of the melt inclusions with the surrounding liquid. The chlorine contents suggest a deeper formation of the melt inclusions which were subsequently modified on ascent to the surface. This model explains the same range of water contents observed from each series of vulcanian eruptions, the absence of melt inclusions with higher water and $CO_2$ contents and the decoupling of the chlorine and water data which may be explained, at least in part, by diffusive re-equilibration of $H_2O$.

**Conclusions**

1.  Plagioclase and quartz hosted melt inclusions sampled from pumice erupted during vulcanian explosions from 1996 to 2004 are rhyolitic in composition (72.8 to 78.7 wt. % $SiO_2$). Dissolved water contents range from 1.19 wt. % to 6.74 wt. % $H_2O$. $CO_2$ levels are < 77 ppm in 9% of the melt inclusions. Chlorine contents range from 2520 to 3270 ppm Cl clustering at ~3000 ppm.

2. The significant cluster of data from 2.8 to 5.4 wt. % $H_2O$ corresponds to pressures between 57-173 MPa and depths of $\sim 2 - 7$ km which indicate a lower conduit/upper magma reservoir.

3. The variability in water contents may reflect decompression crystallization of a volatile saturated magma undergoing closed system degassing with up to $\sim 1$ wt. % $H_2O$ vapor which ponds in the lower conduit/upper magma reservoir prior to eruption.

4. The variability in water contents also can be explained by multi-step decompression in which a batch of magma undergoes a series of decompression steps, water diffusing from the melt inclusion to the matrix. The chlorine contents record the initial entrapment of the melt inclusions, while the $H_2O$ data record the conditions at the time of re-equilibration. The melt inclusion volatile contents then mirror equilibration conditions in the lower conduit/upper magma reservoir, rather than initial entrapment at deeper levels in the reservoir.

5. Vulcanian explosions may provide information regarding the path of magma ascent

 rather than the initial magma conditions at the time of eruption.

**References**

Annen C (2009) From plutons to magma chambers: Thermal constraints on the accumulation of eruptible silicic magma in the upper crust. Earth Planetary Sci Lett 284:409-416

Annen C, Blundy JD, Sparks RSJ (2006) The genesis of intermediate and silicic magmas in deep crustal hot zones. J Petrol 47:505-539

Aspinall WP, Miller AD, Lynch L, Stewart RC, White RA, Power JA (1998) Soufrière Hills eruption, Montserrat 1995-1997: Volcanic earthquake locations and fault plane solutions. Geophys Res Lett 25:3397-3400

Bachmann O, Bergantz GW (2008) Rhyolites and their Source mushes across Tectonic Settings. J Petrol 49:2277-2285

Barclay J, Rutherford MJ, Carroll MR, Murphy MD, Devine JD, Gardner JE, Sparks RSJ (1998) Experimental phase equilibria constraints on pre-eruptive storage conditions of the Soufrière Hills magma. Geophys Res Lett 25:3437-3440

Behrens H, Ohlhorst S, Holtz F, Champenois M (2004) $CO_2$ solubility in dacitic melts

equilibrated with $H_2O$-$CO_2$ fluids: Implications for modeling the solubility of $CO_2$ in

silicic melts. Geochim Cosmochim Acta 68:4687-4703

Blundy J, Cashman K (2005) Rapid decompression-driven crystallization recorded by melt

inclusions from Mount St. Helens volcano. Geology 33:793-796

Blundy J, Cashman K, Berlo K (2007) Evolving magma conditions beneath Mount St. Helens

inferred from chemical variations in melt inclusions from the 1980-1986 and current

eruptions In: Sherrod DR, Scott WE (eds) A volcano rekindled: The renewed eruption of

Mount St. Helens, 2004-2006

Blundy J. Cashman K (2008) Petrologic reconstruction of magmatic system variables and

processes. Rev Mineral Geochem 69:179-239

Buckley VJE, Sparks RSJ, Wood BJ (2006) Hornblende dehydration reactions during magma

ascent at Soufrière Hills Volcano, Montserrat. Contrib Min Petrol 151:121-140

Burgisser A, Scaillet B, Harshvardhan (2008) Chemical patterns of erupting silicic magmas and

their influence on the amount of degassing during ascent. J Geophys Res Lett

113:B12204

Cashman KV (1992) Groundmass crystallization of Mount St Helens dacite, 1980-1986: a tool

for interpreting shallow magmatic processes. Contrib Min Petrol 109:431-449

Christopher T, Edmonds M, Humphreys MCS, Herd RA (2010) Volcanic gas emissions from
    Soufrière Hills Volcano, Montserrat 1995-2009, with implications for mafic magma
    supply and degassing. Geophys Res Lett 37: L00E04

Clarke AB, Stephens S, Teasdale R, Sparks RSJ, Diller K (2007) Petrologic constraints on the
    decompression history of magma prior to Vulcanian explosions at the Soufrière Hills
    volcano, Montserrat. J Volcanol Geotherm Res 161:261-274

Couch S, Sparks RSJ, Carroll MR (2001) Mineral disequilibrium in lavas explained by
    convective self-mixing in open magma chambers. Nature 411:1037-1039

Couch S, Harford CL, Sparks RSJ, Carroll MR (2003a) Experimental constraints on the
    conditions of formation of highly calcic plagioclase microlites at the Soufrière Hills
    Volcano, Montserrat. J Petrol 44:1455-1475

Couch S, Sparks RSJ, Carroll MR (2003b) The kinetics of degassing-induced crystallization at
    Soufrière Hills Volcano, Montserrat. J Petrol 44:1477-1502

Danyushevsky LV, Sokolov S, Falloon TJ (2002) Melt inclusions in olivine phenocrysts: Using
    diffusive re-equilibration to determine the cooling history of a crystal, with implications
    for the origin of olivine-phyric volcanic rocks. J. Petrol 43:1651-1671

Devine JD, Murphy MD et al. (1998) Petrologic evidence for pre-eruptive pressure-temperature
    conditions and recent reheating of andesitic magma erupting at the Soufrière Hills
    volcano, Montserrat W.I. Geophys Res Lett 25:3669-3672

Druitt TH, Young SR, Baptie B et al (2002) Episodes of cyclic vulcanian explosive activity with fountain collapse at Soufrière Hills Volcano, Montserrat. In: Druitt TH, Kokelaar BP (eds) The eruption of Soufrière Hills Volcano, Montserrat, from 1995 to 1999. London: The Geological Society of London, pp 281-306

Edmonds M., Herd RA, Strutt MH (2006) Tephra deposits associated with a large lava dome collapse, Soufrière Hills Volcano, Montserrat, 12-15 July 2003. J Volcanol Geotherm Res 153:313-330

Edmonds M, Pyle D, Oppenheimer C (2001) A model for degassing at the Soufrière Hills Volcano, Montserrat, West Indies, based on geochemical data. Earth and Planetary Sci Lett 186:159-173

Edmonds M, Pyle D, Oppenheimer C (2002) HCl emissions at Soufrière Hills Volcano, Montserrat, West Indies, during a second phase of dome building: November 1999 to October 2000. Bull Volcanol 64:21-30

Eichelberger JC, Carrigan CR, Westrich HR, Price RH (1986) Non-explosive silicic volcanism. Nature 323:598-602

Gardner CA, White RA (2002) Seismicity, gas emission and deformation from 18 July to 25 September 1995 during the initial phreatic phase of the eruption of Soufrière Hills volcano, Montserrat. In: Druitt TH, Kokelaar BP (eds.) The eruption of Soufrière Hills volcano, Montserrat, from 1995 to 1999. London, Memoirs: Geological Society of London, pp 567-581

Harford CL, Pringle MS, Sparks RSJ, Young SR (2002) The volcanic evolution of Montserrat using $^{40}$Ar/$^{39}$Ar geochronology. In: Druitt, T. H. & Kokelaar, B. P. (eds.) The eruption of Soufrière Hills volcano, Montserrat, from 1995 to 1999. London, Memoirs: Geological Society of London, pp 93-113

Harford CL, Sparks RSJ, Fallick AE (2003) Degassing at the Soufrière Hills Volcano, Montserrat, recorded in matrix glass compositions. J Petrol 44:1503-1523

Herd RA, Edmonds M, Bass VA (2005) Catastrophic lava dome failure at Soufrière Hills Volcano, Montserrat, 12-13 July 2003. J Volcanol Geotherm Res 148:234-252

Humphreys MCS, Edmonds M, Christopher T, Hards V (2010) Magma hybridisation and diffusive exchange recorded in heterogeneous glasses from Soufrière Hills Volcano, Montserrat. Geophys Res Lett 37:L00E06

Humphreys MCS, Menand T, Blundy J, Klimm K (2008) Magma ascent rates in explosive eruptions: Constraints from $H_2O$ diffusion in melt inlcusions. Earth Planet Sci Lett 270:25-40

Jaquet O, Sparks RSJ, Carniel R (2006) Magma memory recorded by statistics of volcanic explosions at the Soufrière Hills volcano, Montserrat. In: Mader HM, Coles SG, Connor CB, Connor LJ (eds) Statistics in volcanology. Geological Society, London: Special Publications of IAVCEI, pp 175-184

Jaupart C, Allègre CJ, (1991) Gas content, eruption rate and instabilities of eruption regime in silicic volcanoes. Earth and Planetary Science Letters 102:413-429

Leschik M, Heide G, Frischat GH et al  (2004) Determination of $H_2O$ and $D_2O$ contents in rhyolitic glasses. Physics and Chemistry of Glasses - European Journal of Glass Science and Technology Part B 45:238-251

Liu Y, Zhang Y, Behrens H (2005) Solubility of $H_2O$ in rhyolitic melts at low pressures and a new empirical model for mixed $H_2O$-$CO_2$ solubility in rhyolitic melts. J Volcanol Geotherm Res 143:219-235

Lowenstern JB (1995) Applications of silicate-melt inclusions to the study of magmatic volatiles. Short course handbook 23:71-99

Mann CP, Stix J (2010) Mafic enclaves record magma mixing at the Soufrière Hills Volcano, Montserrat, West Indies. J Petrol (submitted)

Mattioli GS, Dixon TH, Farina F, Howell E, Jansma PE, Smith AL (1998) GPS measurement of surface deformation around Soufrière Hills volcano, Montserrat from October 1995 to July 1996. Geophys Res Lett 25:3417-3420

Melnik O, Sparks RSJ (2002) Modelling of conduit flow dynamics during explosive activity at Soufrière Hills volcano, Montserrat. In: Druitt TH, Kokelaar BP (eds) The eruption of the Soufrière Hills volcano, Montserrat, from 1995 to 1999. Geological Society, London, Memoirs: Geological Society of London, pp 307-317

Metrich N, Wallace PJ (2008) Volatile abundances in basaltic magmas and their degassing paths tracked by melt inclusions. Rev Mineral Geochem 69:363-402

Morrissey MM, Mastin LG (2000) Vulcanian eruptions. In: Sigurdsson, H. (ed.) Encyclopedia of Volcanoes. San Diego: Academic Press, pp 463-475

Murphy MD, Sparks RSJ, Barclay J, Carroll MR, Brewer TS (2000) Remobilization of andesite magma by intrusion of mafic magma at the Soufrière Hills Volcano, Montserrat, West Indies. J. Petrology 41:21-42

Newman S, Epstein S, Stolper E (1988) Water, carbon dioxide, and hydrogen isotopes in glasses in glasses from the ca. 1340 A.D. eruption of the Mono Craters, California: Constraints on degassing phenomena and initial volatile content. J Volcanol Geotherm Res 35:75-96

Newman S, Lowenstern JB (2002) VC: a silicate melt-$H_2O$-$CO_2$ solution model written in Visual Basic for excel. Comput Geoscis 28:597-604

Newman S, Stopler EM, Epstein S (1986) Measurements of water in rhyolitic glasses: Calibration of an infrared spectroscopic technique. Amer Mineral 71:1527-1541

Qin Z, Lu F, Anderson ATJ (1992) Diffusive re-equilibration of melt and fluid inclusions. American Mineralogist 77:565-576

Robertson R, Cole P, Sparks RSJ et al (1998) The explosive eruption of the Soufrière Hills volcano, Montserrat, West Indies, 17 September 1996. Geophy Res Lett 25:3429-3432

Robertson REA, Aspinall WP, Herd R, Sparks RSJ, Young SR (2000) The 1995-1998 eruption of the Soufrière Hills volcano, Montserrat, WI. Philosophical Transactions of the Royal Society A: Mathematical, Phys Engineering Sci 358:1619-1637

Roman DC, DeAngelis S, Latchman JL, White R (2008) Patterns of volcanotectonic seismicity and stress during the ongoing eruption of the Soufrière Hills volcano, Montserrat (1995-2007) J Volcanol Geotherm Res 173:230-244

Rutherford MJ, Devine JD (2003) Magmatic conditions and magma ascent as indicated by hornblende phase equilibria and reactions in the 1995-2002 Soufrière Hills Magma. J Petrol 44:1433-1453

Self S, Wilson L, Nairn IA (1979) Vulcanian eruption mechanisms. Nature 277:440-443

Severs MJ, Azbej T, Thomas JB, Mandeville CW, Bodnar RJ (2007) Experimental determination of $H_2O$ loss from melt inclusions during laboratory heating: Evidence from raman spectroscopy. Chemical Geol 237:358-371

Signorelli S, Carroll MR (2001) Experimental constraints on the origin of chlorine emissions at the Soufrière Hills volcano, Montserrat. Bull Volcanol 62:431-440.

Skirius CM (1990) Pre-eruptive $H_2O$ and $CO_2$ content of plinian and ash flow bishop tuff magma. Dissertation, University of Chicago, 237.

Sparks RSJ, Young SR, Barclay J et al (1998) Magma production and growth of the lava dome of the Soufrière Hills volcano, Montserrat, West Indies: November 1995 to December 1997. Geophys Res Lett 25:3421-3424

Voight B, Hoblitt RP, Clarke A, Lockhart AB, Miller AD, Lynch L, McMahon J (1998) Remarkable cyclic ground deformation monitored in real-time on Montserrat and it's use in eruption forecasting. Geophysical Research Letters 25:3405-3408

Voight B, Linde AT et al (2006) Unprecedented pressure increase in deep magma reservoir triggered by lava-dome collapse. Geophys Res Lett. doi: 10.1029/2005gl024870

Voight B, Sparks RSJ et al (1999) Magma flow instability and cyclic activity at Soufrière Hills Volcano, Montserrat, British West Indies. Science 283:1138-1142

Wallace PJ, Anderson AT, Davis AM (1999) Gradients in $H_2O$, $CO_2$ and exsolved gas in a large-volume silicic magma system: Interpreting the record preserved in melt inclusions from the Bishop Tuff. J Geophys Res 104:20097 - 20122

Webster JD (1997) Chloride solubility in felsic melts and the role of chloride in magmatic degassing. J Petrol 38:1793-1807

Young SR, Sparks R, Aspinall WP, Lynch L, Miller AD, Robertson R, Shepherd JB (1998) Overview of the eruption of the Soufrière Hills volcano, 18 July 1995 to December 997. Geophys Res Lett 25:3389-3392

Zellmer GF, Sparks RSJ, Hawkesworth CJ, Wiedenbeck M (2003) Magma emplacement and remobilization timescales beneath Montserrat: Insights from Sr and Ba zonation in plagioclase phenocrysts. J Petrol 44:1413-1431

**Fig. 1** Samples A) Photo of pumice used for this study from the 12 July 2003 eruption of the Soufrière Hills volcano. B) Microphotograph of typical plagioclase-hosted melt inclusions analyzed for this study. Note the bubbles within the melt inclusions

Fig 1


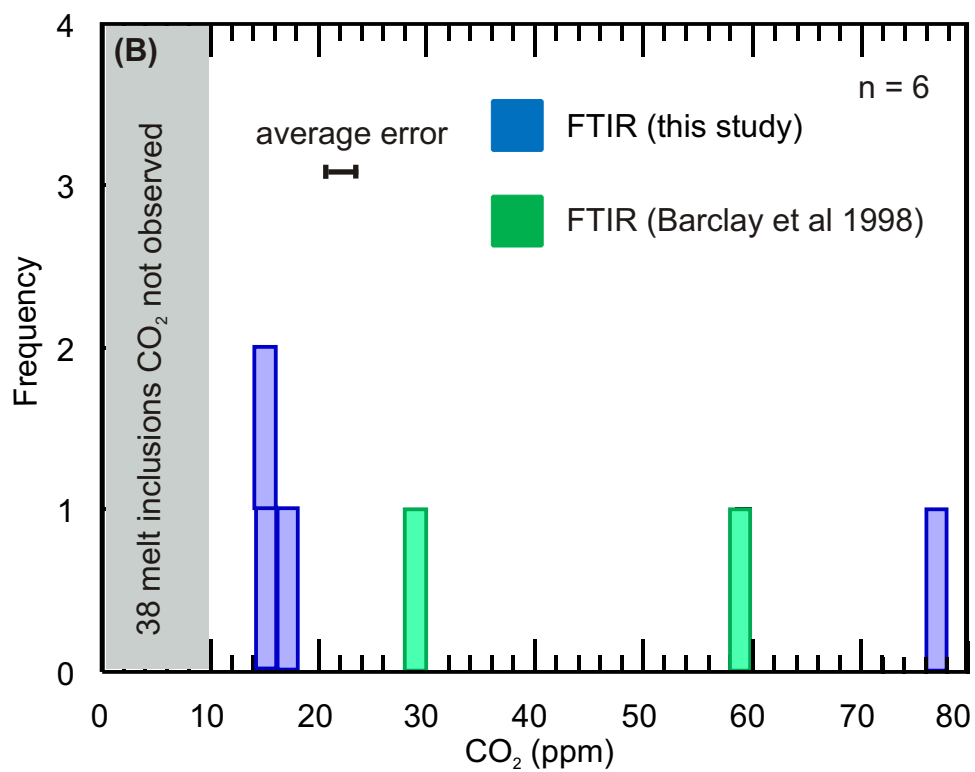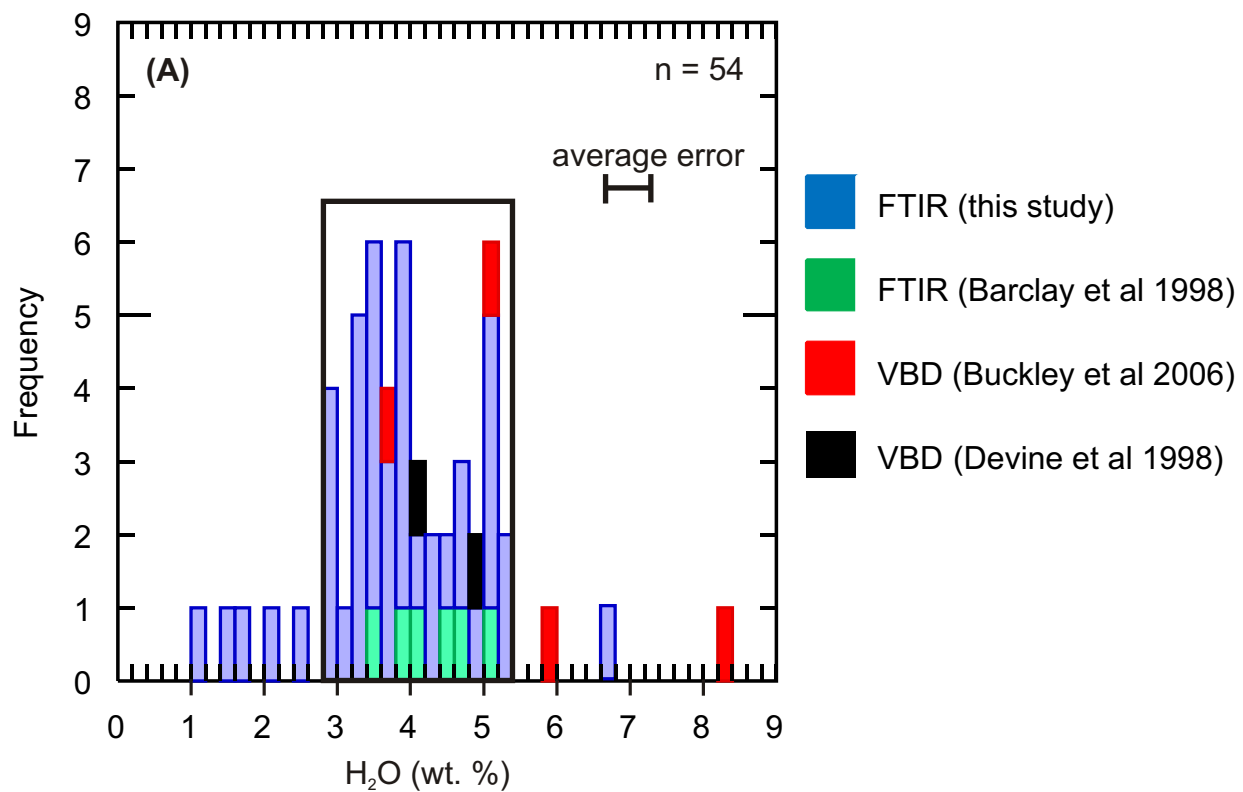
(A)

2 cm

(B)

melt inclusions with
vapor bubbles

20   m
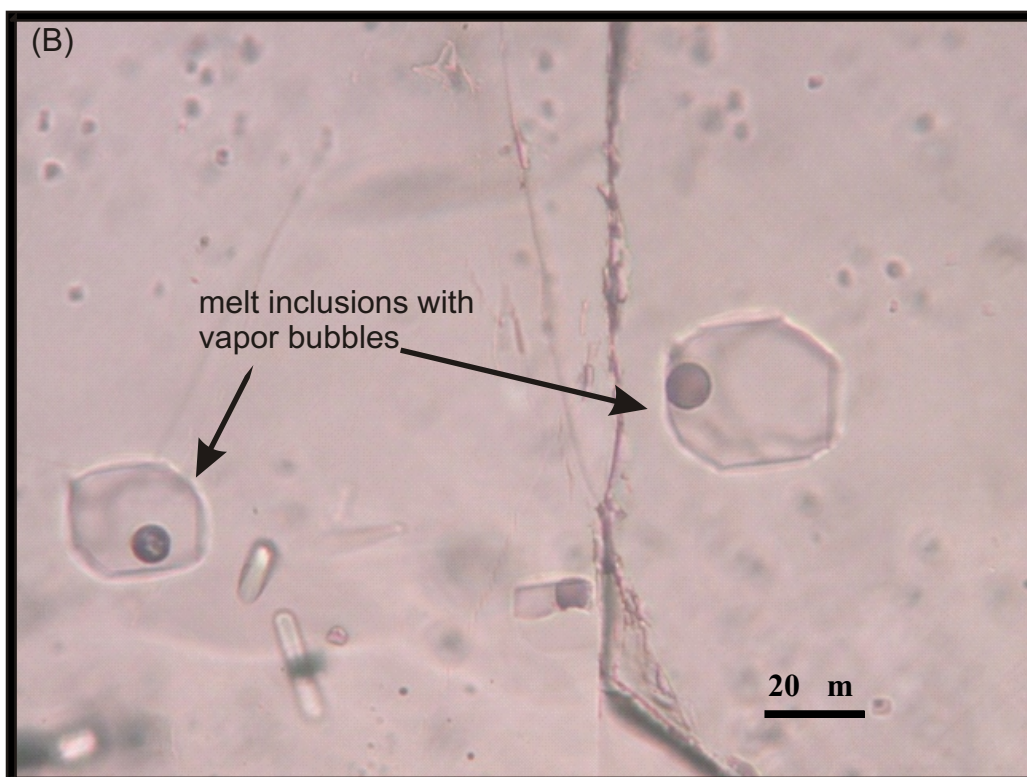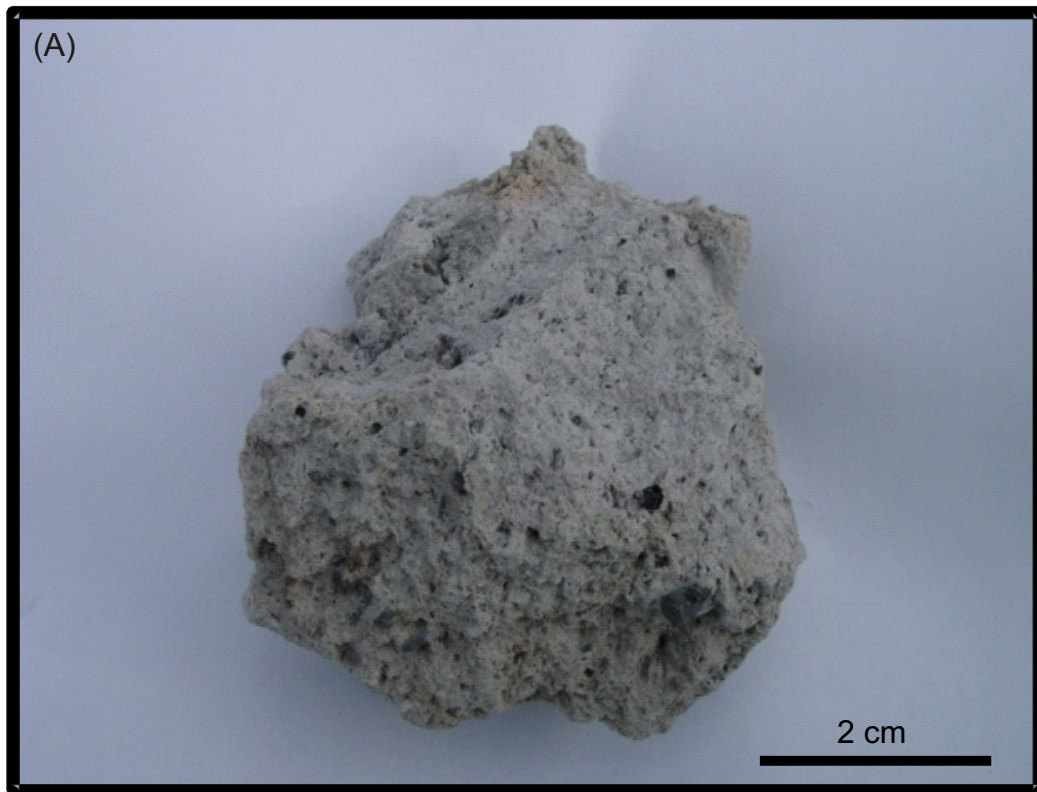
**Fig. 2** Histograms of $H_2O$ and $CO_2$ contents. A) Histogram of our measured $H_2O$ contents compared to previous studies. Black box encloses 81 % of the melt inclusions at water contents between 2.8 - 5.4 wt.% $H_2O$. B) Histogram of our measured $CO_2$ contents compared to previous studies

Fig. 2.

**Fig. 3** Histogram of water in melt inclusions vs frequency demonstrates similar distribution over time. The pumice clast from 1996 ranges from 3.52 – 5.05 wt. % $H_2O$. A pumice clast erupted between 4 August and 21 October 1997 ranges from 2.10 – 5.39 wt. % $H_2O$, while pumice erupted in August 1997 range from 2.82 - 6.74 wt. % $H_2O$. Water contents in pumice erupted in October 1997 range from 3.33 - 4.68 wt. % $H_2O$. Pumice erupted in July 2003 ranges from 1.19 wt. % to 3.96 wt. % $H_2O$ and water contents in pumice erupted March 2004 range from 2.92 – 5.02 wt. % $H_2O$

Fig. 3
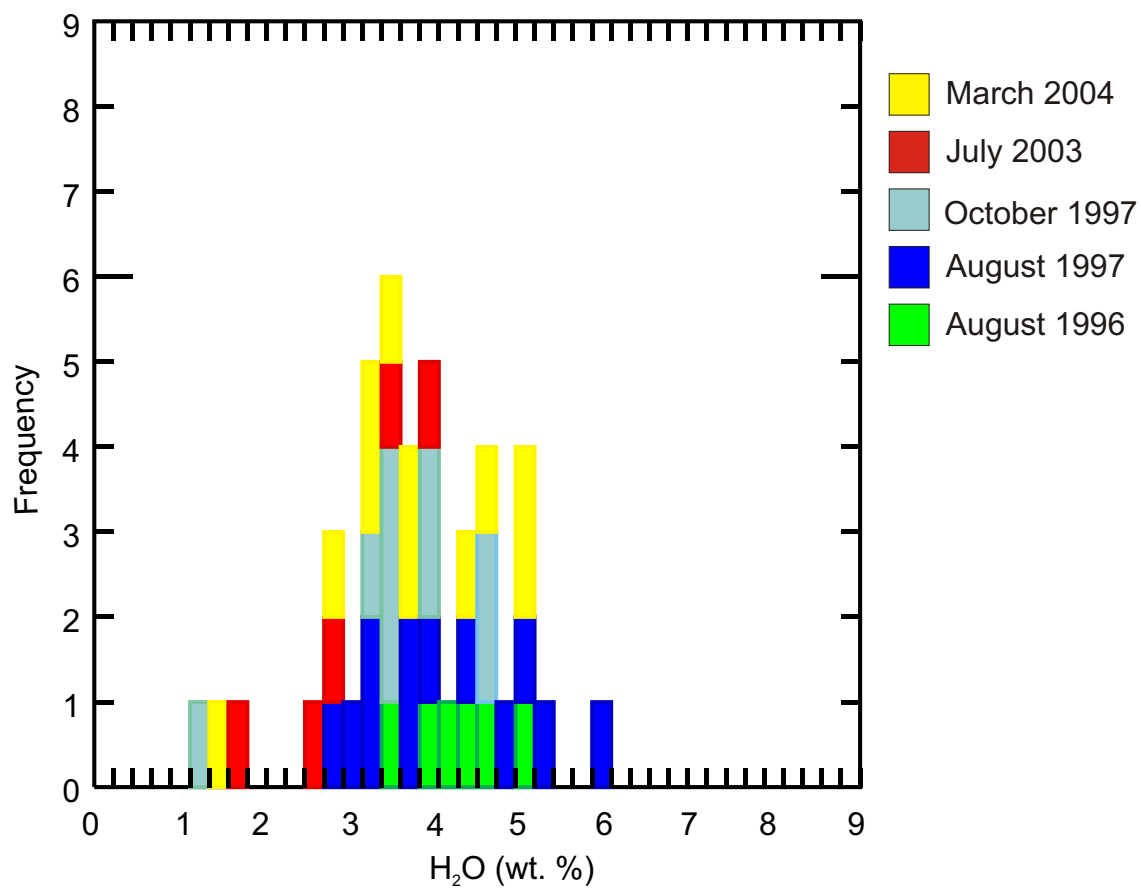
**Fig. 4** Histogram of chlorine content distribution in melt inclusions. A tight cluster is observed

near 3000 ppm Cl

Fig. 4
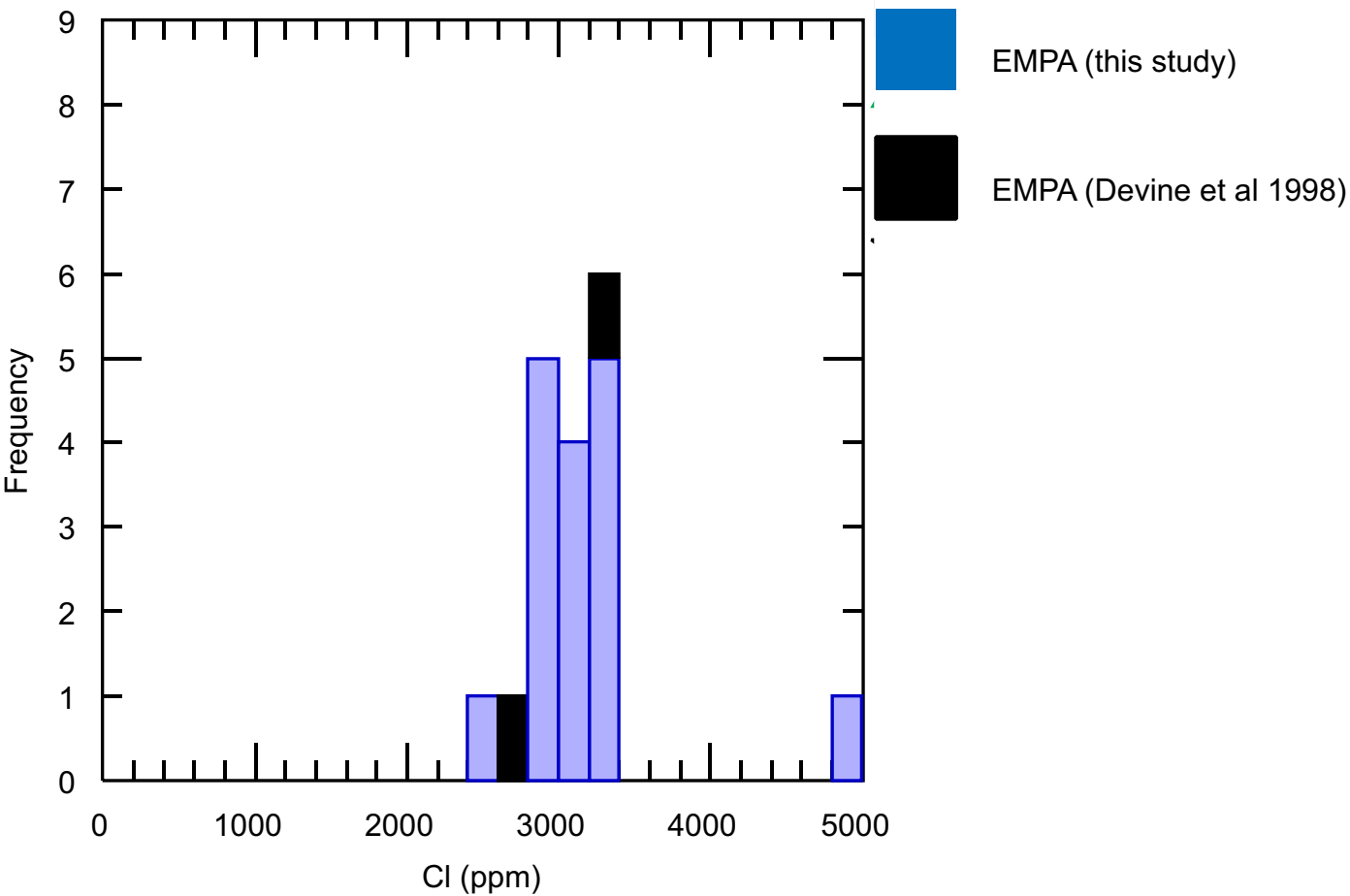
**Fig. 5** Melt inclusion major element data. A) $K_2O$ (wt. %) vs. $SiO_2$ (wt. %) demonstrates slight compatibility of $K_2O$. We include data from Barclay et al. 1998, Buckley et al. 2006 and Devine et al. 1998. Note the occurrence of melt inclusions with significantly high $K_2O$ relative to the others

Fig 5
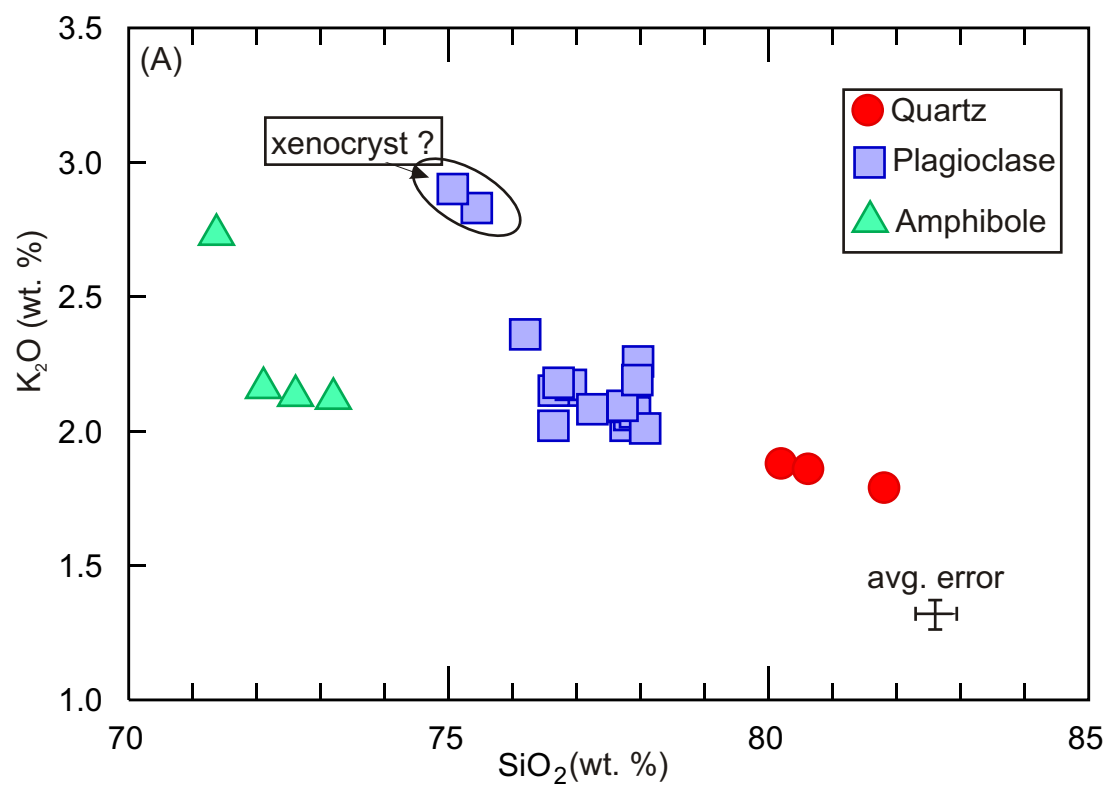
**Fig. 6** SiO$_2$ (wt. %) vs H$_2$O (wt. %) shows possible magma ascent paths. The inset is modified

from Blundy and Cashman (2005). We observe an overall horizontal array which suggests

isobaric crystallization. We include data from Barclay et al. 1998, Buckley et al. 2006 and

Devine et al. 1998. Symbols are the same as in Fig 5.

Fig. 6
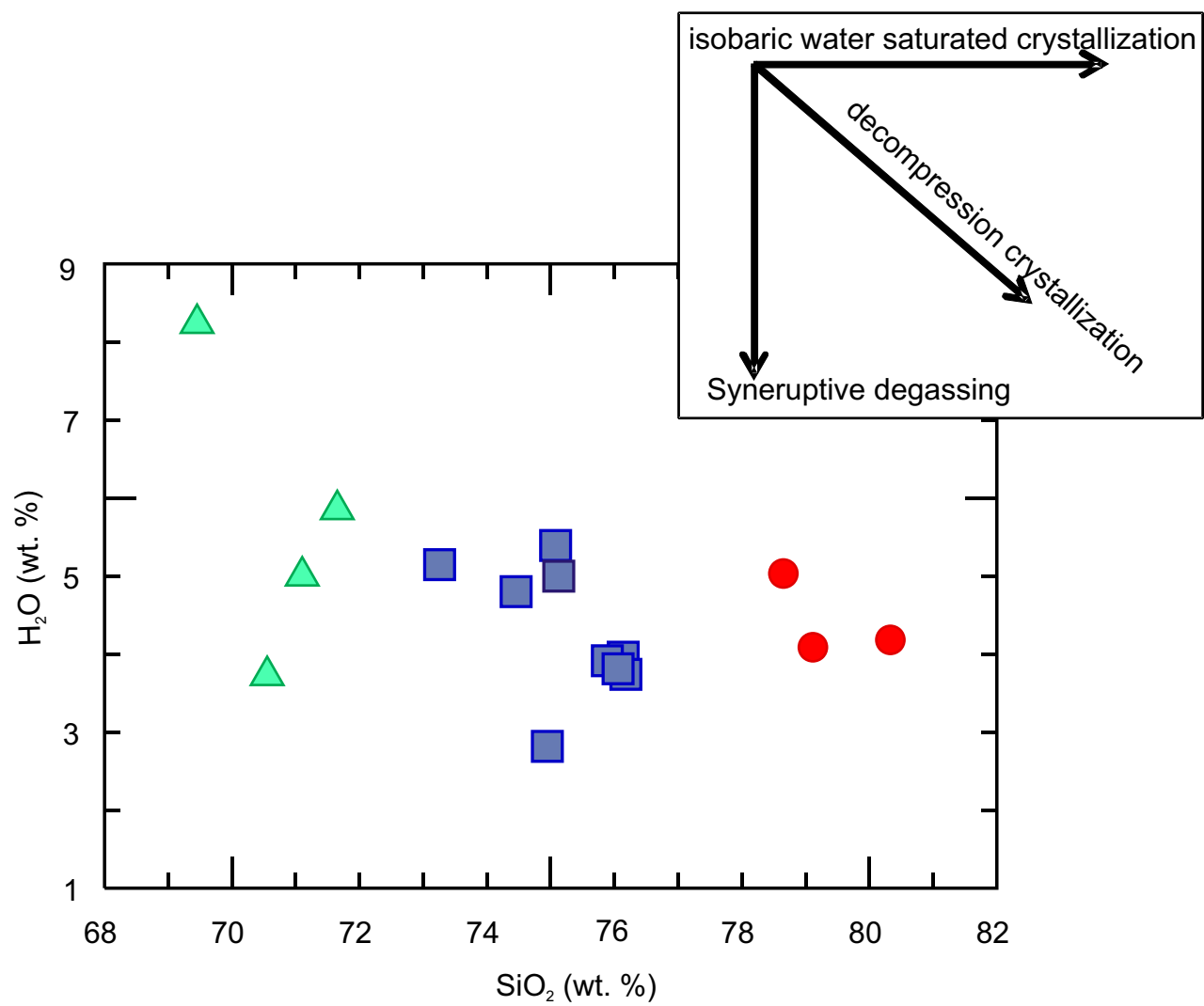
**Fig. 7** Melt inclusion $H_2O$ (wt. %) vs. $CO_2$ (ppm) contents determined by FTIR. Vapor saturation

isobars for 100 and 200 MPa at 850°C and degassing curves were calculated using *VolatileCalc*

(Newman and Lowenstern 2002). The blue degassing curve indicates the effect of a magma

undergoing open-system and closed-system degassing with no initial exsolved vapor. Solid black

line with arrow indicates the path of a magma undergoing degassing at a constant pressure. The

best fit for the data reported in this study is the red line which indicates the ascent path of a

magma experiencing closed-system degassing with ~ 1 wt. % vapor. The solid green line at the

bottom represents melt inclusions with no $CO_2$. Note the different X-Y scales. Data from Barclay

et al. 1998 included

Fig 7
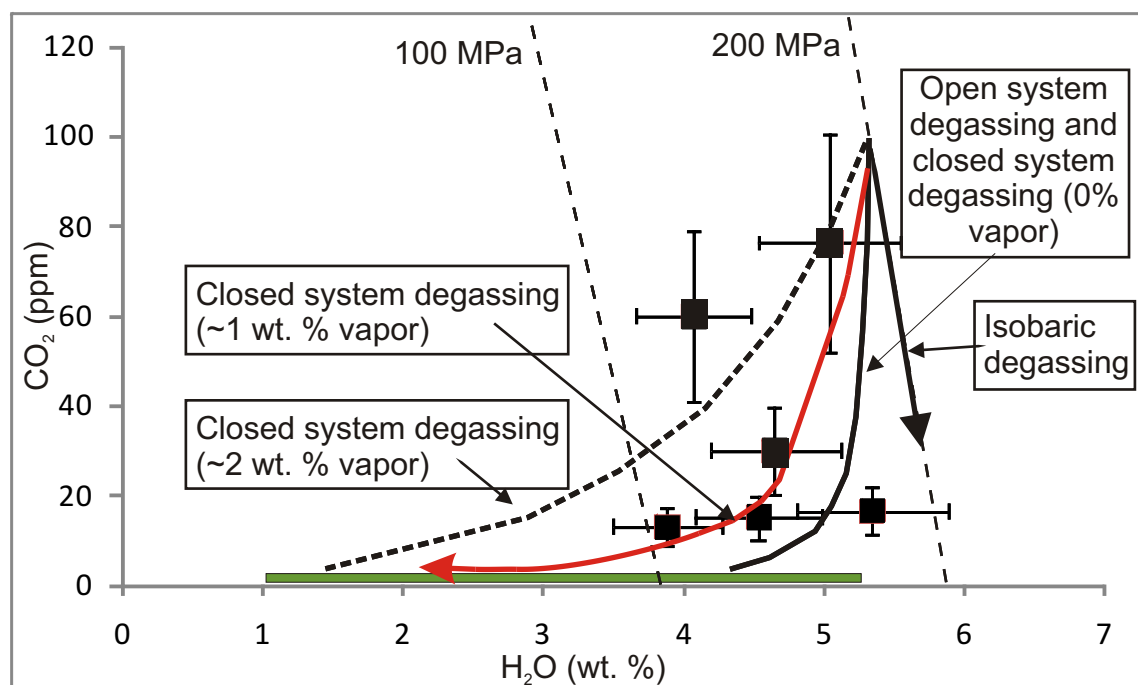
**Fig. 8** Schematic phase diagram of chloride concentration in the silicate liquid vs water

concentration in the silicate liquid. The solid line with arrows indicates isobaric crystallization

with the volatile phase stable, while the dotted line is the suggested decompression degassing

path of the melt inclusions. Data from Barclay et al. 1998 included and diagram modified from

Webster et al. (1997). Host phases of plagioclase and quartz are indicated. Symbols that same as

Fig. 5

Fig 8
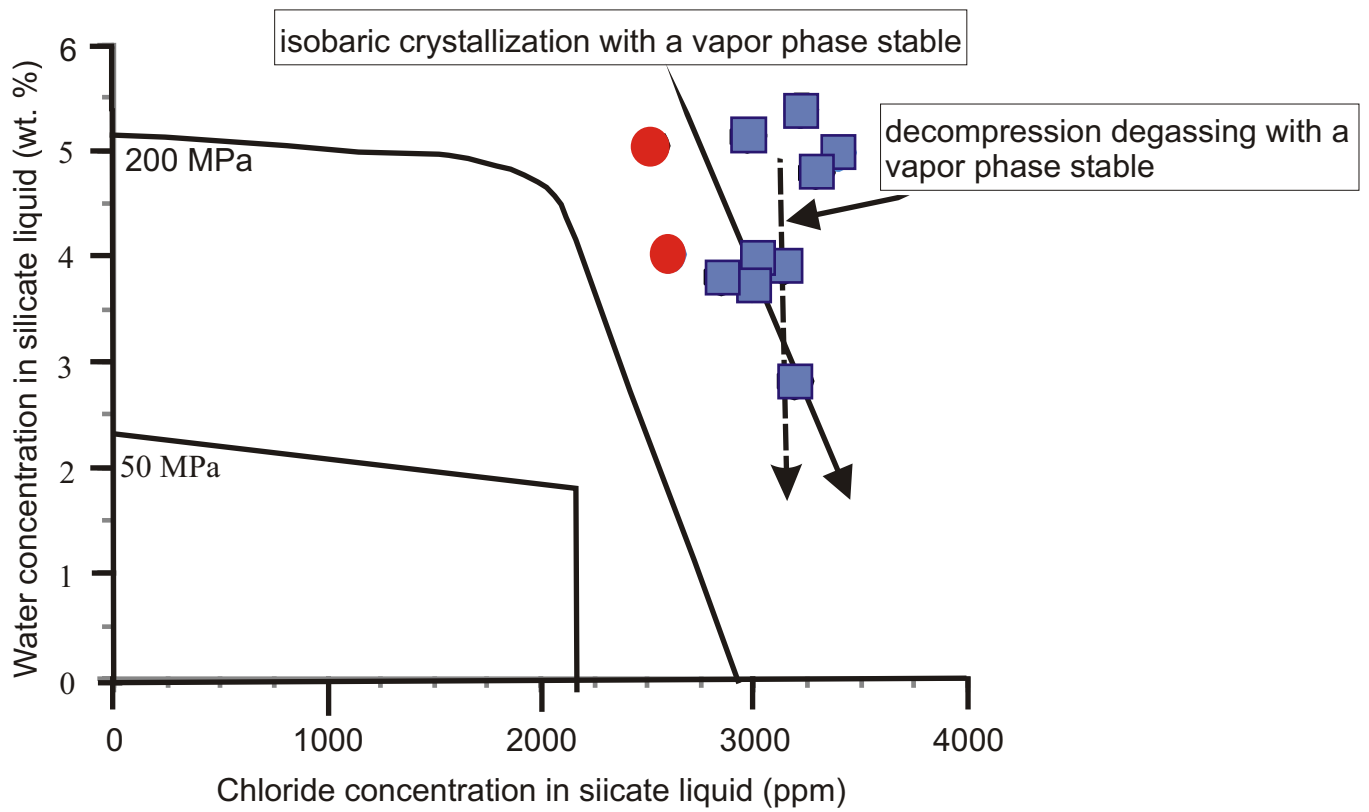
**Fig. 9** Two models which explain the variation in volatile contents at SHV. A) Volatiles are trapped during crystal growth and represent conditions at the time of entrapment. B) Melt inclusions undergo diffusive re-equilibration on ascent to the surface. Symbols same as Fig. 5 and arrows in 9b represent diffusion of water from the melt inclusion to the matrix

Fig 9

(A)

2.6 (km)                    60 (MPa)

4 (km)                      105 (MPa)

6 km                        150 (MPa)

7 km                        180 MPa

(B)

2.6 km                      60 MPa

4 km                        105 MPa

6 km                        150 MPa

7 km                        180 MPa

diffusive re-equilibration
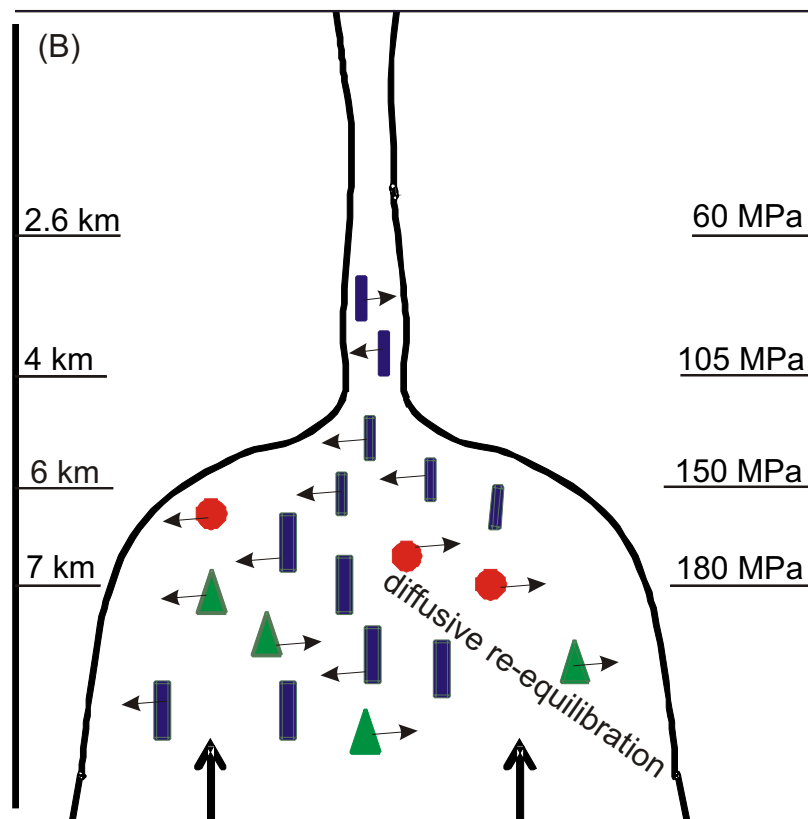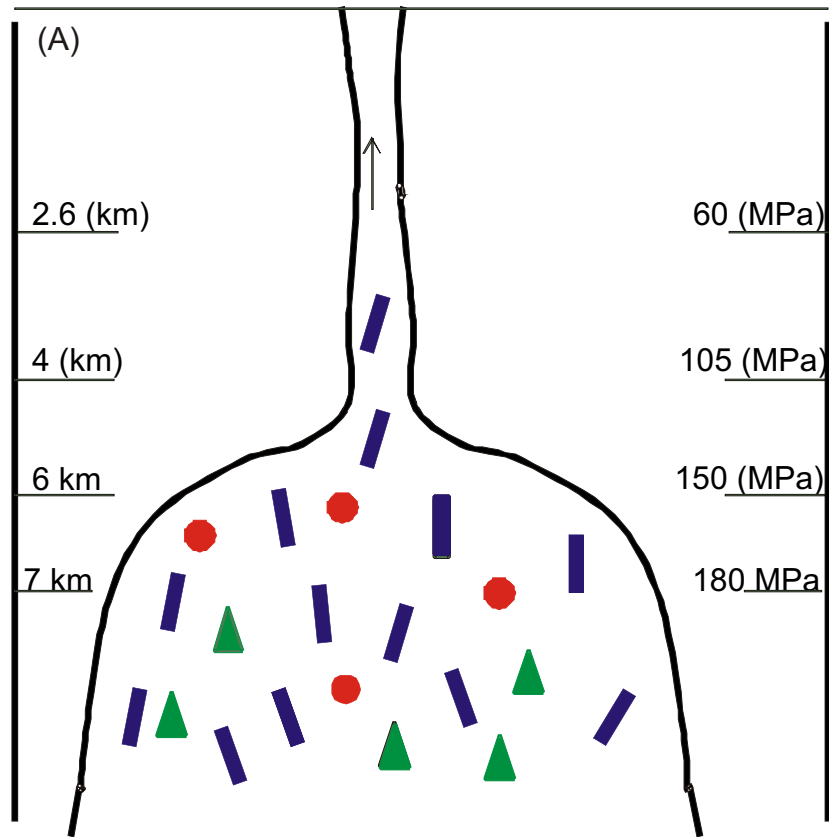
**Supplementary data Table 1. Water values measured by FTIR.**

| SAMPLES | date of analysis | mol. wt. (kg/mole) | abs. 3550 | Density (kg/cubic m) | thickness (cm) | absorptivity (m3/mole*cm) | concentration | H2O wt. % | Avg. % water | 1 SD | Calc. absorbtivity | Calc. Density |
|---|---|---|---|---|---|---|---|---|---|---|---|---|
| MONT1-A-1 -a | Jun-05 | 0.018 | 0.4850 | 2310 | 0.0015 | 0.0755 | 0.0333706 | 3.34 | 3.33 | 0.01 | 0.0755 | 2310 |
| MONT1-A-1 -b | Jun-05 | 0.018 | 0.4830 | 2311 | 0.0015 | 0.0755 | 0.0332186 | 3.32 | | | 0.0755 | 2311 |
| MONT1-A-3-a | Jun-05 | 0.018 | 1.3760 | 2260 | 0.0030 | 0.07 | 0.0521871 | 5.22 | 5.04 | 0.25 | 0.0729 | 2287 |
| MONT1-A-3-b | Jun-05 | 0.018 | 1.3630 | 2291 | 0.0030 | 0.0734 | 0.0486324 | 4.86 | | | 0.0734 | 2291 |
| MONT1-B-1-a | Jun-05 | 0.018 | 1.8560 | 2303 | 0.0050 | 0.0747 | 0.0388388 | 3.88 | 3.88 | 0.01 | 0.0747 | 2303 |
| MONT1-B-1-b | Jun-05 | 0.018 | 1.8520 | 2304 | 0.0050 | 0.0747 | 0.0387383 | 3.87 | | | 0.0747 | 2304 |
| MONT1-C-1-a | Jun-05 | 0.018 | 1.2160 | 2286 | 0.0020 | 0.0728 | 0.0657610 | 6.58 | 6.74 | 0.23 | 0.0711 | 2270 |
| MONT1-C-1-b | Jun-05 | 0.018 | 1.2260 | 2265 | 0.0020 | 0.0706 | 0.0690017 | 6.90 | | | 0.0706 | 2265 |
| MONT3-03-A-1-a | Jun-05 | 0.018 | 0.6669 | 2324 | 0.0030 | 0.077 | 0.0223607 | 2.24 | | | 0.0800 | 2400 |
| MONT3-03-A-2-a | Jun-05 | 0.018 | 0.7397 | 2321 | 0.0030 | 0.0766 | 0.0249634 | 2.50 | | | 0.0766 | 2321 |
| MONT3-03-B-1-a | Jun-05 | 0.018 | 0.9780 | 2310 | 0.0030 | 0.0754 | 0.0336904 | 3.37 | 3.45 | 0.12 | 0.0754 | 2310 |
| MONT3-03-B-1-d | Jun-05 | 0.018 | 1.0219 | 2308 | 0.0030 | 0.0752 | 0.0353269 | 3.53 | | | 0.0752 | 2308 |
| MONT3-03-B-1-e | Jun-05 | 0.018 | 0.9959 | 2309 | 0.0030 | 0.0753 | 0.0343675 | 3.44 | | | 0.0753 | 2309 |
| MONT3-03-B-3-a | Jun-05 | 0.018 | 0.9070 | 2313 | 0.0030 | 0.0758 | 0.0310394 | 3.10 | | | 0.0758 | 2313 |
| MONT3-03-C-2-a | Jun-05 | 0.018 | 1.1130 | 2321 | 0.0045 | 0.0766 | 0.0250410 | 2.50 | 2.59 | 0.12 | 0.0766 | 2321 |
| MONT3-03-C-2-b | Jun-05 | 0.018 | 1.1840 | 2319 | 0.0045 | 0.0764 | 0.0267311 | 2.67 | | | 0.0764 | 2319 |
| MONT3-03-C-3-a | Jun-05 | 0.018 | 0.6350 | 2333 | 0.0040 | 0.0778 | 0.0157432 | 1.57 | 1.65 | 0.11 | 0.0779 | 2333 |
| MONT3-03-C-3-b | Jun-05 | 0.018 | 0.6950 | 2331 | 0.0040 | 0.0777 | 0.0172677 | 1.73 | | | 0.0777 | 2331 |
| MONT3-03-D-1-a | Jun-05 | 0.018 | 1.1320 | 2303 | 0.0030 | 0.0746 | 0.0395335 | 3.95 | 3.96 | 0.04 | 0.0746 | 2303 |
| MONT3-03-D-1-b | Jun-05 | 0.018 | 1.1470 | 2302 | 0.0030 | 0.0745 | 0.0401285 | 4.01 | | | 0.0745 | 2302 |
| MONT3-03-D-1-c | Jun-05 | 0.018 | 1.1220 | 2303 | 0.0030 | 0.0747 | 0.0391318 | 3.91 | | | 0.0747 | 2303 |
| MONT3-03-D-2-a | Jun-05 | 0.018 | 0.5450 | 2317 | 0.0020 | 0.0762 | 0.0277816 | 2.78 | | | 0.0762 | 2317 |
| CM283-A-1-a | Aug-06 | 0.018 | 0.82303 | 2276 | 0.0018 | 0.0718 | 0.0503639 | 5.04 | 5.04 | 0.00 | 0.0732 | 2289 |
| CM283-A-1-b | Aug-06 | 0.018 | 0.82329 | 2276 | 0.0018 | 0.0718 | 0.0503798 | 5.04 | | | 0.0731 | 2289 |
| CM283-C-1-a | Aug-06 | 0.018 | 1.0943 | 2304 | 0.003 | 0.0748 | 0.0380981 | 3.81 | 3.74 | 0.10 | 0.0748 | 2304 |
| CM283-C-1-b | Aug-06 | 0.018 | 1.05692 | 2306 | 0.003 | 0.075 | 0.0366668 | 3.67 | | | 0.0750 | 2306 |
| CM283-C-2-a | Aug-06 | 0.018 | 0.78938 | 2311 | 0.0025 | 0.0756 | 0.0325310 | 3.25 | 3.24 | 0.02 | 0.0756 | 2311 |
| CM283-C-2-b | Aug-06 | 0.018 | 0.78246 | 2312 | 0.0025 | 0.0756 | 0.0322318 | 3.22 | | | 0.0756 | 2312 |
| CM283-D-1-a | Aug-06 | 0.018 | 1.1204 | 2303 | 0.003 | 0.0747 | 0.0390760 | 3.91 | 3.91 | 0.01 | 0.0747 | 2303 |
| CM283-D-1-b | Aug-06 | 0.018 | 1.1238 | 2303 | 0.003 | 0.0747 | 0.0391946 | 3.92 | | | 0.0747 | 2303 |
| CM283-D-2-a | Aug-06 | 0.018 | 0.7145 | 2316 | 0.0025 | 0.076 | 0.0292269 | 2.92 | 2.93 | 0.02 | 0.0760 | 2316 |
| CM283-D-2-b | Aug-06 | 0.018 | 0.7194 | 2315 | 0.0025 | 0.076 | 0.0294400 | 2.94 | | | 0.0760 | 2315 |
| CM283-D-3-a | Aug-06 | 0.018 | 1.1064 | 2317 | 0.004 | 0.0762 | 0.0281996 | 2.82 | | | 0.0762 | 2317 |
| CM283-D-3-b | Aug-06 | 0.018 | 1.0756 | 2318 | 0.004 | 0.0763 | 0.0273669 | 2.74 | 2.82 | 0.05 | 0.0763 | 2318 |
| CM283-D-3-c | Aug-06 | 0.018 | 1.1032 | 2317 | 0.004 | 0.0762 | 0.0281181 | 2.81 | | | 0.0762 | 2317 |
| CM283-D-4-b | Aug-06 | 0.018 | 1.7948 | 2305 | 0.005 | 0.0749 | 0.0374253 | 3.74 | 3.74 | 0.00 | 0.0749 | 2305 |
| CM283-D-4-c | Aug-06 | 0.018 | 1.7915 | 2305 | 0.005 | 0.0749 | 0.0373565 | 3.74 | | | 0.0749 | 2305 |
| CM283-F-1-a | Aug-06 | 0.018 | 0.81506 | 2298 | 0.002 | 0.0741 | 0.0430788 | 4.31 | 4.34 | 0.24 | 0.0741 | 2298 |
| CM283-F-1-b | Aug-06 | 0.018 | 0.8721 | 2294 | 0.002 | 0.0737 | 0.0464246 | 4.64 | | | 0.0737 | 2294 |
| CM283-F-1-c | Aug-06 | 0.018 | 0.826 | 2297 | 0.002 | 0.0741 | 0.0436760 | 4.37 | | | 0.0741 | 2297 |
| CM283-H-1-a | Aug-06 | 0.018 | 1.316 | 2293 | 0.003 | 0.0736 | 0.0467870 | 4.68 | 5.15 | 0.10 | 0.0736 | 2293 |
| CM283-H-1-b | Aug-06 | 0.018 | 1.415 | 2288 | 0.003 | 0.0731 | 0.0507615 | 5.08 | | | 0.0731 | 2288 |
| CM283-H-1-c | Aug-06 | 0.018 | 1.449 | 2287 | 0.003 | 0.0729 | 0.0521466 | 5.21 | | | 0.0729 | 2287 |
| CM283-H-2-a | Aug-06 | 0.018 | 2.00461 | 2284 | 0.004 | 0.0726 | 0.0544014 | 5.44 | 5.34 | 0.34 | 0.0726 | 2284 |
| CM283-H-2-b | Aug-06 | 0.018 | 2.15552 | 2278 | 0.004 | 0.072 | 0.0591396 | 5.91 | | | 0.0720 | 2278 |
| CM283-H-2-c | Aug-06 | 0.018 | 1.94165 | 2286 | 0.004 | 0.0729 | 0.0524300 | 5.24 | | | 0.0729 | 2286 |
| CM283-H-3-a | Aug-06 | 0.018 | 1.55757 | 2293 | 0.0035 | 0.0735 | 0.0475292 | 4.75 | 4.80 | 0.01 | 0.0735 | 2293 |
| CM283-H-3-b | Aug-06 | 0.018 | 1.57491 | 2292 | 0.0035 | 0.0735 | 0.0480793 | 4.81 | | | 0.0735 | 2292 |
| CM283-H-3-c | Aug-06 | 0.018 | 1.57002 | 2292 | 0.0035 | 0.0735 | 0.0479300 | 4.79 | | | 0.0735 | 2292 |
| CM942-A-1-c | Aug-06 | 0.018 | 0.42357 | 2337 | 0.0035 | 0.0784 | 0.0118893 | 1.19 | 1.19 | 0.01 | 0.0784 | 2337 |
| CM942-A-1-d | Aug-06 | 0.018 | 0.4276 | 2337 | 0.0035 | 0.0784 | 0.0120024 | 1.20 | | | 0.0784 | 2337 |
| CM942-B-1-a | Aug-06 | 0.018 | 0.82844 | 2309 | 0.0025 | 0.0754 | 0.0342609 | 3.43 | 3.51 | | 0.0753 | 2309 |
| CM942-B-1-d | Aug-06 | 0.018 | 0.8634 | 2307 | 0.0025 | 0.0751 | 0.0358804 | 3.59 | | | 0.0751 | 2307 |
| CM942-B-2-a | Aug-06 | 0.018 | 0.8627 | 2300 | 0.0022 | 0.0744 | 0.0412486 | 4.12 | 4.01 | 0.16 | 0.0744 | 2300 |

| | | | | | | | | | | | | |
|---|---|---|---|---|---|---|---|---|---|---|---|---|
| CM942-B-2-b | Aug-06 | 0.018 | 0.8205 | 2303 | 0.0022 | 0.0747 | 0.0390224 | 3.90 | | | 0.0747 | 2303 |
| CM942-B-5-a | Aug-06 | 0.018 | 1.327 | 2293 | 0.003 | 0.0736 | 0.0471781 | 4.72 | 4.68 | 0.05 | 0.0736 | 2293 |
| CM942-B-5-b | Aug-06 | 0.018 | 1.3103 | 2294 | 0.003 | 0.0737 | 0.0465009 | 4.65 | | | 0.0737 | 2294 |
| CM942-C-1-f | Aug-08 | 0.018 | 0.9692 | 2310 | 0.003 | 0.0755 | 0.0333431 | 3.33 | 3.32 | 0.01 | 0.0755 | 2310 |
| CM942-C-1-i | Aug-06 | 0.018 | 0.964 | 2311 | 0.003 | 0.0755 | 0.0331498 | 3.31 | | | 0.0755 | 2311 |
| CM942-C-2-a | Aug-06 | 0.018 | 0.56117 | 2303 | 0.002 | 0.0747 | 0.0293577 | 2.94 | 2.94 | 0.00 | 0.0760 | 2315 |
| CM942-C-2-b | Aug-06 | 0.018 | 0.56117 | 2303 | 0.002 | 0.0747 | 0.0293577 | 2.94 | | | 0.0760 | 2315 |
| CM942-C-3-a | Aug-06 | 0.018 | 1.0075 | 2309 | 0.003 | 0.0753 | 0.0347678 | 3.48 | 3.47 | 0.02 | 0.0753 | 2309 |
| CM942-C-3-b | Aug-06 | 0.018 | 1.0008 | 2309 | 0.003 | 0.0753 | 0.0345366 | 3.45 | | | 0.0753 | 2309 |
| CM942-C-3-d | Aug-06 | 0.018 | 1.0098 | 2308 | 0.003 | 0.0753 | 0.0348623 | 3.49 | | | 0.0753 | 2308 |
| CM942-C2-1-a | Aug-06 | 0.018 | 0.865 | 2307 | 0.0025 | 0.0751 | 0.0359469 | 3.59 | 3.59 | 0.01 | 0.0751 | 2307 |
| CM942-C2-1-b | Aug-06 | 0.018 | 0.8632 | 2307 | 0.0025 | 0.0751 | 0.0358721 | 3.59 | | | 0.0751 | 2307 |
| CM942-E-1-a | Aug-06 | 0.018 | 0.8747 | 2294 | 0.002 | 0.0737 | 0.0465630 | 4.66 | 4.67 | 0.02 | 0.0737 | 2294 |
| CM942-E-1-b | Aug-06 | 0.018 | 0.8783 | 2293 | 0.002 | 0.0736 | 0.0468386 | 4.68 | | | 0.0736 | 2293 |
| MVO1243-A-1-c | Aug-06 | 0.018 | 1.1727 | 2289 | 0.0025 | 0.0731 | 0.0504610 | 5.05 | 5.03 | 0.03 | 0.0731 | 2289 |
| MVO1243-A-1-d | Aug-06 | 0.018 | 1.165 | 2289 | 0.0025 | 0.0732 | 0.0500612 | 5.01 | | | 0.0732 | 2289 |
| MVO1243-A-2-b | Aug-06 | 0.018 | 1.1962 | 2287 | 0.0025 | 0.073 | 0.0515878 | 5.16 | 5.09 | 0.08 | 0.0730 | 2287 |
| MVO1243-A-2-c | Aug-06 | 0.018 | 1.169 | 2289 | 0.0025 | 0.0732 | 0.0502331 | 5.02 | | | 0.0732 | 2289 |
| MVO1243-A-2-d | Aug-06 | 0.018 | 1.1674 | 2289 | 0.0025 | 0.0732 | 0.0501644 | 5.02 | | | 0.0732 | 2289 |
| MVO1243-A-3-a | Aug-06 | 0.018 | 0.61776 | 2312 | 0.002 | 0.0757 | 0.0317672 | 3.18 | 3.18 | 0.01 | 0.0757 | 2312 |
| MVO1243-A-3-b | Aug-06 | 0.018 | 0.62119 | 2312 | 0.002 | 0.0757 | 0.0319436 | 3.19 | | | 0.0757 | 2312 |
| MVO1243-A-4-b | Aug-06 | 0.018 | 0.669 | 2309 | 0.002 | 0.0753 | 0.0346298 | 3.46 | 3.42 | 0.06 | 0.0753 | 2309 |
| MVO1243-A-4-a | Aug-06 | 0.018 | 0.6533 | 2310 | 0.002 | 0.0754 | 0.0337576 | 3.38 | | | 0.0754 | 2310 |
| MVO1243-C-2-a | Aug-06 | 0.018 | 1.73617 | 2307 | 0.005 | 0.0751 | 0.0360751 | 3.61 | 3.61 | 0.00 | 0.0751 | 2307 |
| MVO1243-C-2-b | Aug-06 | 0.018 | 1.7393 | 2307 | 0.005 | 0.0751 | 0.0361401 | 3.61 | | | 0.0751 | 2307 |
| MVO1243-C-3-a | Aug-06 | 0.018 | 0.9129 | 2304 | 0.0025 | 0.0748 | 0.0381392 | 3.81 | 3.81 | 0.01 | 0.0748 | 2304 |
| MVO1243-C-3-b | Aug-06 | 0.018 | 0.9099 | 2305 | 0.0025 | 0.0748 | 0.0379974 | 3.80 | | | 0.0748 | 2305 |
| MVO1243-D-1-a | Aug-06 | 0.018 | 0.5071 | 2316 | 0.0018 | 0.0761 | 0.0287720 | 2.88 | 2.92 | 0.07 | 0.0761 | 2316 |
| MVO1243-D-1-b | Aug-06 | 0.018 | 0.5225 | 2315 | 0.0018 | 0.076 | 0.0296976 | 2.97 | | | 0.0760 | 2315 |
| MVO1243-D-3-a | Aug-06 | 0.018 | 0.2541 | 2335 | 0.0018 | 0.0781 | 0.0139337 | 1.39 | 1.41 | 0.02 | 0.0781 | 2335 |
| MVO1243-D-3-b | Aug-06 | 0.018 | 0.2596 | 2334 | 0.0018 | 0.0781 | 0.0142414 | 1.42 | | | 0.0781 | 2334 |
| MVO1243-D-4-a | Aug-06 | 0.018 | 0.5691 | 2311 | 0.0018 | 0.0756 | 0.0325737 | 3.26 | 3.31 | 0.07 | 0.0756 | 2311 |
| MVO1243-D-4-b | Aug-06 | 0.018 | 0.5854 | 2310 | 0.0018 | 0.0754 | 0.0336101 | 3.36 | | | 0.0754 | 2310 |
| MVO1243-E-2-a | Aug-06 | 0.018 | 1.0105 | 2299 | 0.0025 | 0.0742 | 0.0426507 | 4.27 | 4.33 | 0.09 | 0.0742 | 2299 |
| MVO1243-E-2-b | Aug-06 | 0.018 | 1.0384 | 2297 | 0.0025 | 0.074 | 0.0439850 | 4.40 | | | 0.0740 | 2297 |

**Supplemental data Table 2: Molecular CO2 measured by FTIR.**

| SAMPLE | mol. wt. (kg/mole) | abs. 2350 | Density (kg/m³) | Thickness (micron) | thickness (cm) | absorptivity (m³/mole*cm) | concentration | CO2 wt. % | CO2 ppm | Average ppm | 1 SD |
|---|---|---|---|---|---|---|---|---|---|---|---|
| Mont1_A_3_a | 0.044 | 0.016 | 2315.5 | 30 | 0.0030 | 1.214 | 0.000083 | 0.008 | 82.96 | 76.17 | 10 |
| Mont1_A_3_b | 0.044 | 0.0133 | 2315.9 | 30 | 0.0030 | 1.214 | 0.000069 | 0.007 | 69.38 | | |
| Mont1_B_1_a | 0.044 | 0.005 | 2306.0 | 50 | 0.0050 | 1.214 | 0.000016 | 0.002 | 15.72 | 16.16 | 1 |
| Mont1_B_1_b | 0.044 | 0.0053 | 2314.0 | 50 | 0.0050 | 1.214 | 0.000017 | 0.002 | 16.60 | | |
| MVO283-H-3-b | 0.044 | 0.00419 | 2298.8 | 40 | 0.004 | 1.214 | 0.000017 | 0.002 | 16.52 | 16.52 | |
| MVO1243-C-2-a | 0.044 | 0.00409 | 2316.6 | 50 | 0.005 | 1.214 | 0.000013 | 0.001 | 12.80 | 15.19 | 3 |
| MVO1243-C-2-b | 0.044 | 0.00562 | 2316.6 | 50 | 0.005 | 1.214 | 0.000018 | 0.002 | 17.59 | | |

Supplementary data Table 3. Normalized electron microprobe analyses of melt inlcusions.

| name | sample | host | erutpion date | type | Na2O | FeO | K20 | SiO2 | MnO | CaO | Al2O3 | TiO2 | MgO | P2O5 | Total | Cl |
|---|---|---|---|---|---|---|---|---|---|---|---|---|---|---|---|---|
| MONT1 | pumice | Quartz | 1997 | melt incl. | 4.42 | 1.56 | 1.88 | 78.65 | 0.09 | 1.8 | 11.12 | 0.18 | 0.26 | 0.04 | 100 | 2520 |
| MONT1 | pumice | Plag. | 1997 | melt incl. | 4.2 | 1.77 | 2.15 | 75.08 | 0.12 | 2.64 | 13.45 | 0.23 | 0.28 | 0.08 | 100 | 3223 |
| MONT3 | pumice | Plag. | 7/12/2003 | melt incl. | 4.62 | 1.71 | 2.02 | 76.14 | 0.11 | 2.09 | 12.76 | 0.18 | 0.3 | 0.06 | 99.99 | 3026 |
| MVO942 | pumice | Plag. | Oct. 1997 | melt incl. | 4.33 | 1.64 | 2.2 | 75.89 | 0.11 | 2.02 | 13.24 | 0.23 | 0.29 | 0.03 | 99.98 | 3150 |
| MVO283 | pumice | Plag. | 8/1/1997 | melt incl. | 4.55 | 1.74 | 2.15 | 74.95 | 0.09 | 2.39 | 13.51 | 0.24 | 0.32 | 0.05 | 99.99 | 3270 |
| MVO283 | pumice | Plag. | 8/1/1997 | melt incl. | 4.51 | 1.66 | 2.06 | 76.18 | 0.1 | 2.18 | 12.76 | 0.21 | 0.29 | 0.05 | 100 | 2979 |
| MVO283 | pumice | Plag. | 8/1/1997 | melt incl. | 4.39 | 1.57 | 2.36 | 74.36 | 0.07 | 2.53 | 14.11 | 0.25 | 0.31 | 0.05 | 100 | 2960 |
| MVO283 | pumice | Plag. | 8/1/1997 | melt incl. | 4.79 | 1.43 | 2.83 | 73.26 | 0.1 | 2.4 | 14.75 | 0.13 | 0.25 | 0.05 | 99.99 | 3180 |
| MVO283 | pumice | Plag. | 8/1/1997 | melt incl. | 4.58 | 1.4 | 2.78 | 74.46 | 0.1 | 2.13 | 14 | 0.2 | 0.24 | 0.11 | 100 | 3260 |
| MVO283 | pumice | Plag. | 8/1/1997 | melt incl. | 5.04 | 1.5 | 2.9 | 72.83 | 0.09 | 2.25 | 14.85 | 0.16 | 0.3 | 0.08 | 100 | 3250 |
| MVO1243 | pumice | Plag. | 3/4/2004 | melt incl. | 4.77 | 1.53 | 2.09 | 76.06 | 0.08 | 1.99 | 12.97 | 0.21 | 0.26 | 0.03 | 99.99 | 2855 |

Diagram A) Temperature comparison for pumice glass.
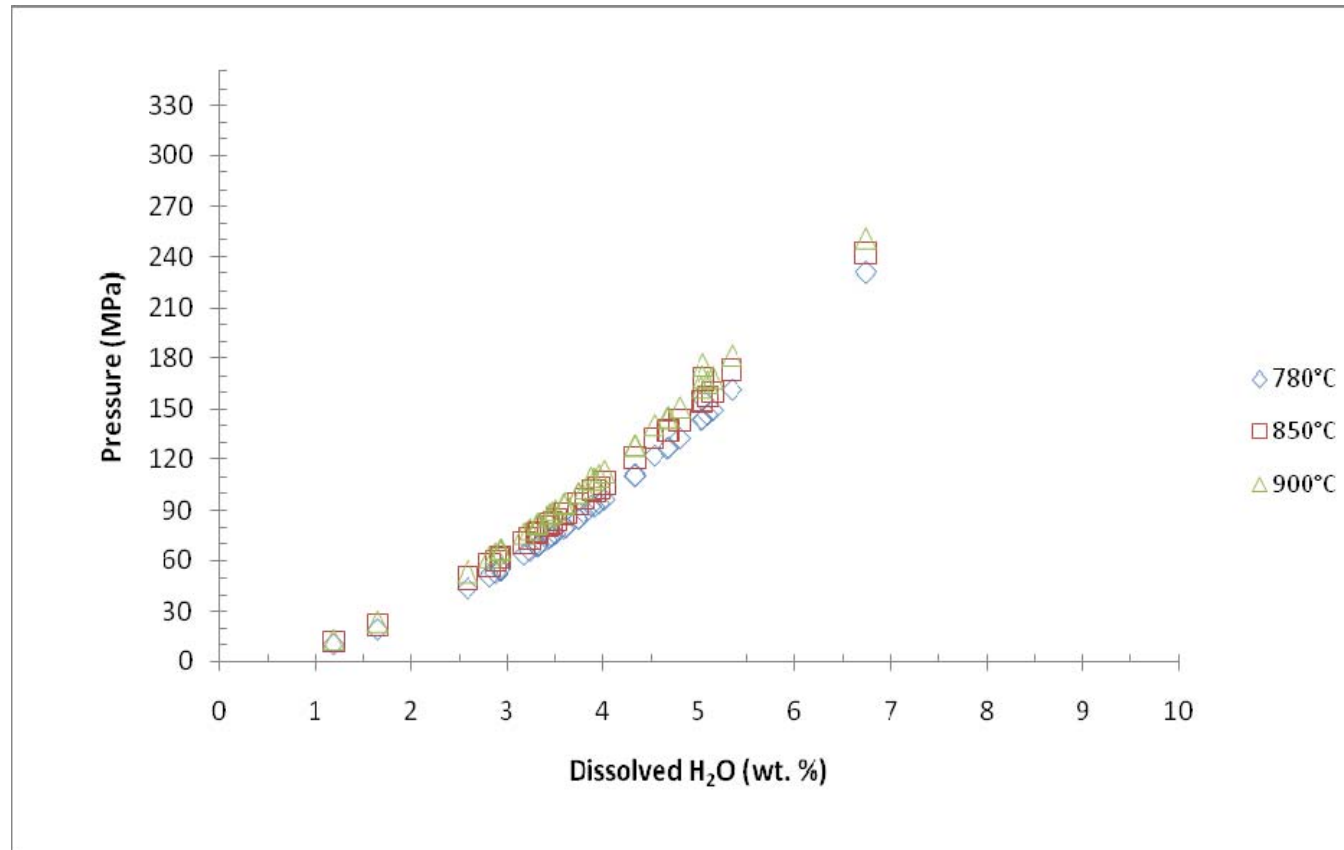
## Link to Chapter 3

In Chapter 1 we established the petrogenesis of the mafic magma from the crust/mantle boundary to the formation of mafic enclaves, which represent a hybrid mixture between the mafic magma and the andesitic host. In Chapter 2 we showed the presence of a rhyolitic $H_2O -$ Cl rich magma residing at lower conduit/upper reservoir conditions. The vulcanian explosions tap the uppermost portions of the magma reservoir during eruptions. In Chapter 3 we develop a synthetic model linking the ongoing activity to the inputs of mafic magma sustaining the eruption chemically, thermally and physically. We hypothesis that the SHV magmatic system is in a steady state and suggest indicators which would indicate a change in the magmatic system and possibly in the eruptive activity.

**Chapter 3**

# Steady-state behavior of the Soufrière Hills volcano, Montserrat

**Crystal Mann and John Stix**

**Abstract**

Mechanisms which control the steady state of a volcanic system are important to our understanding of the reawakening and longevity of volcanic eruptions. From 1995 to 2006 the magmas at the Soufriere Hills volcano (SHV) have remained andesitic in composition, hosting mafic enclaves. To understand the role of mafic input for the magmatic system at SHV, we examine evolution of magma and volatiles from the deep crust and upper mantle through mid - crustal levels to the shallow reservoir. At deep levels primative magma crystallizes amphibole, producing an evolved basaltic liquid, with $CO_2$ degassing isobarically and decompressionally. This differentiated liquid rises to mid-crustal levels where it interacts with andesitic magma, forming mafic enclaves of basalt to basaltic andesite in composition. During enclave formation and subsequent ascent, volatiles such as water, chlorine and sulfur are lost from the hybrid magmas as they rise towards the surface. The replenishment of the andesitic reservoir by mafic magma is the catalyst for the ongoing eruptions by providing heat, mass and volatiles to the system.

**Introduction**

Implicit in active, steady-state magmatic systems is their persistent activity and unchanging behavior in terms of composition and eruptions. Volcanologists examine compositional changes within magmas to better understand their potential for eruption. To deduce these compositional variations taking place at depth, clues are revealed in the chemical and volatile signatures of magma erupted at the surface. A key goal is to identify the underlying mechanism or mechanisms which drive persistently active volcanoes.

The Soufrière Hills volcano (SHV) is a youthful structure (3950 ± 70 years BP) (Harford *et al.*, 2002) which is persistently active. The current eruption, ongoing since 1995, erupts both

andesitic lava domes and pumice with a limited compositional range ($\sim$58 – 61 wt. % $SiO_2$) and hosts basaltic to basaltic andesitic magmatic enclaves ranging in composition from $\sim$49 to 56 wt. % $SiO_2$. The SHV has erupted similar compositions for the last $\sim$ 4000 years with the same eruptive style (i.e., dome growth and collapse cycles), and mafic enclaves have been present throughout (Rea, 1974; Wadge and Isaacs, 1988). An important difference between past eruptions and the current activity is that prehistoric deposits record slightly more felsic compositions up to 64 wt. % $SiO_2$ (Figure 1).

The mafic enclaves sampled from the ongoing eruption represent hybrid magmas of more mafic compositions mixed with magma from the andesitic reservoir (Mann and Stix, 2010). During the course of the current eruption, the magmatic system appears to be in a steady state, as shown by the characteristic and regular eruptive activity, the limited compositional range of the erupted products, and the 15-year duration of the eruption. We hypothesize that the steady state results from a balance between the andesitic magma evolving by cooling and crystallization on the one hand, and mafic magma providing heat and mass to the andesitic reservoir, sustaining the magmatic system and buffering its evolution (Mann and Stix, 2010; Zellmer et al., 2003). The abundance of mafic magma erupted as enclaves at the surface is negligible but appears to have increased slightly during the course of the eruption (Mann and Stix, 2010). We propose that this persistent activity observed at SHV is controlled by a series of factors internal to the andesitic magma reservoir, and a second set of external factors which influence the behavior and evolution of the andesite magma.

To address these issues, we divide the evolution of the SHV magmatic system into three components: 1) upper mantle and deep crust; 2) mid-crust; and 3) shallow reservoir. By taking this layered approach, we can identify key characteristics of each component and their

contributions to the ongoing eruption. At the lower crust/upper mantle boundary, we recognize differentiation processes at depth which provide the eruption catalyst, from mid-crustal levels we extract information regarding mafic enclave ascent rates and enclave residence times, and from shallow levels we identify abundances and distributions of different volatile species which provide information on the state of the shallow reservoir during and between eruptions.

**Mantle and deep crust**

All rocks erupted from SHV, including andesite and mafic enclaves, show strong evidence of amphibole fractionation from their trough-shaped REE profiles for which middle REE are depleted relative to light REE and heavy REE (Figure 2). This clear amphibole signature, coupled with the absence of olivine and clinopyroxene as crystallizing phases in the andesite and enclaves, provides constraints on pressures of differentiation of the mafic magma, prior to its intrusion into the shallow reservoir. The mafic magma is a high alumina basalt (HAB) with ~5 % phenocrystic amphibole and < 10 % phenocrystic plagioclase (Mann and Stix, 2010; Murphy et al., 2000). The upper limit of amphibole stability in terms of temperature is ~ 1050°C, and experiments on HAB + water demonstrate stability of amphibole to pressures of at least 1 GPa and 15 wt. % $H_2O$ (Foden and Green, 1992). The intrusive basalt is interpreted to be hydrous from these experiments, supported by the presence of acicular amphibole in the framework assemblage of the enclaves and their distinctive REE profiles indicating a significant role for amphibole. The absence of a negative Eu anomaly and the lack of appreciable plagioclase phenocrysts suggest minor involvement of plagioclase during differentiation of the more mafic enclaves. With high water concentrations at high pressure, amphibole fractionation will occur while plagioclase fractionation is suppressed (Yoder and Tilley, 1962).

The crust is estimated to be ~ 25 km thick beneath Montserrat (Christeson *et al.*, 2008). As mantle-derived basalt ponds against cooler crust at the crust/mantle boundary (0.6-0.7 GPa), it is capable of fractionating significant amounts of amphibole with little or no plagioclase (Barclay and Carmichael, 2004; Christeson et al., 2008; Davidson et al., 2007). Clearly water plays a key role in petrogenesis, but we speculate that $CO_2$ may be also present during deep differentiation of basalt (Blundy *et al.*, 2010). $CO_2$ emanates from fumaroles at the surface, while small amounts of dissolved $CO_2$ (<80 ppm) are observed in a few phenocryst hosted melt inclusions from pumices ejected by vulcanian eruptions (Barclay et al., 1998; Hammouya et al., 1998; Mann et al., 2010). During fractional crystallization and open system degassing at 0.6-0.7 GPa, mantle derived $CO_2$ could be the primary exsolving volatile phase (Newman and Lowenstern, 2002).

At these deep levels, the basaltic magmas will crystallize significant amphibole by two means. First, crystallization will occur as magmas rise. Second, as the magmas stall and pond in lower crustal intrusions, further amphibole will crystallize. It is therefore likely that amphibole cumulates are present at these deep crustal levels (Arculus and Wills, 1980; Kiddle et al., 2010). Subjected to new inputs of hot mantle-derived basalts, the cumulates could undergo partial melting. The liquid composition extracted from a partially melted amphibole cumulate carries the same REE signature as a basaltic liquid crystallizing amphibole. Thus, both crystal fractionation of a basaltic liquid and partial melting of an amphibolite cumulate can take place at and near the crust-mantle boundary, with the relative proportions of each controlled by the flux of basalt coming from the mantle. Furthermore, over time the accumulated basaltic magma will become stockpiled at the base of the crust; the thickness of this pile also may influence whether crystal fractionation or partial melting dominates.

**Mid-crustal levels**

We now examine the similar bulk compositions of the enclaves as a function of time and discuss their increasing volume as observed in the field from 1996 to 2002. From the crust/mantle boundary the HAB ascends through the crust and intersects a reservoir at ~ 13 km (Devine et al., 2003; Elsworth et al., 2008; Mann and Stix, 2010; Voight et al., 2010). This mid-crustal reservoir may extend upward to shallow levels (5-6 km; Voight et al., 2010), or it may be distinct from the shallow chamber (Ellsworth et al., 2008). The intruding mafic magma mixes with the andesitic host magma at a mixing horizon located at the contact between the two, forming a hybrid magma (Sparks and Marshall, 1986). The enclaves observed in the andesite are the manifestation and result of this mixing process.

Three types of mafic enclaves are present over the course of the current eruption. Types 1 and 2 include basalt to basaltic andesite while Type 3 is strictly basaltic andesite in composition. Intrusion of mafic magma into the andesitic reservoir is thought to be a catalyst for a new eruption cycle (Murphy *et al.*, 2000). Thus, the SHV reservoir or reservoirs has undergone multiple mafic replenishment events over the course of 15 years, with each intrusion disrupting the mixing horizon by heating the overlying andesite, thereby increasing turbulence, causing overturn of mafic magma, and forming enclaves (Perugini et al., 2007; Wiebe, 1974). The mafic magma close to the new intrusion site is likely to be dislodged and erupted, while cooler magma farther from this site may remain in the chamber for a longer period of time. Under this premise, the mafic enclaves have variable residence times in the andesite reservoir, which helps to explain their overlap in composition from 1996 to 2006.

The proportion of mafic enclaves has increased from < 1 vol. % to 5 vol. % in the erupted products from 1997 to 2002 (Mann and Stix, 2010; Murphy et al., 2000). If the mafic magma has intruded the andesitic reservoir many times, the volume of mafic magma in the reservoir should increase progressively. Hence more mafic magma is available in the reservoir to be processed and remobilized as enclaves. A second possibility is that the flux of mafic magma from deeper levels is increasing with time; this scenario implies that all of the mafic magma is removed from the chamber between eruptive cycles. A third possibility is that the deep plumbing system exploited by the mafic magma from the mantle to the andesitic reservoir has become increasingly well established during the 15-year eruption. As a result, mafic magma is now channeled and transported into the andesite more efficiently today compared to 15 years ago.

The thickness of overgrowth rims on amphibole can be used to determine rates of magma ascent (Rutherford and Devine, 2003; Rutherford and Hill, 1993). In the andesite host, amphibole develops overgrowth rims due to dehydration as it rises slowly to the surface (Buckley *et al.*, 2006). By contrast, the T1 enclaves contain xenocrystic amphibole with overgrowth rims due to heating when incorporated into the mafic magma from the andesitic magma. T2 enclaves contain phenocrystic amphibole without reaction rims. The absence of reaction rims on these crystals suggests rapid ascent of the T2 enclaves once outside of the amphibole stability field. Studies at SHV demonstrate ascent rates on the order of $0.02 \text{ m s}^{-1}$ from 5 kilometers depth at 130 MPa and ~850°C (Rutherford and Hill, 1993). T2 enclaves are rapidly driven upward due to inputs of heat by mafic intrusion (Mann and Stix, 2010). The absence of reaction rims on the amphibole is consistent with a model of T2 enclaves dislodged at depth within the stability field of amphibole and then ascending rapidly to the surface at rates of at least $0.02 \text{ ms}^{-1}$.

**Shallow reservoir**

In this section we examine gas contents of the host andesite and mafic enclaves to understand volatile conditions in the shallow reservoir. The andesite has a very distinct volatile element signature, in which water and chlorine reach significant abundances, while $CO_2$ and S are close to zero. Phenocryst-hosted melt inclusions have water contents which cluster at 2.8 to 5.4 wt. % (Figure 3a) while chlorine clusters at ~ 3000ppm. Using Webster et al. (1997) experimental data indicates pressures close to 200 MPa and depths of ~ 8 km. This depth indicates upper reservoir conditions (Mann et al., 2010; Paulatto et al., 2010; Voight et al., 2010). By contrast, matrix glasses in the mafic enclaves contain very low water contents of < 0.5 wt % $H_2O$ with significant chlorine variability ranging from 400 – 3400 ppm (Figure 3a-b), also containing no measurable $CO_2$ or S. The low water contents of the mafic enclaves suggest that they have efficiently lost water during their ascent to the surface. Some of this dewatering could take place during mixing and the diktytaxitic texture of both the T1 and T2 enclaves. After enclave formation, gas-driven filter pressing may promote further vesiculation and degassing. It has been demonstrated that $K^+$ can diffuse from enclaves into the host andesite (Humphreys *et al.*, 2010). Since $H^+$ is also a fast-diffusing species, it is possible that some water has been transferred from the basalt to the andesite reservoir, either at the mixing horizon or as enclaves rise within the andesite. The range of chlorine contents may be the result of variable residence times and /or variable degassing in the magma reservoir. The lower chlorine contents indicate longer residence times or slower ascent to the surface, hence more degassing.

Although the magma reservoir is thought to reach depths of at least ~ 10 km (Elsworth et al., 2008; Voight et al., 2010), volatiles present at this depth are not recorded in melt inclusions.

The absence of melt inclusions trapping higher water contents may result from multistep decompression observed during vulcanian explosions, in which water diffuses from melt inclusions through host crystals to equilibrate with the surrounding matrix at progressively shallower levels in the magma reservoir (Mann *et al.*, 2010). Alternatively, andesite from deep in the magma chamber is not being erupted. A third possibility is that melt inclusions are being trapped preferentially at shallow depths, perhaps due to significant crystallization at these levels from degassing and/or cooling.

The low $CO_2$ and S suggest that the magmas have been efficiently degassed. The mafic enclaves pond at depth various depths with $CO_2$ lost passively and escaping through fractures in the crust as manifested by the principal volcanic conduit, fumaroles and thermal areas outside the conduit, and faults. The sulfur is degassed from the mafic magma at the mixing horizon, crystallization, and vesiculation at the mixing horizon. The mixing dynamics at this interface promotes loss of gases such as sulfur as a foam layer develops (Mann and Stix, 2010). Although only small amounts of dissolved sulfur are present in the host andesite, $SO_2$ is a pervasive species in the gas plume (Christopher et al., 2010; Edmonds et al., 2003), suggesting that the sulfur is able to segregate from deeper levels in a free gas phase (Voight et al., 2010) and escape at the surface.

If magma residing in the upper parts of the chamber is being erupted preferentially as suggested by our data, we might expect progressively more evolved compositions to be erupted. Simultaneously, however, mixing is taking place at a location or locations much deeper in the chamber. The tendency for shallow andesitic magma to evolve towards dacite is hence counteracted by the addition of mafic magma to andesite at deep levels, which results in homogenization. The end product is a buffered system of intermediate composition (~60 wt. %

$SiO_2$). How might this buffering be disrupted? On the one hand, the eruption of more felsic compositions would demonstrate that the andesite is able to fractionate and evolve with less processing by the mafic magma. In this case, the supply of mafic magma from is reduced. On the other hand, we would observe progressively more mafic material with time, caused by a basaltic plume which has been able to establish an efficient route or pathway through the crust to shallow levels. The T3 mafic enclaves are clear evidence of this phenomenon. These enclaves are significantly more evolved and fractionated than are the T1 and T2 enclaves. All REE are more enriched (Fig. 2). These data prove that the T3 enclaves represent mafic magmas which have crystallized abundant plagioclase at shallow crustal levels.

**Conclusions**

The Soufriere Hills volcano is in a steady state condition which is balanced between the andesitic magma evolving by cooling and crystallization and the mafic magma providing heat and mass to the andesitic reservoir, sustaining the system and buffering its evolution. Periodic replenishment of mafic magma initiates mafic overturn and drives the mafic enclaves towards the surface. The absence of amphibole overgrowth rims in enclaves attest to their rapid ascent. The volume of mafic magma may be increasing with time due to 1) accumulation of mafic magma from repeated intrusions, 2) an increased mantle flux of mafic magma, or 3) increasingly efficient transport of mafic magma from the mantle into the reservoir. Variable water contents and similar chlorine contents in phenocryst-hosted melt inclusions from the andesite reflect eruption of shallow andesitic magma during vulcanian explosions. Conversely, low water contents and variable chlorine contents in the mafic enclaves matrix indicate their efficient degassing and variable residence times in the magma chamber prior to eruption.

## References

Barclay, J., and Carmichael, I.S.E., 2004, A Hornblende Basalt from Western Mexico: Water-saturated Phase Relations Constrain a PressureTemperature Window of Eruptibility: Journal of Petrology, v. 45, p. 485-506.

Barclay, J., Rutherford, M.J., Carroll, M.R., Murphy, M.D., Devine, J.D., Gardner, J.E., and Sparks, R.S.J., 1998, Experimental phase equilibria constraints on pre-eruptive storage conditions of the Soufrière Hills magma: Geophysical Research Letters, v. 25, p. 3437-3440.

Botcharnikov, R.E., Behrens, H., Holtz, F., Koepke, J., and Sato, H., 2004, Sulfur and chlorine solubility in Mt. Unzen rhyodacitic melt at 850 °C and 200 MPa: Chemical Geology, v. 213, p. 207-225.

Buckley, V.J.E., Sparks, R.S., and Wood, B.J., 2006, Hornblende dehydration reactions during magma ascent at Soufrière Hills Volcano, Montserrat: Contributions to Mineralogy & Petrology, v. 151, p. 121-140.

Christeson, G.L., Mann, P., Escalona, A., and Aitken, T.J., 2008, Crustal structure of the Caribbean–northeastern South America arc-continent collision zone: J. Geophys. Res., v. 113, p. B08104.

Christopher, T., Edmonds, M., Humphreys, M.C.S., and Herd, R.A., 2010, Volcanic gas emissions from Soufrière Hills Volcano, Montserrat 1995-2009, with implications for mafic magma supply and degassing: Geophys. Res. Lett., v. 37, p. L00E04.

Davidson, J., Turner, S., Handley, H., Macpherson, C., and Dosseto, A., 2007, Amphibole "sponge" in arc crust?: Geology, v. 35, p. 787-790.

Devine, J.D., Rutherford, M.J., Norton, G.E., and Young, S.R., 2003, Magma Storage Region Processes Inferred from Geochemistry of Fe-Ti Oxides in Andesitic Magma, Soufrière Hills Volcano, Montserrat, W.I: J. Petrology, v. 44, p. 1375-1400.

Edmonds, M., Oppenheimer, C., Pyle, D.M., Herd, R.A., and Thompson, G., 2003, SO2 emissions from Soufrière Hills volcano and their relationship to conduit permeability, hydrothermal interaction and degassing regime: Journal of Volcanology and Geothermal Research, v. 124, p. 23-43.

Edmonds, M., Pyle, D., and Oppenheimer, C., 2002, HCl emissions at Soufrière Hills Volcano, Montserrat, West Indies, during a second phase of dome building: November 1999 to October 2000: Bulletin of Volcanology, v. 64, p. 21-30.

Elsworth, D., Mattioli, G.S., Taron, J., Voight, B., and Herd, R., 2008, Implications of magma transfer between multiple reservoirs on eruption cycling: Science, v. 322, p. 246-248.

Foden, J.D., and Green, D.H., 1992, Possible role of amphibole in the origin of andesite: some experimental and natural evidence: Contributions to Mineralogy and Petrology, v. 109, p. 479-493.

Hammouya, G., Allard, P., Jean-Baptiste, P., Parello, F., Semet, M.P., and Young, S.R., 1998, Pre and syn-eruptive geochemistry of volcanic gases from Soufrière Hills volcano, Montserrat W.I.: Geophysical Research Letters, v. 25, p. 3685-3688.

Harford, C.L., Pringle, M.S., Sparks, R.S., and Young, S.R., 2002, The volcanic evolution of Montserrat using $^{40}$Ar/$^{39}$Ar geochronology, *in* Druitt, T.H., and Kokelaar, B.P., eds., The eruption of Soufrière Hills volcano, Montserrat, from 1995 to 1999, Volume 21: London, Memoirs, Geological Society of London, p. 93-113.

Humphreys, M.C.S., Edmonds, M., Christopher, T., and Hards, V., 2010, Magma hybridisation and diffusive exchange recorded in heterogeneous glasses from Soufrière Hills Volcano, Montserrat: Geophys. Res. Lett., v. 37, p. L00E06.

Mann, C.P., and Stix, J., 2010, Mafic enclaves record magma mixing at the Soufrière Hills Volcano, Montserrat, West Indies: Journal of Petrology, v. submitted.

Mann, C.P., Wallace, P., and Stix, J., 2010, Phenocryst hosted melt inclusions mirror lower conduit and upper magma reservoir conditions at the time of eruption, Soufrière Hills volcano, Montserrat, West Indies: submitted.

Murphy, M.D., Sparks, R.S.J., Barclay, J., Carroll, M.R., and Brewer, T.S., 2000, Remobilization of Andesite Magma by Intrusion of Mafic Magma at the Soufrière Hills Volcano, Montserrat, West Indies: J. Petrology, v. 41, p. 21-42.

Newman, S., and Lowenstern, J.B., 2002, VC: a silicate melt-H2O-CO2 solution model written in Visual Basic for excel: Computers & Geosciences, v. 28, p. 597-604.

Paulatto, M., Minshull, T.A., and Henstock, T.J., 2010, Constraints on an intrusive system beneath the Soufrière Hills Volcano, Montserrat, from finite difference modeling of a controlled source seismic experiment: Geophysical Research Letters, v. 37, p. 5.

Perugini, D., Valentini, L., and Poli, G., 2007, Insights into magma chamber processes from the analysis of size distribution of enclaves in lava flows: A case study from Vulcano Island (Southern Italy): Journal of Volcanology and Geothermal Research, v. 166, p. 193-203.

Rea, W.J., 1974, The volcanic geology and petrology of Montserrat, West Indies: Journal of the Geological Society, v. 130, p. 341-366.

Roggensack, K., and Moore, G., 2008, Constraints on mixed-fluid ($H_2O$ and $CO_2$) solubility in arc basalts: New experiments require new models: Geological Society of America *Abstracts with Programs*, v. 40, p. 7.

Rutherford, M.J., and Devine, J.D., 2003, Magmatic Conditions and Magma Ascent as Indicated by Hornblende Phase Equilibria and Reactions in the 1995-2002 Soufrière Hills Magma: J. Petrology, v. 44, p. 1433-1453.

Signorelli, S., and Carroll, M.R., 2001, Experimental constraints on the origin of chlorine emissions at the Soufrière Hills volcano, Montserrat: Bulletin of Volcanology, v. 62, p. 431-440.

Sparks, R.S.J., and Marshall, L.A., 1986, Thermal and mechanical constraints on mixing between mafic and silicic magmas: Journal of Volcanology and Geothermal Research, v. 29, p. 99-124.

Voight, B., Widiwijayanti, C., Mattioli, G., Elsworth, D., Hidayat, D., and Strutt, M., 2010, Magma-sponge hypothesis and stratovolcanoes: Case for a compressible reservoir and quasi-steady deep influx at Soufrière Hills Volcano, Montserrat: Geophys. Res. Lett., v. 37, p. L00E05.

Wadge, G., 1984, Comparison of volcanic production rates and subduction rates in the Lesser Antilles and Central America: Geology, v. 12, p. 555-558.

Wadge, G., and Isaacs, M.C., 1988, Mapping the volcanic hazards from Soufrière Hills Volcano, Montserrat, West Indies using an image processor: Journal of the Geological Society, v. 145, p. 541-551.

Watson, E.B., and Jurewicz, S.R., 1984, Behavior of Alkalies during Diffusive Interaction of Granitic Xenoliths with Basaltic Magma: The Journal of Geology, v. 92, p. 121-131.

Webster, J.D., 1997, Chloride Solubility in Felsic Melts and the Role of Chloride in Magmatic Degassing: J. Petrology, v. 38, p. 1793-1807.

Wiebe, R.A., 1974, Coexisting Intermediate and Basic Magmas, Ingonish, Cape Breton Island: The Journal of Geology, v. 82, p. 74-87.

Yoder, H.S.J., and Tilley, C.E., 1962, Origin of Basalt Magmas: An Experimental Study of Natural and Synthetic Rock Systems: J. Petrology, v. 3, p. 342-532.

Zellmer, G.F., Hawkesworth, C.J., Sparks, R.S.J., Thomas, L.E., Harford, C.L., Brewer, T.S., and Loughlin, S.C., 2003, Geochemical Evolution of the Soufrière Hills Volcano, Montserrat, Lesser Antilles Volcanic Arc: J. Petrology, v. 44, p. 1349-1374.

Figure 1. SHV andesite and mafic enclaves over time. Data from Harford et al. (2002); Murphy et al. (2000); Zellmer et al. (2003)

Figure 1
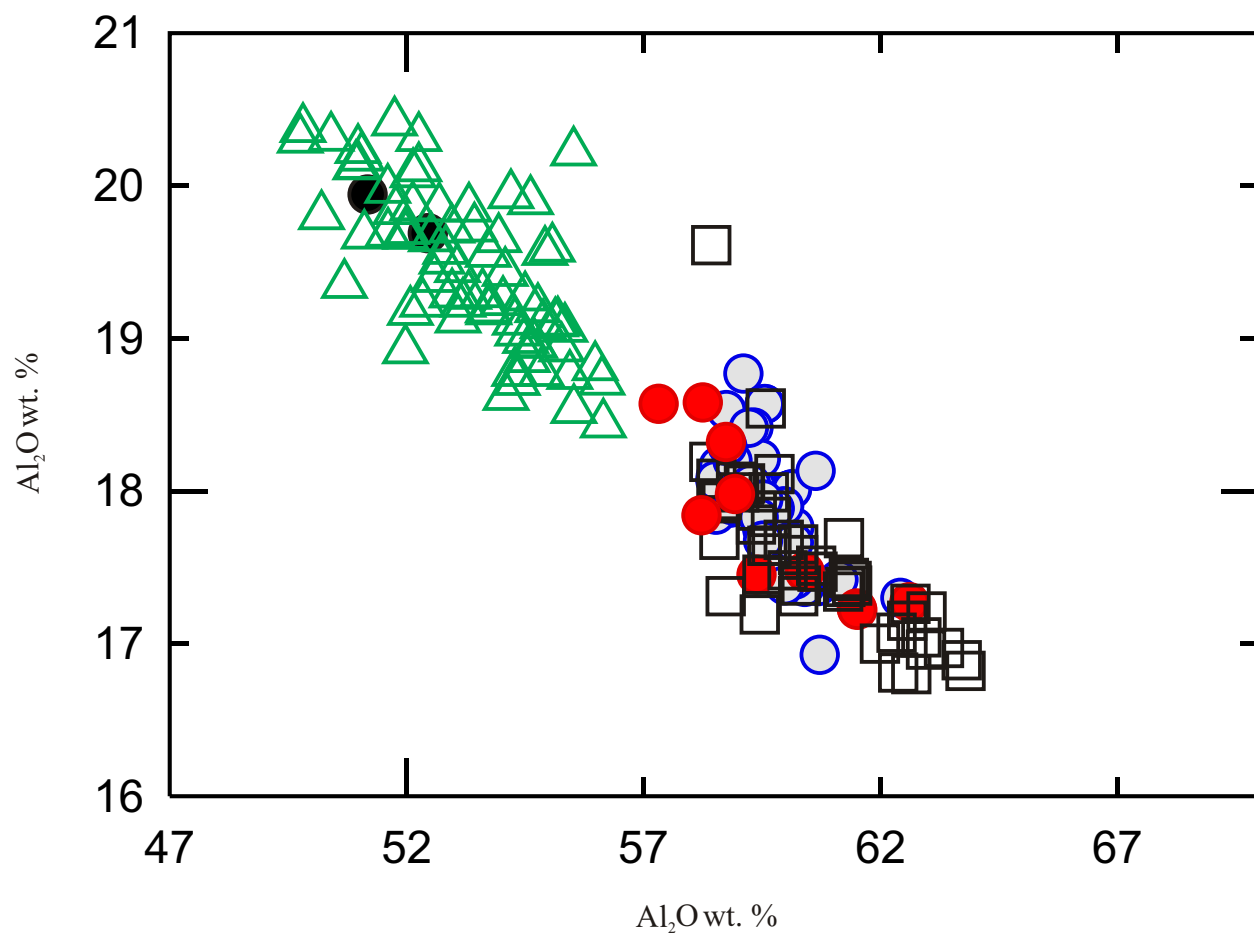


Mafic enclaves 1996 to present
Mafic enclaves prior to 1996
Andesite dome rock prior to 1996
Andesite dome rock 1996 to present
Pumice 1996 to present

Figure 2. REE patterns for mafic enclaves (T1, T2 and T3) and host andesite. Note enriched
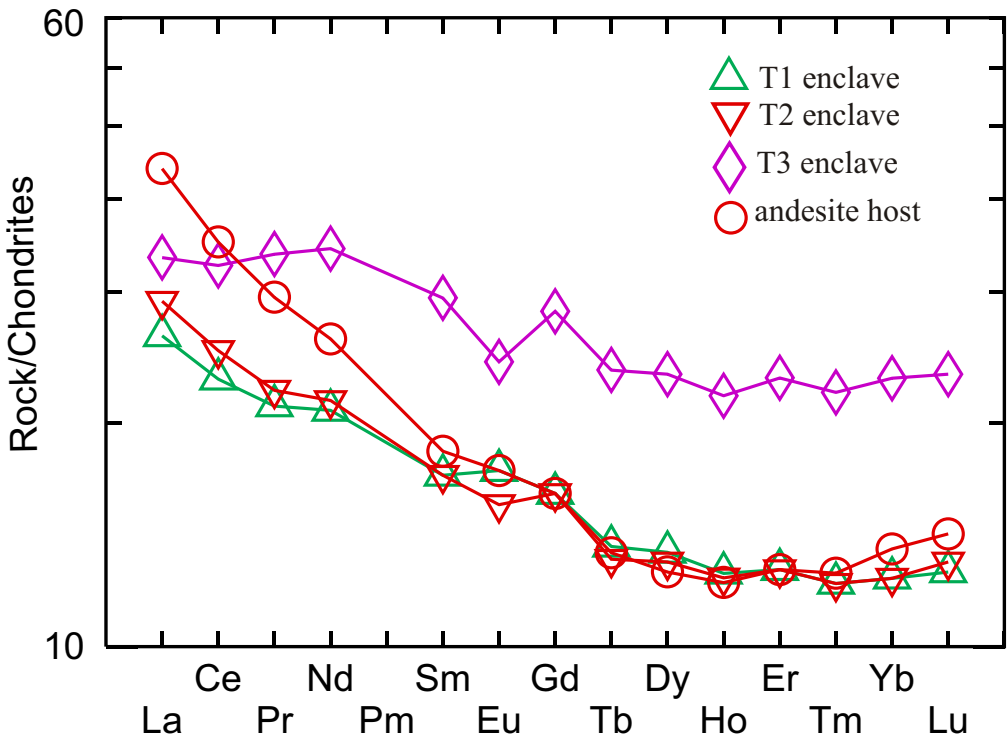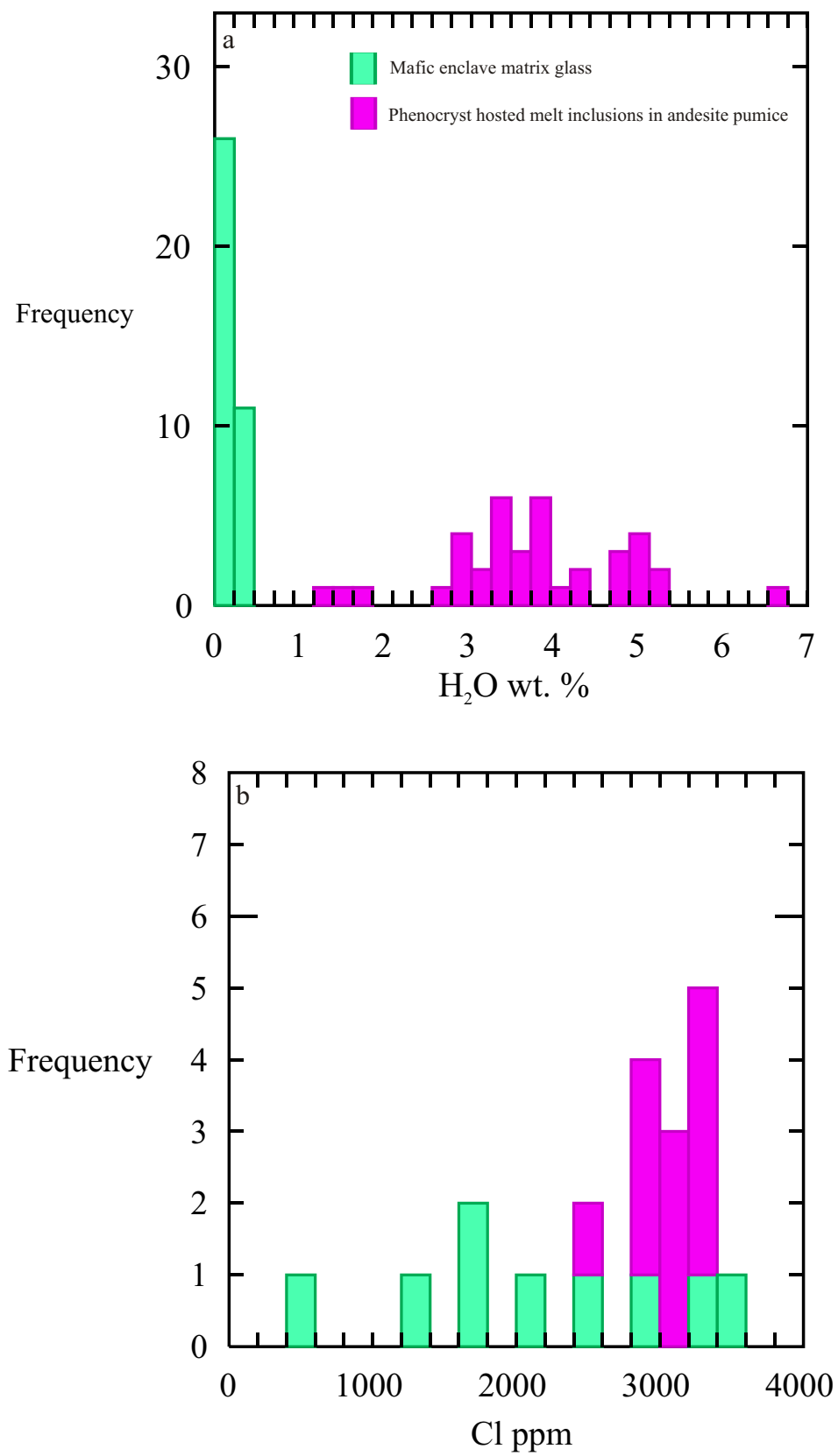
REE's for T3.

Figure 2

Figure 3. A) Water contents for mafic enclaves and explosively erupted phenocryst hosted melt inclusions. Data from Mann and Stix (2010); B) Chlorine contents for mafic enclaves and explosively erupted phenocryst hosted melt inclusions. Data from Mann and Stix (2010)

Figure 3

# Conclusions

*Main findings*

1. The mafic enclaves observed in the block and ash flow deposits at the Soufrière Hills volcano, Montserrat, represent differentiated basaltic magma mixed with the andesitic host prior to enclave formation.

2. Amphibole plays a major role in differentiation of the replenishing basaltic magma, and some batches also fractionate significant plagioclase.

3. Based on their chemistry, mineralogy, and petrology, the mafic enclaves can be grouped into three types (T1, T2, T3). Types T1 and T2 represent the basaltic magma mixed with the host andesite. Type T3 represents a differentiated basaltic magma which has undergone significant fractionation of both amphibole and plagioclase with little mixing.

4. Vulcanian explosions tap the uppermost portions of an andesitic reservoir which is $H_2O$ – Cl rich and depleted in $CO_2$ and S.

5. The mafic magma contributes mass, volume, heat and volatiles ($H_2O$, $CO_2$, S, Cl) to the magmatic system.

6. The magmatic system at SHV is in a steady state. The tendency for the andesitic reservoir to cool and crystallize is counteracted by periodic inputs of mafic magma. This buffering effect prevents the andesite from evolving to more silicic compositions.

## Contributions to knowledge

My petrologic study of the mafic enclaves provides better constraints on the role of the mafic magma to the ongoing eruption at the Soufrière Hills volcano. I have demonstrated that the mafic magma is a catalyst for the ongoing eruption; it also buffers the andesite compositionally and thermally. Without inputs of mafic magma, the andesite would not erupt. The mafic magma provides volatiles which help drive the dynamics of the magmatic system and contribute to its explosivity. Careful monitoring of changes towards more evolved compositions may indicate a change in the input of mafic magma at depth. Since mafic enclaves are present in many arc volcanic lavas, they appear to be a catalyst for magma chamber dynamics and volcanic eruptions in many cases.

## Topics for future research

An undetermined variable is the timescales between mixing and eruption. To understand ascent rates and residence times, further work using mobile element diffusion rates such as Na and K across enclave margins could help to constrain ascent rates. Solubility relationships between water and chlorine during magma ascent can reveal ascent pathways; for example, do the enclaves rise directly from depth or do they move up in multiple increments, stall and partly degas before further ascent? Lower chlorine contents in the T1 enclaves would support our model of rapid ascent. Further work on temperatures and pressures of enclave formation would be useful to estimate more precisely where the enclaves are forming. If we assume that the mafic magma and andesite are mixing and we have evidence for contemporaneous eruption, then the two magmas must be in the same reservoir at some point. The current reservoir models are 1) two magma chambers, one at shallow depth and one deeper, or 2) a vertically extensive reservoir

which fluxes hot magma from depth through it. The enclave formation temperatures would help to refine the appropriate reservoir model.

Another key question is the ultimate source of the mafic magma and the host andesite. Stable isotope geochemistry (O, D/H) and radiogenic isotopes (Sr, Nd, Pb) determined for the host andesite and the mafic enclaves would be useful to compare their respective sources. This source identification would improve our model of mafic enclave petrogenesis and could help with identifying long-term factors for steady state behavior of the magma reservoir.